The Extension of Colloid Chemistry from Aqueous to Non-Aqueous Media with Application to Nanofluid Research

by

Dan Clary

A dissertation submitted to the Graduate Faculty of
Auburn University
in partial fulfillment of the
requirements for the Degree of
Doctor of Philosophy

Auburn, Alabama
December 12, 2011

Keywords: colloid, nanoparticle, photochemistry, kinetics, organosol

Approved by

German Mills, Chair, Associate Professor of Chemistry
Rik Blumenthal, Associate Professor of Chemistry
Vince Cammarata, Associate Professor of Chemistry
Wei Zhan, Assistant Professor of Chemistry

Abstract

Nanofluids are colloids whose design is specific to the study and application of heat transfer systems. Metals typically have thermal conductivities which are several times higher than that of traditional cooling liquids such as water or ethylene glycol. The suspension of metal particles in a cooling fluid is expected to yield a nanofluid with enhanced thermal transport properties relative to the base solvent. During the course of the current study, several colloidal suspensions were prepared and the thermal properties of the resulting suspensions were evaluated when appropriate. Due to the surplus of literature available which describes aqueous colloids, the current work will diverge and place the bulk of its emphasis on suspensions in nonpolar solvents.

Cyclodextrins are cyclic molecules composed of glucose units. The inner cavity of cyclodextrins is noted for its ability to form stable inclusion complexes with a wide variety of guests. A cyclodextrin-glucose host-guest complex was prepared and utilized as both a salt reductant and a particle stabilizer in the generation of aqueous metal colloids including Ag, Au, Pd, and Pt. The resulting colloids demonstrated remarkable stability—3 years and running, in some cases—and have been evaluated for thermal conductivity. Evaluation of the reaction products when the complex is used to reduce Pd^{2+} demonstrated a unique comproportionation reaction in which the guest undergoes a two electron oxidation to produce a Pd atom. The resulting atom reduces a neighboring Pd^{2+} ion to yield two Pd^{+} ions. The monovalent species, in

contrast to Pd^{2+}, can then oxidize the host to form atoms which rapidly aggregate to yield particles.

Highly stable, crystalline copper(II) oxide particles were prepared which can be isolated as a powder and redispursed in low dielectric media such as hydrocarbons or chloroform. Mass concentrations of up to 20% (1.65 M) were achieved in octane, dodecane, and eicosane and remained stable for at least ten days at room temperature as observed by visible spectroscopy. Quasi-spherical particle shape was observed with the largest fraction possessing a diameter of 9 nm and 90% of the population existing within the range of 5 to 15 nm. The colloidal systems were characterized using FAA, XRD, TEM, UV-Vis, DSC, and a simple device inspired by Newton's Law of cooling which was employed to measure cooling/heating rates. Thermodynamic measurements of sodium oleate-stabilized CuO particles suspended in dodecane and eicosane reveal a decrease in C_p, ΔH_{fus}, and cooling/heating rates of the resulting colloid with large increases in particle mass concentration.

Irradiation with 350 nm photons of anhydrous, air-free octane or toluene solutions of copper(II) oleate containing benzophenone as a photosensitizer and oleoylsarcosine as a stabilizer resulted in metallic Cu particles with nanometer dimensions. Evidence is presented that implicates the hydrocarbon as the predominant H-atom donor in the generation of reductive benzophenone ketyl radicals and a kinetic model is constructed to rationalize the rate dependencies with respect to the Cu^{2+}/Cu^{+} step. Rates of both Cu^{2+} consumption and Cu formation vary linearly with light intensity and exhibit a first-order dependence on benzophenone concentration but the latter step shows little dependence otherwise. The initial rate of reactant consumption decreases with increasing concentration of cupric ions or sarcosine. Quenching of the excited state of benzophenone by the stabilizer occurs with a rate constant of

$k_4 = 1.6 \times 10^5$ M^{-1} s^{-1} and is explained by the formation of a contact ion pair between the reduced chromophore and oxidized sarcosine which ultimately decays by back electron transfer. The rate decrease induced by cupric ions results from the quenching of the excited state of benzophenone by the copper(II) complex with a rate constant of $k_5 = 6.1 \times 10^5$ M^{-1} s^{-1}. The resulting colloids proved to be stable in an anaerobic environment for at least a month and require more than 12 hours to oxidize upon exposure to air. Upon removal of the octane solvent, the particles can be redispersed in a variety of low dielectric media such as chloroform, carbon tetrachloride, hexane, or toluene.

UV irradiation of octane solutions containing Ag neodecanoate, $Pd(acac)_2$, or $Pt(acac)_2$ in the presence of benzophenone and oleoyl sarcosine resulted in crystalline metal particles. Rates of metal formation in the absence of BP for $Pd(acac)_2$ and $Pt(acac)_2$ were $r_i = 3.4\times10^{-8}$ M/s and $r_i = 4.7\times10^{-8}$ M/s, respectively, which are 2-4 times slower than the analgous reactions conducted in the presence of the chromophore. The direct irradiation of Ag(OOR), on the other hand, resulted in no reaction. In the presence of BP, silver atoms were formed with a rate constant of 4.2×10^{-7} M/s. The resulting octane colloids were evaluated for enhancements in thermal conductivity (TC) using the Thermal HotDisk method. Increases in k_{rel} of up to 10% were observed for the Ag and Pt systems at [M] = 5 mM which are far larger than what Maxwell's theory predicts for a colloid of such low volume fraction ($\sim5\times10^{-5}$ vol%).

Acknowledgments

I would like to graciously thank Professor German Mills for continued guidance throughout this program. Additional appreciation is given to the advisory committee which consists of Dr. Rik Blumenthal, Dr. Vince Cammarata, Dr. Wei Zhan, and the outside reader, Dr. Rob Jackson. This section would be far from complete without recognizing Professor Anne Gorden. Guilty of being overwhelmingly helpful and knowledgable, and having an office across the hall from mine, Dr. Gorden was instrumental in my success for her friendly guidance and help with the organic and organometallic aspects of my research. Gratitude is given to the U.S. Department of Energy for providing funding for this project under the EPSCoR/DOE implement Award Number DE-SC0002470. The author would also like to respectfully acknowledge Professor Jay Khodadadi of the Auburn University Mechanical Engineering Department for assembling and heading the research cluster that made this grant possible. The greatest thanks of all goes to my loving wife who is my inspiration.

Table of Contents

List of Tables

List of Figures

Chapter 1

Introduction

Introduction to Colloid Chemistry

The dispersion of tiny particles in a medium of interest to produce a material with unique properties, such as stained glass and ceramics in the early days, inspired a movement in science which has long been termed colloid chemistry. The simplest definition of a colloid is a two-phase system in which one component is very small, containing nm or μm dimensions, and is stably dispersed in the other phase, as shown in Figure 1.1.[1] Dispersed bubbles in a liquid to form a foam, liquid droplets in a gas to form an aerosol, and solid particles in a liquid to form a sol are examples of common types of colloids. Specific, practical examples correspondingly include the foam atop a beer, spray paint, and sun tan lotion. Although colloidal particles can range in size, *d*, from 1 nm to 10 μm and can be comprised of various materials, the current brief will only consider metal and metal oxide particles where d≤50 nm in the longest dimension. This reduction in size of a material to nm dimensions results in unique electronic properties as the density of states and the electron confinement lengths decrease with decreasing particle size. These unique properties have inspired the use of nanometer-sized crystallites in the fields of spectroscopy,[2-6] biology and medicine,[5,7,8] catalysis,[9] imaging,[10] fuel cell research,[11-13] water purification,[14] and the fabrication of materials with enhanced thermal properties.[15-19]

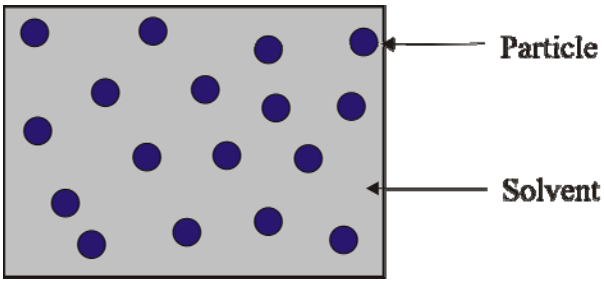

Figure 1.1. Schematic defining a typical colloid.

Fundamentals of Particle Growth and Stabilization

One key challenge facing colloid chemists is the preparation of stable suspensions; that is, particles that remain in solution without undesirable aggregation for a period sufficient to outlast the demand. This can be understood by considering the generic potential energy diagram shown in Figure 1.2. This example uses metal as a model but the same principle applies to particle growth in general. When dissolved metal ions are reduced the immediate result is a solution of highly energetic atoms that will rapidly form tiny clusters (2 - 10 Å dia), called nuclei, in order to achieve a lower energy.[20] These nuclei then combine to form small (<1 nm dia.) clusters.[21] Unless thwarted, this nucleation and growth process will continue until the clusters combine to form large aggregates that will precipitate from solution. Along this potential energy landscape in proceeding from highly energetic atoms to the bulk material, however, exist local minima corresponding to various particle sizes and geometries at which growth can be arrested. This is typically achieved by kinetically stabilizing the particles, which is the basis of forming nanoparticles.[22]

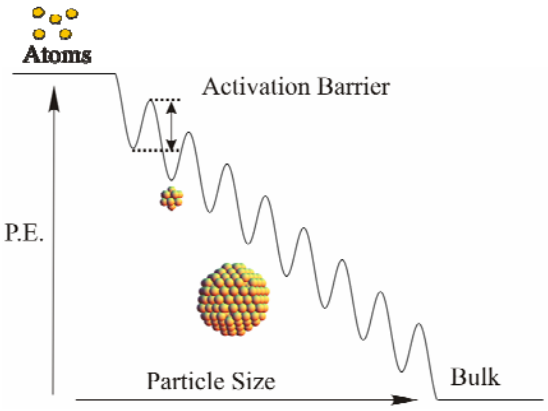

Figure 1.2. Generic potential energy diagram depicting particle nucleation and growth. Energetic atoms rapidly combine to form tiny nuclei which evolve into clusters then particles. Local minima about the P.E. landscape allow opportunities to arrest growth and produce stable particles.

Attraction between atoms and molecules occurs when permanent or induced dipoles align. In neutral, nonpolar atoms, electron motion causes rapidly oscillating dipoles which lead to London dispersion forces that result in van der Waals interactions. It is energetically favorable for dipole oscillations in neighboring atoms to occur in resonance. Nanoparticles thus become large assemblies of coherent oscillators which develop long-range attractions that exceed distances of attraction between two atoms.[1] In order to overcome these attractions, two general modes of kinetic stabilization can be harnessed, namely electrostatic and steric.[23] In an electrolyte solution, the distribution of ions about a particle surface occurs in two layers, a compact inner layer and a diffuse outer layer.[24] Electrostatic stabilization is a Coulombic effect resulting from repulsion of these electrical double layers which envelope the particles. One example of this mode of stabilization includes the gold colloids prepared by Turkevich in which $HAuCl_4$ was reduced and stabilized by sodium citrate[21] and can be rationalized by considering Figure 1.3. As two particles approach one another, the diffuse outer layers overlap and the interaction of like-charged particles comprising the dense, inner layers yield a repulsive force that may be sufficient to overcome the van der Waals attraction. But if the approaching particles

have sufficient kinetic energy, either due to excessive size or to the input of thermal energy, then dislocation of the surface layers may occur allowing particle contact and fusion.

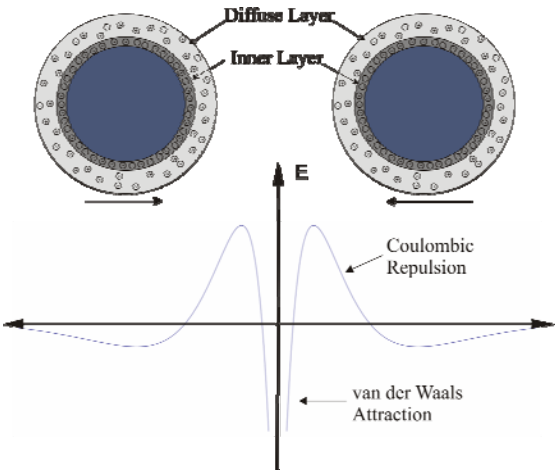

Figure 1.3. Model illustrating electrostatic repulsion of approaching particles. At very close intervals, van der Waals interactions produce an attractive force but repulsion of like-charged ions enveloping the particle may be sufficient to overcome this attraction preventing particle collision and subsequent agglomeration.

Steric stabilization, on the other hand, is achieved by the coordination of large, bulky ligands to the particle surface that provide a physical "cushion" between colliding particles as illustrated in Figure 1.4. This latter mode is supported by a plethora of possibilities and literature data. Polymers such as PVA,[25-28] PVP,[29] Polyurea (Ley),[30] Poly(acrylonitrile) and poly(acrylic acid),[31] and poly(ethylene glycol)[28,32] are commonly used to stabilize noble metal particles along with phosphines,[33] thiols[34] and amines.[35] Surfactants are widely used in stabilizing not only metal particles but metal oxides as well.[36-39]

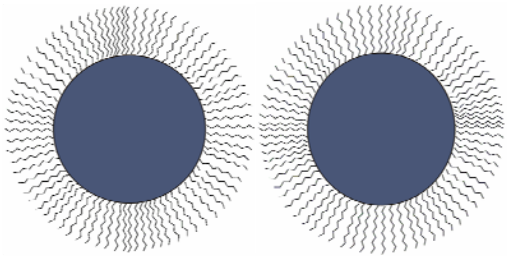

Figure 1.4. Illustration of steric stabilization. Large, bulky ligands adsorbed onto the particle surface provide a physical barrier which may prevent particle contact and subsequent agglomeration.

Particle Preparation

Modern literature contains many methods for the preparation of untold varieties of colloids but the earliest wet chemical technique was reported by Faraday[40] in 1857 who reduced gold chloride with phosphorus to produce colloids that are still stable today and remain on display at the Royal Institution in London.[41] The most basic premise for producing transition metal particles in aqueous solution involves a metal salt, reducing agent, stabilizer, and, typically, an energy input source. Salts commonly used include Ag^{+}, Au^{3+}, Pd^{2+}, Pt^{2+}, Cu^{2+}, Ni^{2+}, Rh^{3+}, and Ir^{3+} but may include the majority of the transition metals. Proper selection of reductant is integral to achieving desired particle morphology. In the case of silver, stronger reducing agents have shown to produce smaller nuclei allowing a narrow size distribution.[42] Diborane and sodium borohydride are popular reductants due to their remarkable reducing capability and have been employed in the preparation of various colloidal systems spanning the majority of the d-block elements.[43] Alcohols can be used as reducing agents in basic solution producing the corresponding aldehyde or ketone[25-27,29,44-46] while hydrogen has been employed in the preparation of Pd, Pt, Rh, and Ir colloids.[47-51] Of the multiple stabilizing agents previously listed, many can also act as the reductant, as is the case with sugars[52] and PVA.[29] While heat is

the most commonly used energy input source, reduction can also be driven by gamma irradiation,[53] light irradiation,[54] microwave irradiation,[55] and applied electrochemical potential.[56]

In general, hydrophilic stabilizers yield water soluble particles while lipophilic ligands provide particles capable of being dispersed in nonpolar media. The in-situ generation of metal or metal oxide crystallites in organic media possessing small dielectric constants (~15 or less) presents a formidable challenge due in large part to the incompatibility of the polar starting materials with the nonpolar solvent. This obstacle has previously been overcome by employing a two-phase system whereby aqueous metal salts are extracted into an organic layer with the aid of a phase transfer agent which may include phosphines or quaternary amines. Salt reduction ensues by the addition of a compatible reducing agent such as hydrazine.[57-67] Provided that salt dissolution can be achieved, reduction at times can be made possible in the organic phase by the input of thermal energy. Silver lactate, for example, was thermally decomposed in mineral oil in the presence of Kornatin SH as a reductant as well as a stabilizer to produce particles in large concentrations that were stable for weeks.[68] Further methods of thermally decomposing various organic-soluble salts of silver and gold lead to isolable particles which could be dispersed in an assortment of low-dielectric solvents, including hexane, heptane, chloroform, toluene, cyclohexane, MIBK, THF, and benzene.[35,69,70] Additional achievements in nonpolar media include the electrochemical generation of silver in DMSO[71] and the formation of silver-encapsulated reverse micelles that could be isolated then dispersed in hexane.[72]

Nanoparticles on the Global Energy Stage

Rising energy demands resulting from technological advancements and rapid population growth have inspired innovative thinking. The current global energy demand sums to ~13 tera

watts (TW) whereas by the year 2050 this number is predicted to rise to ~23 TW.[73] In order to address the concern of energy shortage while also considering the preservation of the environment, researchers have turned to renewable energy sources. Environmentally benign resources include hydroelectric, which may yield an additional 0.5 TW, the harvesting of geothermal energy integrated over the entire earth's surface (12 TW), globally extracted wind power (2-4 TW), and the sum the solar energy reaching the earth's surface (120,000 TW).[74] As the world encroaches a never-seen-before energy crisis, attention is turned, in society, in government, in industry, and in science, to these alternative sources and the development thereof. Creating and commissioning new energy resources, however, is a daunting task that may not be readily achievable in an appropriate time frame. With a steadily growing population and skyrocketing demands, it is necessary to also investigate means of increasing the efficiency with which energy is consumed. The concepts of phase change materials (PCMs) and nanofluids may offer a significant reduction in residential and commercial energy consumption by greatly enhancing the efficiency with which thermal energy is used and stored.

Phase Change Materials

Amongst the alternative energy sources previously mentioned, solar energy is a promising resource and harnessing the sun's energy is achievable; however, further challenges ensue. While the sun radiates bountifully during daylight hours, darkness brings a period devoid of solar energy which demands novel storage technologies. A current effort to address the challenge of thermal energy storage involves the use of a phase change material. PCMs offer an efficient mode of storage by making use of a material's enthalpy of fusion, which is the latent heat associated with a phase transition. An ideal PCM could store energy received from the sun

during the day for later use in a variety of applications such as heating of water, space heating, or the generation of electricity.[75]

In order for a PCM to be useful, the material must first meet several criteria. An ideal PCM will have a melting point capable of being adjusted to the needs of a given application, a large latent heat, and high thermal conductivity (TC).[76] Furthermore, it would be beneficial if the material experiences a small volume change during phase transition and be chemically inert. The set point of storage can be tailored in hydrocarbon-based PCMs by simply lengthening or shortening the chain. Eicosane, for example, experiences a phase change between 35 and 36 °C and also offers the benefit of negligible volume change during freezing and melting.[77] Although a promising candidate, hydrocarbons posses a low thermal conductivity. One manner by which researchers hope to enhance the latent heat and the rate at which the phase change occurs is through the suspension of small metal or metal oxide particles.[17,77] Metallic copper particles, for example, were dispersed in paraffin and while heating and cooling of the resulting liquid became faster, the latent heat decreased with increasing particle concentration.[78]

Nanofluids

Heat generating processes and machines including materials production, electronic devices, combustion engines, fuel cells, batteries, and power plants require a means by which excess heat can be removed. Traditional cooling processes involve exposing the system to a medium which is capable of extracting heat and transferring it to the surroundings. Such a medium may include forced air, water, ethylene glycol, or other cooling liquid; however, many of these compounds have a low thermal conductivity relative to the materials composing the

system, such as metals, silicon, and ceramics.[18,19] These demands create a need for improved cooling technologies.

In 1873 Maxwell proposed dispersing metallic particles in a given solvent to produce a heat transfer medium with enhanced thermal properties.[79] This notion was founded on the knowledge that metals tend to have much higher thermal conductivity (TC) than common liquids. Copper, for example, has a conductivity about 700 times larger than that of water and about 3000 times greater than engine oil.[80] Novel heat transfer liquids were initially attempted by dispersing micro- to millimeter sized particles but attempts were met with little success due to immediate sedimentation of the particles. In the past decade, however, researchers have turned to traditional colloid chemistry for inspiration. After suspending nanometer-sized copper(II) oxide in water and measuring the resulting enhancement of TC of the mixture, the term "nanofluid" was coined and has since become widely accepted.[15] In practice, a nanofluid is a colloid whose design is specific to the study and application of heat transfer technology.

While nanofluids themselves are not a renewable energy source, they may offer the ability to use current energy sources with greater efficiency. The automotive industry has invested interest in these technologies in the hope of improving combustion engine, electric motor, and battery cooling capacities as well as reducing the size of cooling devices such as radiators and heater cores.[81,82] Recently, a 4% enhancement in engine cooling capacity was reported with the use of a 2 vol% Cu/water/ethylene glycol nanofluid.[83] This limited improvement, however, was attributed to a need for conventional radiator systems to be adapted to facilitate these modified fluids. Society’s appetite for advanced electronic devices has inspired enhanced performance with more compact sizes which result in greater heat generation per unit volume. By forcing an aqueous alumina suspension over a micro-electronic cooling

block, a 40% increase in cooling efficiency was achieved with respect to deionised water; however, the deposition of particle aggregates in microchannel heat sinks lead to equipment failure.[81] Industrial chillers are a large consumer of energy in commercial production and the high laminar flow rates reduce the threat of particle precipitation; CuO nanofluids achieved a 40% improvement in heat exchange.[84] From Maxwell's early vision to these recent developments, nanofluids have emerged as a viable tool for improved energy consumption.

With many milestones ahead, efforts were launched to find the ideal combinations of particle and solvent which would maximize heat transport.[85-93] Several studies have considered the dispersion of Cu, Fe, Au, and Ag in water[90] and ethylene glycol;[94] Al_2O_3, CuO, SiC, and TiO_2 in water;[88,92,95] and multiwalled carbon nanotubes (MWNT) in oil,[96] decene/ethylene glycol/water,[97] and water.[98] Copper(II) oxide remains on the forefront due to its ease of production, dispersity in various media, and stability toward oxidation.[86,87,89,99-102] Commercial Al powders from Shenzhen Junye Nano Material Ltd., China were dispersed in paraffin (T_m = 58-60 °C) and an increase in TC was observed.[78] Alumina was also dispersed in paraffin and a 10% increase TC was reported[16] while a 30% increase was reported for Al particles dispersed in water.[103] Oil-based nanofluids have recently appeared in greater number.[104-106] Silver particles supported on silica dispersed in transformer oil produced a TC increase of 15% but the particles only remained stable for one hour.[107] Isolable, oleic acid-coated Ag particles were redispersed in hexane and chloroform to produce a 17% TC enhancement. While stable for two months at room temperature, these particles precipitated rapidly at elevated temperatures.[108] Metallic Cu was deposited on MWCNTs and dispersed in water and ethylene glycol to yield a 35% increase in TC. These composite particles remained in solution for up to 20 days but showed early evidence of oxidation.[109] Copper(II) oxide deposited on graphene showed a 90% TC

enhancement in a water/ethylene glycol mixture compared to the unmodified solvent.[110] While various colloidal systems have shown potential for application as nanofluids, particle instability remains a challenging issue.

The migration of heat through a nanofluid is a time-dependent process that remains under intense investigation predominantly by thermal engineers but with much debate. Four principle modes of heat transfer have been identified:[111] (i) collisions between solvent molecules (solvent TC), (ii) conduction within the suspended particles, (iii) Brownian motion of particles resulting in interparticle collisions, and (iv) collisions or other thermal interactions between solvent molecules and particles. The conduction of heat via collisions between solvent molecules is well understood in pure liquids and enhancements in modified solutions are typically reported as a comparison of heat transport properties of the nanofluid with the starting solvent. TC in solids is known to be higher than in liquids which validates the theory that conduction within the particles may contribute to enhanced heat flow. Phonons migrate through solid particles in random directions when the particles are large and polycrystalline, or amorphous. On the other hand, when particle size is smaller than the mean free path of the phonons, which is on the order of 40 nm at room temperature for alumina,[112] ballistic conduction occurs in which phonons "jump" directly from the lower surface of the particle to the upper.[113] Brownian motion is considered by many to be the dominant mode of enhancement[113-115] while others claim that particle collision is a very slow process relative to solvent molecule collisions and therefore Brownian motion cannot contribute to the enhancement.[115-118] Particle aggregation is thought to enhance TC by reducing thermal resistance[113,119] but a strong opposition to this theory exists providing evidence that only well dispersed, stable colloids produce a clear increase in TC.[85,120] Nanolayering is an additional model that has recently been introduced in which liquid layers about the particle

surface are more highly ordered than the bulk solvent and are expected to act as a thermal interface between the particle and bulk solvent.[101,121-125] Although nanolayering models were successful in describing TC enhancements, it was demonstrated that an incorrect derivation in the layering model[123] produced the agreement with experimental results[124].

Amidst the recent surge in nanofluid literature, there exist certain obstacles that hinder the evolution of this field: Lack of agreement in experimental data and theoretical models, inadequate colloid characterization, and particle instability. Science, technology, and engineering are changing. Gone are the days when scientists and engineers work exclusively within their respective communities. In order for nanofluid research to achieve its potential, scientists and engineers will need to form an interdisciplinary union involving symbiotic collaboration. Scientists must develop well characterized, stable colloids for subjects of investigation while engineers must work to understand the mechanisms leading to TC enhancement and develop useful models. The authors of several recent reviews have reached out to the nanofluid community challenging researchers to address the obstacle of particle instability.[84,120,126] The current work is an attempt to embrace that challenge by developing novel colloids, and corresponding synthetic regimes, including rigorous characterization and emphasis on robust particle stability. A phase change material will also be briefly considered by dispersing metal oxide particles in paraffin and analyzing the resulting thermal properties.

References

(1) Vincent, B. Introduction to Colloidal Dispersions. In *Colloid Science: Principles, methods, and applications*; Cosgrove, T., Ed.; Blackwell Publishing: Ames, 2005; pp 1-13.

(2) Jin, R. *Angewandte Chemie, International Edition in English* **2010**, *49*, 2826-2829.

(3) Kerker, M. *Applied Optics* **1991**, *30*, 4699-4705.

(4) Lombardi, J. R.; Birke, R. L. *Accounts of Chemical Research* **2009**, *42*, 734-742.

(5) Schlücker, S. *ChemPhysChem* **2009**, *10*, 1344-1354.

(6) Stiles, P. L.; Dieringer, J. A.; Shah, N. C.; Van Duyne, R. P. *Annual Review of Analytical Chemistry* **2008**, *1*, 601-626.

(7) Boisselier, R.; Astruc, D. *Chemical Society Reviews* **2009**, *38*, 1759-1782.

(8) Ghosh, P.; Han, G.; De, M.; Kim, C. K.; Rotello, V. M. *Advanced Drug Delivery Reviews* **2008**, *60*.

(9) *Nanoparticles and Catalysis*; Astruc, D., Ed.; Wiley: Weinheim, 2008.

(10) Grouchko, M.; Magdassi, S. *Journal of Materials Chemistry* **2009**, *19*, 3057-3062.

(11) Schmidt, T.; Noeske, M.; Gasteiger, H. A.; Behm, R. J.; Britz, P.; Brijoux, W.; Bönnemann, H. *Langmuir* **1997**, *13*, 2591-2595.

(12) Götz, M.; Wendt, H. *Electrochimica Acta* **1998**, *43*, 3637-3644.

(13) Schmidt, T. J.; Noeske, M.; Gasteiger, H. A.; Behm, R. J.; Britz, P.; Bönnemann, H. *Journal of the Electrochemical Society* **1998**, *145*, 925-931.

(14) Anshup, T. P. *Thin Solid Films* **2009**, *517*, 6441-6478.

(15) Choi, U. S. Enhancing Thermal Conductivity of Fluids with Nanoparticles. In *Developments and Applications in Non-Newtonian Flows*; Siginer, D. A., Wang, H. P., Eds.; ASME: New York, 1995; Vol. 66; pp 99-105.

(16) Ho, C. J.; Gao, J. Y. *Int. Commun. Heat Mass Transfer* **2009**, *36*, 467-470.

(17) Khodadai, J. M. Nanoparticle-Enhanced Phase Change Materials (NEPCM) with Great Potential for Improved Thermal Energy Storgae. U.S. Patent Application 20090236079, September 24, 2009., 2009.

(18) Das, S. K.; Choi, U. S.; Patel, H. E. *Heat Transfer Engineering* **2006**, *27*, 3-19.

(19) Wongwises, S.; Daungthongsuk, W. *Renewable Sustainable Energy Rev.* **2007**, *11*, 797-817.

(20) Leisner, T.; Rosched, C.; Wolf, S.; Granzer, F.; Wöste, L. *Surface Review and Letters* **1996**, *3*, 1105-1108.

(21) Turkevich, J.; Stevenson, P. C.; Hillier, J. *Disc. Faraday Soc.* **1951**, *11*, 55-75.

(22) Bönnemann, H.; Richards, R. M. *European Journal of Inorganic Chemistry* **2001**, 2455-2480.

(23) *Clusters and Colloids*; Schmid, G., Ed.; VCH: Weinheim, 1994, pp 469-473.

(24) Aiken III, J. D.; Finke, R. G. *Journal of Molecular Catalysis A: Chemical* **1999**, *145*, 1-44.

(25) Hirai, H.; Nakao, Y.; Toshima, N.; Adachi, K. *Chemistry Letters* **1976**, 905-910.

(26) Hirai, H.; Nakao, Y.; Toshima, N. *J. Macromol. Sci. Chem.* **1978**, *A 12*, 1117-1141.

(27) Hirai, H.; Nakao, Y.; Toshima, N. *J. Macromol. Sci. Chem.* **1979**, *A 13*, 727-750.

(28) Longenberger, L.; Mills, G. *J. Phys. Chem.* **1995**, *99*, 475-478.

(29) Hirai, H.; Nakao, Y.; Toshima, N. *Chemistry Letters* **1978**, 545-548.

(30) Ley, S. V.; Mitchel, C.; Pears, D.; Ramarao, C.; Yu, J. Q.; Zhou, W. Z. *Organic Letters* **2003**, *5*, 4665-4668.

(31) Demir, M. M.; Gulgun, M. A.; Menceloglu, Y. Z.; Erman, B.; Abramchuk, S. S.; Makhaeva, E. E.; Khokhlov, A. R.; Matveeva, V. G.; Sullman, M. G. *Macromlecules* **2004**, *37*, 1787-1792.

(32) Pillai, U. R.; Sahle-Demessie, E. *J. Mol. Catal.* **2004**, *222*, 153-158.

(33) Schmid, G. *Polyhedron* **1998**, *7*, 2321-2329.

(34) Sardar, R.; Funston, A. M.; Mulvaney, P.; Murray, R. W. *Langmuir* **2009**, *25*, 13840-13851.

(35) Hiramatsu, H.; Osterloh, F. E. *Chemistry of Materials* **2004**, *16*, 2509-2511.

(36) Bönnemann, H.; Braun, G.; Brijoux, W.; Brinkmann, R.; Tilling, A. S.; Seevogel, K. *Inorganica Chimica Acta* **1998**, *270*, 95-110.

(37) Gosh, S.; Gomathi, A.; Rao, C. N. R. *Journal of Nanoscience and Nanotechnology* **2009**, *9*, 5214-5222.

(38) Qiang, A. H.; Zhao, L. M.; Xu, C. J.; Zhou, M. *Journal of Dispersion Science and Technology* **2007**, *28*.

(39) Li, C. C.; Chang, M. H. *Materials Letters* **2004**, *58*, 3903-3907.

(40) Faraday, M. *Philos. Trans.* **1857**, *147*, 145-181.

(41) Tweney, R. D. *Perspectives on Science* **2006**, *14*, 97-121.

(42) Leisner, T.; Rosche, C.; Wolf, S.; Granser, F.; Wöste, L. *Surface Review and Letters* **1996**, *3*, 1105-1108.

(43) Sonti, S. V.; Bose, A. *Journal of Colloid and Interface Science* **1995**, *170*, 575-585.

(44) Toshima, N.; Yonezawa, T. *New Journal of Chemistry* **1998**, 1179-1201.

(45) Toshima, N.; Hirakawa, K. *Polymer Journal (Tokyo, Japan)* **1999**, *31*, 1127-1132.

(46) Lu, P.; Teranishi, T.; Asakura, K.; Miyake, M.; Toshima, N. *Journal of Physical Chemistry B* **1999**, *103*, 9673-9682.

(47) Rampino, L. D.; Nord, F. F. *J. Am. Chem. Soc.* **1941**, *63*, 2745-2749.

(48) Rampino, L. D.; Nord, F. F. *J. Am. Chem. Soc.* **1941**, *63*, 3268.

(49) Rampino, L. D.; Nord, F. F. *J. Am. Chem. Soc.* **1943**, *65*, 2121-2125.

(50) Hernandez, L.; Nord, F. F. *J. Colloid Sci.* **1948**, *3*, 363-375.

(51) Dunsworth, W. P.; Nord, F. F. *J. Am. Chem. Soc.* **1950**, *72*, 4197-4198.

(52) Panigrahi, S.; Subrata, K.; Kumar, S.; Sudip, N.; Snigdhamayee, P.; Soumen, B.; Pal, T. *Polyhedron* **2006**, *25*, 1263-1269.

(53) Wang, Z.; Zu, X.; Jingbo, L. *Nanoparticles* **2010**, 323-338.

(54) Sakamoto, M.; Fujistuka, M.; Majima, T. *Journal of Photochemistry and Photobiology, C: Photochemistry Reviews* **2009**, *10*, 33-56.

(55) Nadagouda, M. N.; Speth, T. F.; Varma, R. S. *Accounts of Chemical Research* **2011**, *44*, 469-478.

(56) Coutanceau, C.; Brimaud, S.; Lamy, C.; Leger, J. M.; Dubau, L.; Rousseau, S.; Vigier, F. *Electrochimica Acta* **2008**, *53*, 6865-6880.

(57) Brust, M.; Walker, J. M.; Bethell, D.; Schiffrin, D. J.; Whyman, R. *Journal of the Chemical Society, Chemical Communications* **1994**, 801-802.

(58) Esumi, K.; Shiratori, M.; Ishizuka, H.; Tano, T.; Torigoe, K.; Meguro, K. *Langmuir* **1991**, *7*, 457-459.

(59) Manna, A.; Imae, T.; Iida, M.; Hisamatsu, N. *Langmuir* **2001**, *17*, 6000-6004.

(60) Nath, S.; Praharaj, S.; Panigrahi, S.; Ghosch, S. K.; Kundu, S.; Basu, S.; Pal, T. *Langmuir* **2005**, *21*, 10405-10408.

(61) Song, X.; Sun, S.; Zhang, W.; Yin, Z. *Journal of Colloid and Interface Science* **2004**, *273*.

(62) Xun, F.; Wei, Y.; Yusheng, L.; Debao, W.; Huaqiang, S.; Fengyuan, Y. *Journal of Dispersion Science and Technology* **2005**, *26*, 575-580.

(63) Lala, N.; Lalbegi, S. P.; Adyanthaya, S. D.; Sastry, M. *Langmuir* **2001**, *17*, 3766-3768.

(64) Zeiri, L.; Efrima, S. *J. Phys. Chem.* **1992**, *96, 5908-5917*.

(65) Vorobyova, S. A.; Lesnikovich, A. I.; Sobal, N. S. *Colloids Surf. A* **1999**, *152*, 375-379.

(66) Kang, S. Y.; Kim, K. *Langmuir* **1998**, *14*.

(67) Yang, J.; Lee, J. Y.; Chen, L. X.; Too, H. P. *Journal of Physical Chemistry B* **2005**, *109*, 5468-5472.

(68) Bönneman, H.; Bladergroen, B.; Linkov, V. M. *Applied Organometallic Chemistry* **2005**, *19*, 768-773.

(69) Yamamoto, M.; Kashiwagi, Y.; Nakamoto, M. *Langmuir* **2006**, *22*, 8581-8586.

(70) Rao, C. R. K.; Trivedi, D. C. *Materials Chemistry and Physics* **2006**, *99*, 354-360.

(71) Wadkar, M. M.; Chaudhari, V. R.; Haram, S. K. *Journal of Physical Chemistry B* **2006**, *110*.

(72) Taleb, A.; Petit, C.; Pileni, M. P. *Chemistry of Materials* **1997**, *9*, 950-959.

(73) Wiesz, P. B. *Phys. Today* **2004**, *57*, 47-52.

(74) Kamat, P. V. *J. Phys. Chem. C* **2007**, *111*, 2834-2860.

(75) Shukla, A.; Buddhi, D.; Sawhney, R. L. *Renewable Sustainable Energy Rev.* **2009**, *13*, 2119-2125.

(76) Fan, L.; Khodadadi, J. M. *Renewable Sustainable Energy Rev.* **2011**, *15*, 24-46.

(77) Sharma, A.; Tyagi, V. V.; Chen, C. R.; Buddhi, D. *Renewable Sustainable Energy Rev.* **2009**, *13*, 318-345.

(78) Wu, S.; Zhu, D.; Zhang, X.; Huang, J. *Energy & Fuels* **2010**, *24*, 1894-1898.

(79) Maxwell, J. C. *Treatise on Electricity and Magnetism*; Clarendon Press: Oxford, 1873.

(80) Bejan, A.; Kraus, A. D. *Heat Transfer Handbook*; John Wiley and Sons Inc.: Hoboken, 2003.

(81) Wang, X. Q.; Mujumdar, A. S. *J. Chem. Eng.* **2008**, *25*, 631-648.

(82) Sarit, K. D. *Heat Transfer Engineering* **2006**, *27*, 1-2.

(83) Leong, K. Y.; Saidur, R.; Kazi, S. N.; Mamun, A. H. *Appl. Therm. Eng.* **2010**, *30*, 2685-2692.

(84) Saidur, R.; Leong, K. Y.; Mohammed, H. A. *Renewable Sustainable Energy Rev.* **2011**, *15*, 1646-1668.

(85) Lee, D.; Kim, J.-W.; Kim, B. G. *J. Phys. Chem. B* **2006**, *110*, 4323-4328.

(86) Lee, S.; Choi, S.; Eastman, J. A. *J. Heat. Transfer* **1999**, *121*.

(87) Das, S. K.; Putra, N.; Theisen, P.; Roetzel, W. *J. Heat Transfer* **2003**, *125*, 567-574.

(88) Murshed, S. M. S.; Leong, K. C.; Yang, C. *Int. J. Therm. Sci.* **2005**, *44*, 367-373.

(89) Eastman, J. A.; Choi, S. U. S.; Li, S.; Yu, W.; Thompson, L. J. *Appl. Phys. Lett.* **2001**, *78*, 718-720.

(90) Xuan, Y.; Li, Q. *Int. J. Heat Fluid Flow* **2000**, *21*, 58-64.

(91) Patel, H. E.; Das, S. K.; Sundararajan, T.; Nair, A. S.; George, B.; Pradeep, T. *Appl. Phys. Lett.* **2003**, *83*, 2931-2934.

(92) Xie, H.; Wang, J.; Xi, T.; Liu, Y. *Int. J. Thermophys.* **2002**, *23*, 571-580.

(93) Xie, H.; Lee, H.; Youn, W.; Choi, M. *Appl. Phys. Lett.* **2003**, *94*.

(94) Hong, T. K.; Yang, H. S.; Choi, C. J. *J. Appl. Phys.* **2005**, *97*, 0643111-0643114.

(95) Xie, H.; Wang, J.; Xi, T.; Liu, Y.; Ai, F.; Wu, Q. *J. Appl. Phys.* **2002**, *91*, 4568-4572.

(96) Choi, S. U. S.; Zhang, Z. G.; Yu, W.; Lockwood, F. E.; Grulke, E. A. *Appl. Phys. Lett.* **2001**, *79*, 2252-2254.

(97) Xie, H.; Lee, H.; You, W.; Choi, M. *J Appl. Phys.* **2003**, *94*, 4967-4971.

(98) Assael, M. J.; Chen, C. F.; Metaxa, I.; Wakeham, W. A. *Int. J. Thermophys.* **2004**, *25*, 971-985.

(99) Jang, S. P.; Choi, S. U. S. *Appl. Phys. Lett.* **2004**, *84*, 4316-4318.

(100) Kumar, D. H.; Patel, H. E.; Kumar, V. R. R.; Sundararajan, T.; Pradeep, T.; Das, S. K. *Phys. Rev. Lett.* **2004**, *93*, 144301.

(101) Xue, Q.; Xu, W. M. *Mater. Chem. Phys.* **2005**, *90*, 298-301.

(102) Yu, W.; Choi, S. U. S. *J. Nanoparticle Res.* **2003**, *5*, 167-171.

(103) Wang, X. J.; Li, X. F.; Yang, S. *Energy & Fuels* **2009**, *23*.

(104) Choi, C.; Yoo, H. S.; Oh, J. M. *Curr. Appl. Phys.* **2008**, *8*, 710-712.

(105) Xuan, Y.; Li, Q. *J. Heat Fluid Flow* **2000**, *21*, 158-164.

(106) Chen, L.; Xie, H. *Colloids and Surfaces* **2009**, *352*, 136-140.

(107) Both, S. S.; Ndungu, P.; Bladergroen, B. J. *Ind. Eng. Chem. Res.* **2011**, *50*, 3071-3077.

(108) Li, D.; Hong, B.; Fang, W.; Guo, Y.; Lin, R. *Industrial & Engineering Chemistry Research* **2010**, *49*, 1697-1702.

(109) Jha, N.; Ramaprabhu, S. *J. Phys. Chem. C* **2008**, *112*, 9315-9319.

(110) Baby, T. T.; Sundara, R. *J. Phys. Chem. C* **2011**, *115*, 8527-8533.

(111) Jang, S. P.; Choi, S. U. S. *Applied Physics Letters* **2004**, *84*, 4316-4318.

(112) Carslaw, H. S.; Jaeger, J. C. *Conduction of Heat in Solids*; Oxford University Press: New York, 1967.

(113) Azizian, R.; Dorodchi, E.; Moghtaderi, B. *Ind. Eng. Chem. Res.* **2011**, Articles ASAP, 9/1/2011.

(114) Keblinski, P.; Phillpot, S. R.; Choi, S. U. S.; Eastman, J. A. *International Journal of Heat and Mass Transfer* **2002**, *45*, 855-863.

(115) Koo, J.; Kleinstreuer, C. *Int. Commun. Heat Mass Transfer* **2005**, *32*, 1111-1118.

(116) Jang, S. P.; Choi, S. U. S. *J. Heat Transfer* **2007**, *129*, 618-625.

(117) Koo, J.; Kleinstreuer, C. A. *J. Nanoparticle Res.* **2004**, *6*, 577-588.

(118) Shukla, R. K.; Dhir, V. K. *J. Heat Transfer* **2008**, *130*, 042406-042419.

(119) Gao, J. W.; Zheng, R. T.; Ohtani, H.; Zhu, D. S.; Chen, G. *Nano Letters* **2009**, *9*, 4128-4132.

(120) Wong, K. V.; Castillo, M. J. *Advances in Mechanical Engineering* **2010**, *2010*, 1-9.

(121) Xue, Q. *Phys. Lett. A* **2003**, *307*, 313-317.

(122) Yu, W.; Choi, S. U. S. *J. Nanoparticle Res.* **2004**, *6*, 355-361.

(123) Leong, K. C.; Yang, C.; Murshed, S. M. S. *J. Nanoparticle Res.* **2006**, *8*.

(124) Doroodchi, E.; Evans, T. M.; Moghtaderi, B. *J. Nanoparticle Res.* **2009**, *11*, 1501-1507.

(125) Lee, D. *Langmuir* **2007**, *23*, 6011-6018.

(126) Godson, L.; Raja, B.; Mohan Lal, D.; Wongwises, S. *Renewable Sustainable Energy Rev.* **2010**, *14*, 629-641.

Chapter 2

Preparation of Aqueous Noble Metal Colloids

Introduction

The application of metal colloids in the fields of catalysis,[1] SERS,[2] biology,[3] and medicine[4] has inspired innovative methods for the generation of stable particle suspensions composed of materials which are appropriate for the desired application. Metal particles have successfully been stabilized using bulky organic molecules such as surfactants,[5] polymers,[6] sugars,[7] biomolecules,[8] dendrimers,[9] calixarenes,[10] and sarcosines.[11,12] Over the past two decades, cyclodextrins (CDs) have also been introduced as bio-friendly, environmentally "green" stabilizers of noble metal particles.[13]

CDs are macrocyclic oligosaccharides composed of α-(1-4) linked glucopyranose units which assume the shape of a cone as illustrated in Figure 2.1.[14] Naturally occurring CDs include the α-, β-, and γ- forms which consist of 6, 7, and 8 glucose monomers, respectively, where β-CD is the most common. The outer diameter spans 15.4 Å, while the inner cavity ranges from 6.0-6.5 Å with a volume of 262 Å^3,[15] and a polarity similar to that of ethanol.[16] The great significance of CDs are their ability to form inclusion complexes with a wide variety of polar, nonpolar, charged, or radical molecules; in fact, CDs have been described as "all purpose molecular containers".[17] The driving force of complex formation has been attributed to several factors including van der Waals forces, hydrophobic interactions, electronic effects, and steric effects[18] but the key factor is likely the enthalpically favorable release of water molecules from the cavity which are displaced by the guest to achieve a lower energy state.[19] In all cases, however, the guest is bound at least partially within the cavity.[20] Once included, the guest

molecule experiences changes in physiochemical properties such as solubility enhancement, stability toward degradation, control of volatility and sublimation, spatial isolation from incompatible compounds, and controlled release rates in the case of drugs and flavors.[15] The rich chemistry of CDs has enabled its use in the food industry,[21] pharmaceuticals,[22] cosmetics,[23] environmental protection and cleaning,[24] bioconservation,[25] and in the textile industry.[26]

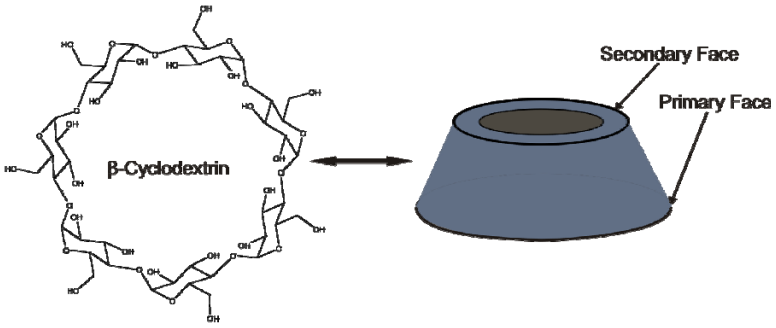

Figure 2. 1 Molecular structure of β-CD (left) which exists in the shape of a cone (right). The narrow opening terminates with secondary hydroxyl groups and the wide opening if faced with primary alcohols.

Since their introduction as a particle stabilizer,[27] CDs have become common in the colloid literature. Selective modification of the primary hydroxyl groups about the outer CD edge allows for the generation of functionalized derivatives. Stable colloids of gold,[28,29] palladium,[29-32] and platinum[32] have been achieved using *per*-6-thiolated *β*-CD after initial reduction of metal salts (precursors of metal particles) by $NaBH_4$. Additional modifications at the primary face of *β*-CD include the grafting of acrylic acid to stabilize Ag colloids[33] and adamantyl-derivatized poly(propylene imine) to disperse gold particles.[34] Modification of the secondary hydroxyl at the C2 position of *α*-CD resulted in hydroxypropyl-*α*−CD which was used as both a reducing agent and stabilizer in the generation of Pd particles.[35] Following metal ion reduction by $NaBH_4$, unmodified *α*-CD has been employed to stabilize silver particles[36]

while the β form has been similarly used in the stabilization of silver,[36-39] gold,[40] and palladium[39,41] colloids. Basic solutions of β-CD and Ag^{+} and Au^{3+} result in metallic particles without the aid of an additional reducing agent.[42] An early investigation also reports the reduction of Pd^{2+} in basic solutions of β-CD at 70 °C over the course of minutes but these results were not reproducible with modern starting materials.[43] This phenomenon is likely due to the presence of reductive impurities complexed in the host cavity.[44] Stable suspensions were also produced by laser ablation of gold metal in the presence of unmodified β-CD[45] or through the thermal decomposition of 1,5-(cyclooctadiene) dimethylplatinum(II) in supercritical CO_2.[46] Host-guest complexes of β-CD with phenylsilane have also been prepared for the synthesis of silver particles.[47] Similarly, gold salts have been reduced with $NaBH_4$ followed subsequent stabilization by inclusion complexes of α-CD with alkane thiols[48] or β-CD with 4-amino thiophenol,[49] the block copolymer Pluronic F127,[50] and thio[2-(benzoylamino)ethylamine.[51]

The ongoing quest for highly stable colloids which possess enhanced heat transfer properties has lead nanofluid research to the use of noble metal particles due to their well-known resistance toward oxidation and the large thermal conductivity (TC) of the corresponding bulk metals. Stable suspensions of gold particles ranging from 2-45 nm were prepared by the citrate method and were evaluated by the thermal hotwire (THW) and parallel plate (GAP) methods for enhancements in (TC). The maximum amount of increase, however, was 1.4% for 40 nm particles at 0.11 % vol while in other formulations of sizes and concentrations actually resulted in a decrease in TC.[52] Gold particles in the ionic liquid 1-methylimidazole, on the other hand, achieved a 13% increase in TC (THW) for a 10^{-3} %vol but the majority of the samples investigated suffered rapid particle precipitation.[53] Bimetallic Au/Pd particles stabilized by PVP were reported to produce an increase in thermal diffusivity but no corresponding values for TC

were provided.[54] Ethylene glycol suspensions of silver particles achieved an initial enhancement in TC of 15% but particle agglomeration reduced this value after 30 days.[55] Prefabricated Ag particles (Sigma-Aldrich) dispersed in deionised water without the aid of a stabilizer achieved an increase in TC of 80% but no information was provided regarding colloidal stability.[56] Similarly, ethanolic solutions of PVP-stabilized silver achieved an increase in TC of 60% but, again, no report of stability was provided.[57] The current work reports a synthesis for the preparation of a β-cyclodextrin—glucose (CD-Glu) complex which is used as a salt reductant and particle stabilizer in the generation of Ag, Au, Pd, and Pt colloids. Whereas Ag^{+} and Au^{3+} are readily reduced in basic solutions of unmodified CD,[42] the Pd^{2+} and Pt^{2+} salts require the aid of the included glucopyranose. The prepared colloids are then be evaluated for enhancement in TC while monitoring particle stability.

Experimental

Caution: Piranha etch is a hazardous material that should only be handled by trained personnel using appropriate personal protective measures. Waste from this material should only be disposed of by approved procedures.[58] Uniformly labeled (UL-) ^{13}C Glu was purchased from Omicronbio while all other reagents were purchased from Aldrich and used as-received. Absorbance spectra were obtained on a Shimadzu UV-2450 spectrophotometer, XRD patterns on a Bruker D8, ^{13}C NMR spectra on a Bruker Avance 400 nuclear magnetic resonance spectrometer, and thermal conductivity measurements were conducted with a Hot Disk Transient Plane Source TC detector.[59] Electron micrographs were obtained on a Zeiss EM10 transmission electron microscope at 60 keV. Specimens were prepared by evaporating one drop of colloid, previously diluted to 0.1 mM when necessary, onto a Cu/formvar 300 mesh grid while particle

size analysis involved counting a minimum of 200 particles per sample.[60] Deionised water was supplied by a Barnstead EasyPure II ultrafiltration system and all glassware was cleaned with fresh piranha etch prior to use.

The procedure for preparing CD-Glu complexes was adapted from literature techniques.[61] Into 20 mL of deionised water, 2.4 g of glucose (Glu) and 1.0 g of β-CD (15:1 mole ratio) were added with stirring at 90 °C for 2 h before being slowly cooled to room temperature. Selective precipitation was achieved by adding 8 mL of acetonitrile to the mixture followed by submersion in a thermostatic bath at -5 °C. After 15 minutes, the solution was sufficiently turbid to be filtered through a 0.2 μm Gelman filter. Under similar conditions in the absence of Glu, β-CD rapidly precipitates at 15 °C but in the current procedure, no turbidity was present at this temperature after extended periods of time. Excess Glu was removed by rinsing several times with 5 mL aliquots of 0 °C ethanol (95 %). The product was then dried in a vacuum oven at 60 °C prior to storage. The process was repeated under similar conditions using UL-^{13}C Glu for evaluation of the complex via carbon NMR.

Colloids of Ag, Au, Pd, and Pt were prepared in the concentration range of 0.1 to 5.0 mM while [CD-Glu] and [NaOH] were fixed at 5 and 15 mM, respectively. Aqueous solutions of $AgClO_4$, $NaAuCl_4$, K_2PdCl_4, or K_2PtCl_4 were combined with CD-Glu and NaOH, which was added last, to achieve a final volume of 25 mL in a 50 mL boiling flask. The mixtures were then refluxed at 100 °C until color change was complete, which typically occurred within 5 minutes for Ag and Au or 30 min for Pd and Pt.

Results and Discussion

Figures 2.2A-2.2C display ^{13}C NMR spectra, obtained in D_2O, corresponding to β-CD, UL-^{13}C Glu, and the CD-^{13}C Glu complex, respectively. As expected, the peaks corresponding to CD are all singlets whereas those for the labeled Glu are multiplets enabling easy distinction between the two species. The appearance in Figure 2.2C of both singlets and multiplets is clear evidence that Glu is present in the complex. When equal quantities of β-CD(aq) and Glu(aq) were combined at 25 °C and the equilibrium presented in equation 1 was achieved, the free sugar concentration was measured with a glucose meter. Assuming a host-guest ratio of 1:1, an equilibrium constant of 420 ±120 was reported.[62] In the present study, a 1.279 g/L solution of CD-Glu, corresponding to a concentration range of 0.973 to 1.13 mM depending on the fraction of host molecules possessing an included guest (0-100%), was enzymatically analyzed at 37 °C for free glucose.[63] A Glu concentration of 330 μM was observed which, under the assumption that the glucose oxidase/peroxidase does not react with complexed Glu, corresponds to an equilibrium constant of $5\text{-}7\times10^4$. This value is an order of magnitude larger than that which was previously reported[62] which suggests that either the two techniques do not agree well or that different types of complexes are possible and may be made accessible at higher temperatures. Attempts to quantify the guest via NMR were unsuccessful.

$$CD + Glu \rightleftharpoons CD\text{-}Glu \qquad (1)$$

When basic solutions of $AgClO_4$, $NaAuCl_4$, K_2PdCl_4, or K_2PtCl_4 were refluxed in the presence of CD-Glu, metal particles with nanometer dimensions where achieved. Absorbance spectra of the corresponding red, yellow, dilute-black, and light-brown colored solutions are

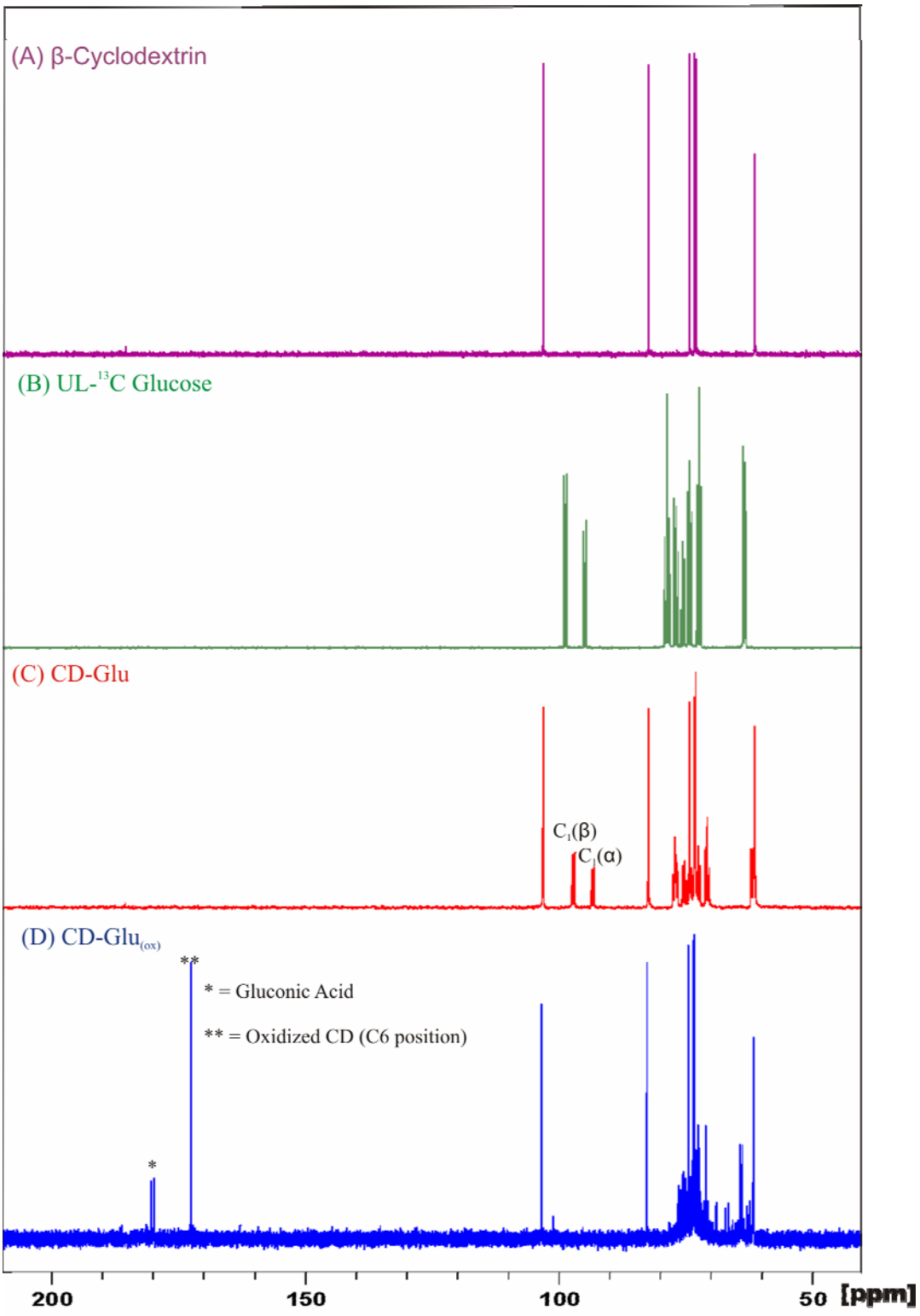

Figure 2. 2. Carbon NMR spectra of (A) β-CD, (B) uniformly labled ^{13}C glucose, (C) CD-Glu complex prepared with labeled Glu, and (D) the oxidized form of (C) resulting from the reduction of 5 mM Pd^{2+} in basic solution.

presented in Figure 2.3 along with a photograph of each colloid shown in the inset. Complete ion reduction was confirmed in a series of control experiments involving each metal salt when the addition of $NaBH_4$, followed by heating, produced no increase in color. Sharp peaks at 400 and 520 nm for Ag and Au, respectively, correspond to the collective oscillation of electrons about the particle surfaces while the broad absorption continua throughout the visible region of the Pd and Pt spectra is a result of the superposition of interband excitations with plasma resonances.[64] In the cases of Pd and Pt, the same experiment performed with unmodified CD,

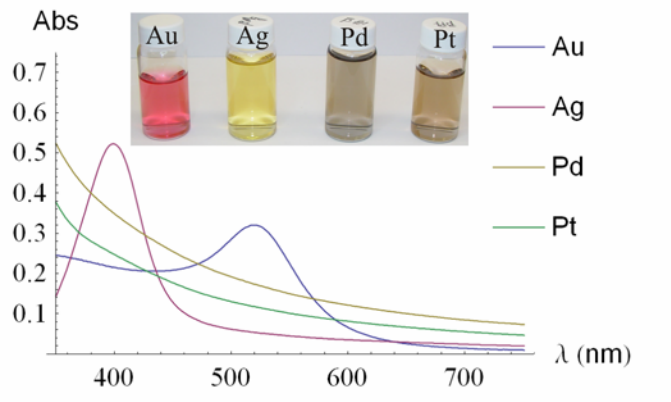

Figure 2. 3. Absorption spectra of 0.1 mM Au, 0.025 mM Ag, 0.1 mM Pd, and 0.5 mM Pt with a photograph of the corresponding colloids (inset).

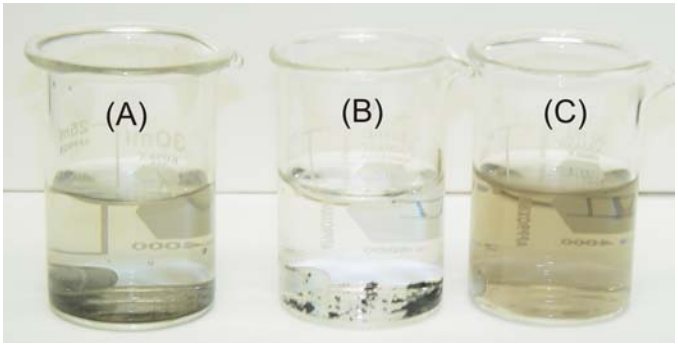

Figure 2. 4. Photograph taken 24 hours after preparation of Pd (A) and Pt (B) in basic solutions of glucose and Pt (C) prepared under identical conditions using CD-Glu in place of the lone sugar. The image exemplifies the need to use the host-guest complex in order to achieve particle stability in the cases of Pd and Pt.

rather than the complex, resulted in no reaction. Moreover, an additional control experiment using the same concentration of glucose, in lieu of the complex, resulted in the formation of particles which rapidly precipitate. Figures 2.4A and 2.4B display photographs of the glucose-prepared Pd and Pt colloids taken 24 hours after the reaction was complete. Figure 2.4C, on the other hand, is a similar image of a stable Pt colloid that was prepared with the CD-Glu complex.

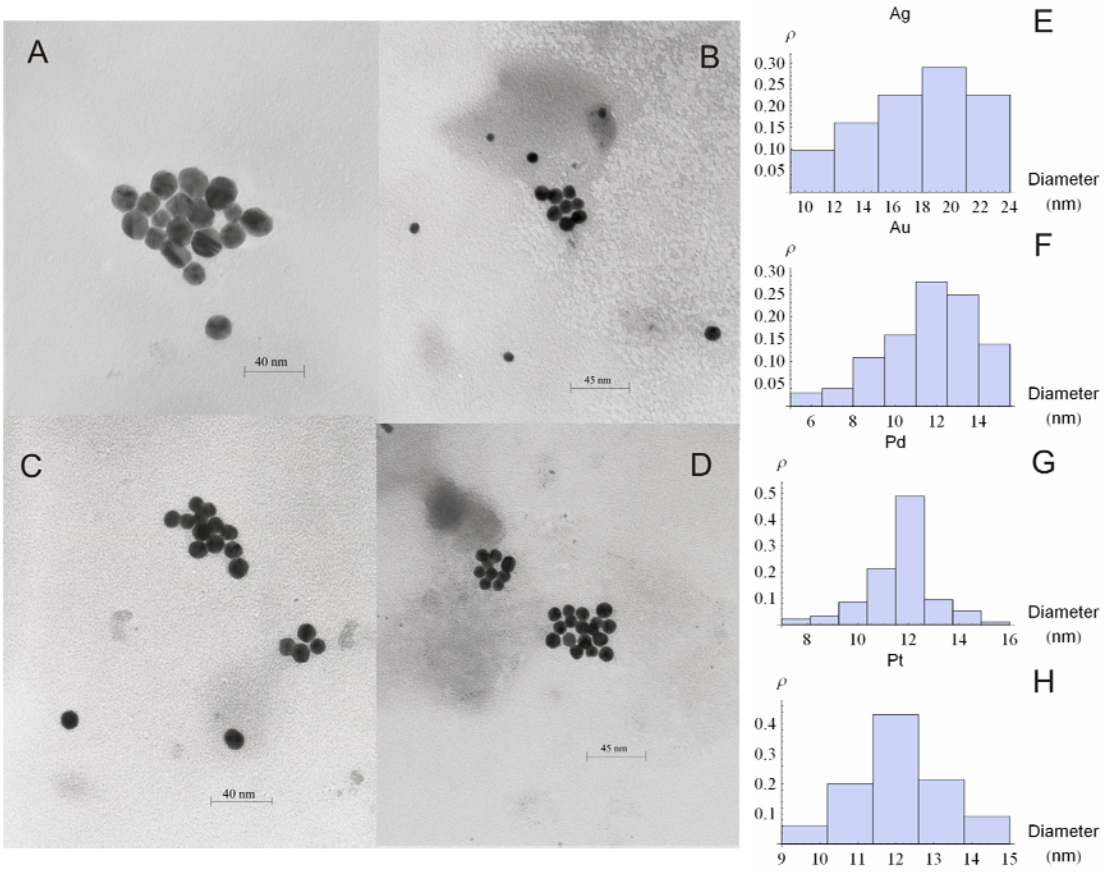

Figure 2. 5. TEM images of (A) Ag, (B) Au, (C) Pd, and (D) Pt along with the corresponding histograms of particle diameters (E-H).

The electron micrographs presented in Figures 2.5A-2.5D demonstrate that the particles possess fairly spherical morphology while the histograms in Figures 2.5E-2.5H reveal average particle

diameters of 18, 11, 12, and 12 nm for Ag, Au, Pd, and Pt, and provide the corresponding size distributions. Colloidal stability was evaluated by visible inspection and in all cases, the 0.1 mM samples remain in solution for very long periods of time. At the time of publication, the eldest sample in possession was 0.1 mM Au which after three years displayed no evidence of precipitation. Samples of Ag, Pd and Pt of equal concentration had similarly been shelved for well over one year without evidence of flocculation. XRD was employed to verify the crystallinity of each colloid by evaporating a 5.0 mM suspension and analyzing the resulting powder. The 2θ peaks shown in Figure 2.6 are in good agreement with those published by the JCPDS.[65]

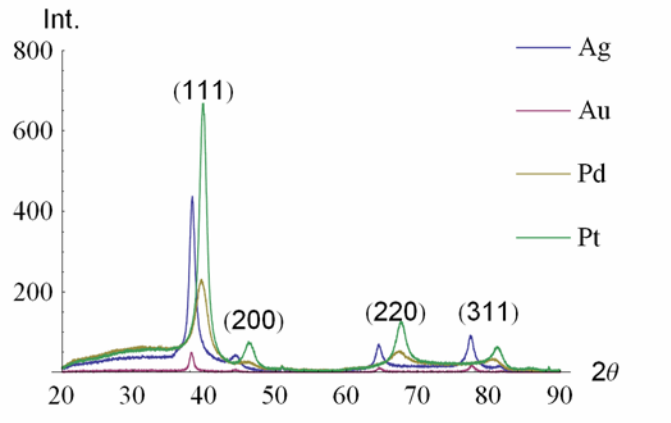

Figure 2. 6. Powder diffraction data corresponding to the fcc-crystalline noble metal particles prepared during the current investigation.

Salt reduction is expected to occur according to equations 2 & 3 where $CD_{(ox)}$ denotes

$$\text{CD-Glu} \rightleftharpoons CD_{(ox)} + \text{gluconic acid} + x\ H^+ + x\ e^- \quad (2)$$

$$M^{n+} + ne^- \rightarrow M \quad (3)$$

the oxidized form of cyclodextrin and $x \geq 4$ depending on the extent of host oxidation; however, under our basic conditions, gluconic acid is converted to gluconate. Because Ag^{+} and Au^{3+} can readily oxidize unmodified CD as well as glucose,[7,42] the extent to which the host vs. guest are oxidized during the generation of silver and gold colloids has not been considered. In order to evaluate the major reaction products in the generation of palladium, however, a 5 mM Pd sample was anaerobically prepared in the presence of 10 mM CD-Glu with D_2O as the solvent. The sealed sample was then subjected to numerous freeze/thaw cycles to promote particle flocculation prior to being filtered through a 0.2 μm Gelman syringe filter for analysis. The corresponding ^{13}C NMR spectrum is shown in Figure 2.2D where the generation of gluconate as a reaction product is made evident by the doublet centered at 180.1 ppm.[66] Spiking a control sample, under the above conditions, with analytical grade sodium gluconate gave rise to a singlet at 180.1 ppm supporting the proposed identity of gluconate as a reaction product. The decay of the $C_1\beta$ and $C_1\alpha$ doublets centered at 98.7 and 94.9, respectively, in Figure 2.2C provides further evidence for the oxidation of Glu at the C_1 position to form gluconate. The singlet centered at 172.5 ppm in Figure 2.2D, which is absent in Figure 2.2C, has been assigned to the oxidation of the C_6 primary hydroxyl group of CD.[67]

Enzymatic analysis[63] of the above reaction products revealed a gluconate concentration of 2.3 mM. With 10 mM electrons needed to reduce 5 mM Pd^{2+}, these data indicate that the major reductant is thus the host which is significant due to the results of earlier control experiments which demonstrated that basic solutions of unmodified CD were incapable of reducing Pd^{2+} and Pt^{2+}. A control experiment was conducted to confirm that Pd particles are not catalyzing the oxidation of CD. No reaction occurred after adding 1 mL of 0.1 mM Pd colloid to a solution containing 0.5 mM Pd^{2+}, 5 mM CD, and 15 mM NaOH and heating to

100 °C for 30 min. A comproportionation reaction is thus tentatively proposed to solve the dilemma of Glu not being the sole reductant, as mentioned earlier; note that atom-atom combination to form particles does not solve this dilemma. In this mechanism, Pd^{2+} undergoes a two electron reduction by the encaged Glu, according to equation 4, generating a zero-valent Pd atom. One Pd atom then undergoes comproportionation with a Pd^{2+} ion to yield two Pd^{+}, according to equation 5, where the two monovalent ions likely exist as a dimer. This reaction

$$Pd^{2+} + \text{CD-Glu} \rightarrow Pd + \text{CD} + \text{Gluconate} + 2H^{+} \quad (4)$$

$$Pd + Pd^{2+} \rightarrow 2\ Pd^{+} \quad (5)$$

$$2\ Pd^{+} + \text{CD} \rightarrow 2\ Pd + \text{CD}_{(ox)} + 2\ H^{+} \quad (6)$$

competes favorably with the aggregation of atoms to form particles. Pd atoms on the surface of particles have never been observed to reduce Pd^{2+} ions to form Pd^{+}. Reaction 5 seems reasonable because in the radiolytic reduction of aq. Pd^{2+}, dimeric Pd^{+} was produced which remained stable for several hours.[68] Steps 4 and 5 agree with a previous study in which researchers combined relatively small amounts of a Pd^{0} complex with an excess of Pd^{2+} in the presence of a material which favors the complexation of Pd^{+}. Single crystal X-Ray analysis of the isolated product revealed the presence of dimeric Pd^{+} complexes and some residual Pd^{0} but no divalent metal ions.[69] A similar mechanism has recently been proposed in which the comproportionation of two nascent Au atoms with two Au^{3+} ions yields two Au^{+} and a long lived dimer of Au^{2+}.[70] The unique step in the current schema, however, is equation 6 which proposes that the Pd^{+} dimer is capable of oxidizing the CD host under the current conditions. Another possible step involves the monoelectronic reduction of two Pd^{2+} by Glu to yield two Pd^{+} as illustrated in step 7. This step,

$$2\ Pd^{2+} + \text{CD-Glu} \rightarrow 2\ Pd^{+} + \text{CD} + \text{Gluconate} \quad (7)$$

however, is expected to occur with negligible probability because, to the best of our knowledge, no 1 electron reduction of metal ions by glucose has been reported. The two electron reduction in step 4 is thus more likely. The most probable path would involve the coordination of two Pd^{2+} ions to the CD.

The efficacy of nanofluids is typically evaluated by their relative TC values, $k_{rel,}$ where k_{rel} = k_{nf}/k_{sol}, k_{nf} = nanofluid TC and k_{sol} = TC of the solvent. According to Maxwell's theory for nanofluids composed of non-interacting, spherical particles, k_{rel} is expected in vary according to equation 8 where k_p = TC of the dispersed metal and ϕ = the volume fraction of particles.[71] Corresponding TC values for each bulk metal are listed in Table 2.1.[72]

$$k_{rel} = (1+2\beta\phi)/(1-\beta\phi) \qquad \beta = (k_p-k_{sol})/(k_p+2k_{sol}) \tag{8}$$

	10 °C	20 °C	30 °C	40 °C	50 °C
Ag	429.	429.	428.	428.	428.
Au	319.	318.	317.	317.	316.
Pd	72.	72.	72.	72.	72.
Pt	72.	72.	72.	72.	72.

Table 2.1. Reference TC values (W/m/°C) for each metal assessed during the current study.

Thermal conductivity measurements were performed on aqueous solutions comprised of 0.1-5.0 mM metal, 5 mM CD-Glu, and 15 mM NaOH (based on starting concentrations). A 10 mL sample of colloid was deposited in a pyrex sample holder fitted with a cover containing a slit to accommodate the Thermal Hot Disk sensor. The sample containers were inserted into matching cavities within an aluminum block submerged in a thermostatic bath. Samples were equilibrated until they remained at the desired temperature, ±0.1 °C, for 5 minutes and the reported TC value is the average of five different measurements. Figure 2.7 presents a plot of data obtained from two control experiments which evaluated the TC of deionised water and a

blank solution containing 5 mM CD-Glu and 15 mM NaOH. The objective of this step was to isolate any background contribution from these reagents; the blank showed negligible change in TC relative to pure water.

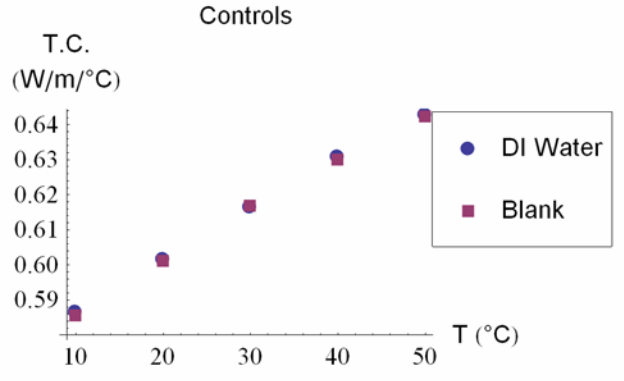

Figure 2. 7. Plots of thermal conductivity vs. T for deionized water and a blank consisting of 5 mM CD-Glu and 15 mM NaOH.

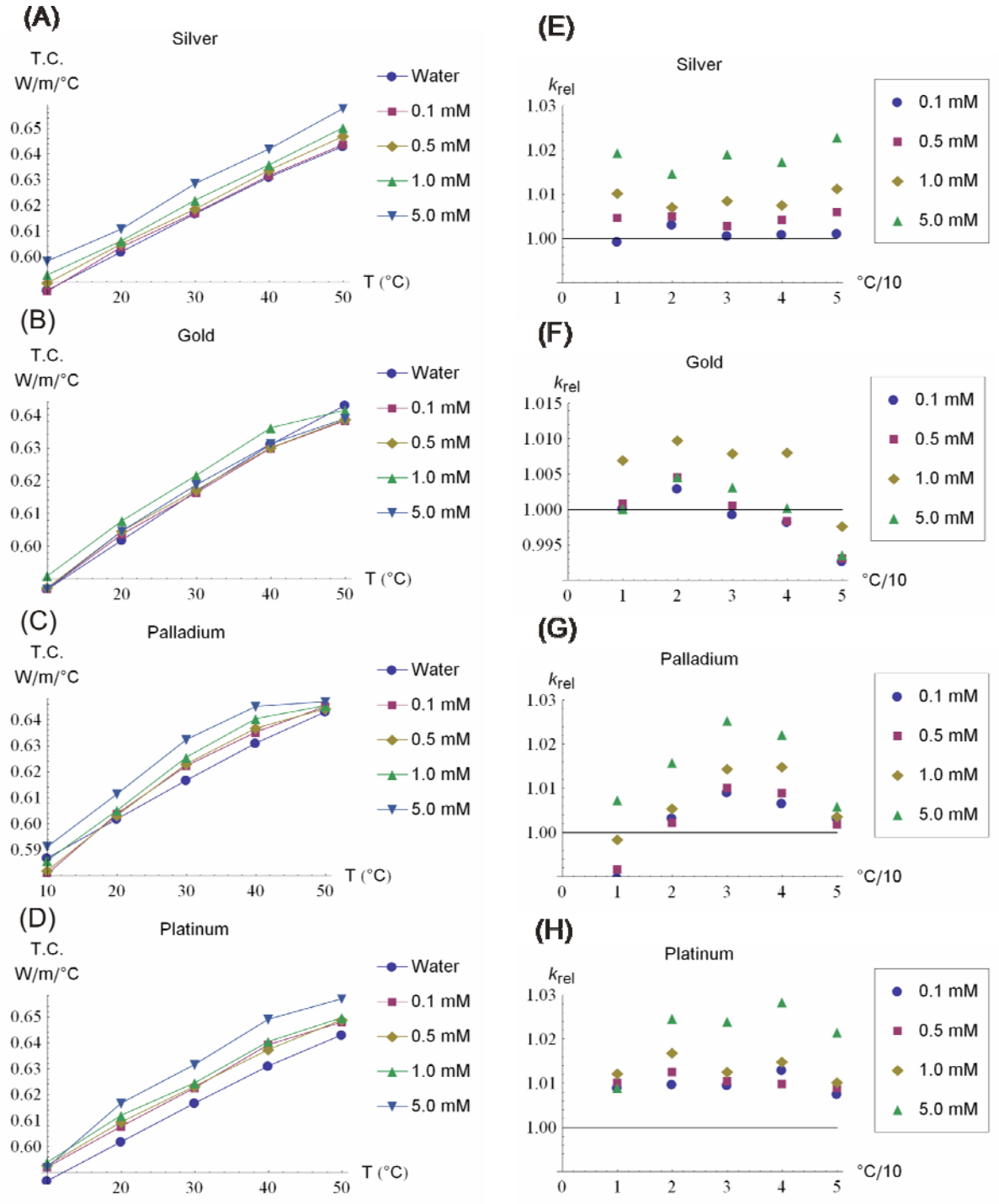

Figure 2. 8. Plots of absolute TC (W/m/°C) as a function of T (°C) (A-D) with matching plots of relative TC (E-H).

Each sample was evaluated at 10, 20, 30, 40 and 50 °C with the absolute TC values plotted in Figures 2.8A-2.8D and plots of k_{rel} presented in Figures 2.8E-2.8H. Table 2.2 summarizes the change in TC for each nanofluid at 40 °C relative to deionised water; the value obtained for water at this temperature was 0.631 W/m/K which is in good agreement with the reference value.[72] The largest increase observed was 2.9% for 5.0 mM Pt. Over the current temperature range, the TC of water is nearly linear; however, inspection of the curves in Figures 2.8B-2.8D which correspond to [M] = 5.0 mM, reveals a significant decrease in slope over the region from 40 to 50 °C. This is a clear indication of particle sedimentation, which was confirmed by visible inspection after recording the final measurement at 50 °C. The same trend is not observed in the silver samples. The slopes in Figure 2.8A all appear to be rather linear due to the increased stability of this colloid at elevated temperatures. Although no visible precipitation was observed in any of the Pt colloids, a slight tail appears at 50 °C for each concentration which suggests particle agglomeration which was insufficient to cause flocculation or a visibly noticeable color change.

	Ag	Au	Pd	Pt
0.1 mM	0.1	0.4	0.8	1.7
0.5 mM	−0.2	−0.2	0.8	0.0
1.0 mM	0.7	0.9	1.5	2.2
5.0 mM	1.3	1.0	1.5	2.9

Table 2.2. Table of values for enhancement of TC (%), relative to deionised water, obtained at 40 °C.

Conclusion

Stable colloids of Ag, Au, Pd, and Pt have been prepared utilizing a CD-Glu host-guest complex as both a reducing agent and particle stabilizer. In all cases, the particles demonstrate remarkable stability at room temperature for very long periods of time—up to three years, thus

far. A unique aspect of the reduction process is the comproportionation of Pd with Pd^{2+} to yield two Pd^{+} ions. As similar trends have previously been observed, it is possible that the two, short-lived, univalent Pd species exist as a dimer which, working in concert, is capable of oxidizing the host. The inability of unmodified CD to reduce Pd^{2+} or Pt^{2+}, under the current conditions, in conjunction with the stoichiometric shortage of gluconate, resulting from salt reduction by the CD-Glu complex, supports the comproportionation mechanism.

Thermal conductivity measurements on each of the 5 mM ($4\text{-}5\times10^{-5}$ vol%) colloids revealed an enhancement in k_{rel} of 1-3%. Although these values appear small, they are two orders of magnitude larger than what is predicted by equation 8. Also predicted by Maxwell's theory is that k_{rel} is a function of the TC of the dispersed particles. The current results deviate from the trend of values listed in Table 2.1 in that the largest enhancement was observed in the Pt colloids and the smallest in Au. These data are at odds with theory because the TC of bulk Au is ~4.5 times larger than that of Pt. On the other hand, the fact that observed enhancements are vastly larger than theoretical predictions lends credibility to the concept.

The projected use of nanofluids is in systems which operate at elevated temperatures. Colloids prepared during the current study display exceptional stability at room temperature—in excess of 3 years in some cases—but upon heating to 50 °C for ~1 hr, all but the Ag sample exhibited at least some evidence of decay. These findings imply that the current standards of aqueous colloids are insufficient to serve in the practical application of nanofluids. Current work is underway to develop viscous colloidal gels that permit the dispersion of much larger concentrations of metal particles. The increased viscosity is a result of polymeric stabilizers which serve to promote long-term particle stability at elevated temperatures. The deviation in TC from classic Maxwell's theory suggests that there is either a very large extent of

experimental error or that the process of thermal conduction in heterogeneous, complex systems, such as nanofluids, is far more complex than pure liquids and solids and requires more detailed theoretical analysis.

References

(1) *Nanoparticles and Catalysis*; Astruc, D., Ed.; Wiley-VCH: Weinheim, 2008.

(2) Jin, R. *Angew. Chem. Int. Ed.* **2010**, *49*, 2826-2829.

(3) De, M.; Ghosh, P. S.; Rotello, V. M. *Adv. Mater.* **2008**, *20*, 4225-4241.

(4) Zhang, L.; Gu, F. X.; Chan, J. M.; Wang, A. Z.; Langer, R. S.; Farokhzad, O. C. *Clin. Pharmacol. Ther.* **2008**, *83*, 761-769.

(5) Chen, C.; Wang, L.; Jiang, G.; Yu, H. *Rev. Adv. Mater. Sci.* **2006**, *11*, 1-18.

(6) Longenberger, L.; Mills, G. *J. Phys. Chem.* **1995**, *99*, 475-478.

(7) Panigrahi, S.; Kundu, S.; Ghosh, S. K.; Nath, S.; Pal, T. *Colloids and Surfaces A: Physiochem. Eng. Aspects* **2005**, *264*, 133-138.

(8) Sperling, R. A.; Parak, W. J. *Phil. Trans. R. Soc. A* **2010**, *368*, 1333-1383.

(9) Bronstein, L. M.; Shifrina, Z. B. *Chem. Rev.* **2011**, *Articles ASAP*, Downloaded 9/1/2011.

(10) Ha, J. M.; Solovyov, A.; Katz, A. *Langmuir* **2009**, *25*, 153-158.

(11) Bönnemann, H.; Botha, S. S.; Bladergroen, B.; Linkov, V. M. *Appl. Organometal. Chem.* **2005**, *19*, 768-773.

(12) Clary, D. R.; Mills, G. *J. Phys. Chem. C* **2011**, *115*, 14656-14663.

(13) Denicourt-Nowicki, A.; Roucoux, A. *Curr. Org. Chem.* **2010**, *14*, 1266-1283.

(14) Dodziuk, H. Molecules with Holes—Cyclodextrins. In *Cyclodextrins and Their Complexes: Chemistry, Analytical Methods, Applications*; Dodziuk, H., Ed.; Wiley-VCH: Weinheim, 2006.

(15) Del Valle, E. M. M. *Process Biochem.* **2004**, *39*, 1033-1046.

(16) Frömming, K. H.; Szejtli, J. *Cyclodextrins in Pharmacy*; Kluwer Academic Publishers: Dordrecht, 1994; Vol. 5.

(17) Stoddart, J. F. *Carbohydr. Res.* **1989**, *192*, 12-15.

(18) Rekharsky, M. V.; Inoue, Y. *Chem. Rev.* **1998**, *98*, 1875-1918.

(19) Szejtli, J. *Chem. Rev.* **1998**, *98*.

(20) Hapiot, F.; Tilloy, S.; Monflier, E. *Chem. Rev.* **2005**, *106*, 767-781.

(21) Astray, G.; Gonzalez-Barreiro, C.; Mejuto, J. C.; Rial-Otero, R.; Simal-Gándara, J. *Food Hydrocolloids* **2009**, *23*, 1631-1640.

(22) Kanwar, J. R.; Long, B. M.; Kanwar, R. K. *Curr. Med. Chem.* **2011**, *18*, 2079-2085.

(23) Duchene, D.; Wouessidjewe, D.; Poelman, M. C. *Cosmetic Science and Technology Series* **1999**, *19*, 275-293.

(24) Lezcano, M.; Ai-Soufi, W.; Novo, M.; Rodriguez-Nunez, E.; Tato, J. V. *J. Agric. Food. Chem.* **2002**, *50*, 108-112.

(25) Dufosse, L.; Souchon, I.; Feron, G.; Latrasse, A.; Spinnler, H. E. *Biotechnol. Prog.* **1999**, *15*, 135-139.

(26) Hedges, R. A. *Chem. Rev.* **1998**, *98*, 2035-2044.

(27) Komiyama, M.; Hirai, H. *Bull. Chem. Soc. Jpn.* **1983**, *56*, 2833-2834.

(28) Liu, J.; Ong, W.; Esteban, R.; Lynn, M. J.; Kaifer, A. E. *Langmuir* **2000**, *16*, 3000-3002.

(29) Liu, J.; Alvarez, J.; Kaifer, A. E. *Adv. Mater.* **2000**, *12*, 1381-1383.

(30) Strimbu, L.; Liu, J.; Kaifer, A. E. *Langmuir* **2003**, *19*, 483-485.

(31) Liu, J.; Alvarez, J.; Ong, W.; Román, E.; Kaifer, A. E. *Langmuir* **2001**, *17*, 6762-6764.

(32) Alvarez, J.; liu, J.; Román, E. *Chem. Commun.* **2000**, 1151-1152.

(33) Hebeish, A.; El-Shafei, A.; Sharaf, S.; Zghloul, S. *Carbohydr. Polym.* **2011**, *84*.

(34) Michels, J. J.; Huskens, J.; Reinhoudt, D. N. *J. Chem. Soc. Perkin Trans. 2* **2002**, 102-105.

(35) Senra, J. D.; Malta, L. F. B.; Da Costa, M. E. H. M.; Michel, R. C.; Aguiar, L. C. S.; Simas, A. B. C.; Antunes, O. A. C. *Adv. Synth. Catal.* **2009**, *351*, 2411-2422.

(36) Ng, C. H. B.; Yang, J.; Fan, W. Y. *J. Phys. Chem. C* **2008**, *112*, 4141-4145.

(37) Yang, Y.; Liu, S.; Kimura, K. *Colloids and Surfaces A: Physiochem. Eng. Aspects* **2006**, *290*, 143-149.

(38) Jaiswal, S.; Duffy, B.; Jiaswal, A. K.; Stobie, N.; McHale, P. *Int. J. Antimicrob. Agents* **2010**, *36*, 280-283.

(39) Kochkar, H.; Aouine, M.; Ghorbel, A.; Berhault, G. *J. Phys. Chem. C* **2011**, *115*, 11364-11373.

(40) Liu, Y.; Male, K. B.; Bouvrette, P.; Luong, J. H. T. *Chem. Mater.* **2003**, *15*, 4172-4180.

(41) Kochkar, H.; Aouine, M.; Ghorbel, A.; Berhault, G. *J. Phys. Chem. C.* **2011**, *115*, 11364-11373.

(42) Pande, S.; Ghosh, K.; Praharaj, S.; Panigrahi, S.; Basu, S.; Jana, S.; Tsukuda, T.; Pal, T. *J. Phys. Chem. C* **2007**, *111*, 10806-10813.

(43) Mandler, D.; Willner, I. *J. Am. Chem. Soc.* **1987**, *109*, 7884-7885.

(44) Lu, P.; Teranishi, T.; Asakura, K.; Miyake, M.; Toshima, N. *Journal of Physical Chemistry B* **1999**, *103*, 9673-9682.

(45) Giuffrida, S.; Ventimiglia, G.; Petralia, S.; Concoci, S.; Sortino, S. *Inorg. Chem.* **2006**, *45*, 508-510.

(46) Gehrke, H.; Pelka, J.; Hartinger, C. G.; Blank, H.; Bleimund, F.; Schneider, R.; Gerthsen, D.; Bräse, S.; Crone, M.; Türk, M.; Marko, D. *Arch. Toxicol.* **2011**, *85*, 799-812.

(47) Kim, B. H.; Kim, S. Y.; Woo, H. G.; Jun, J.; Sohn, H. *J. Nanosci. Nanotechnol.* **2008**, *8*, 5356-5359.

(48) Liu, J.; Xu, R.; Kaifer, A. E. *Langmuir* **1998**, *14*, 7337-7339.

(49) Kim, J. H.; Kim, K. S.; Manesh, K. M.; Santhosh, P.; Goplalan, A. I.; Lee, K. P. *Colloids Surf., A* **2008**, *313*, 612-616.

(50) Jing, B.; Chen, X.; Wang, X.; Zhao, Y.; Qiu, H. *ChemPhysChem* **2008**, *9*, 249-252.

(51) Liu, Y.; Yang, Y. W.; Chen, Y. *Chem. Commun.* **2005**, 4208-4210.

(52) Shalkevich, N.; Escher, W.; Bürgi, T.; Michel, B.; Si-Ahmed, L.; Poulikakos, D. *Langmuir* **2010**, *26*, 663-670.

(53) Wang, B.; Wang, X.; Lou, W.; Hao, J. *Nanoscale Res. Lett.* **2011**, *6*, 259-269.

(54) Sánchez-Ramírez, J. F.; Pérez, J. L. J.; Orea, A. C.; Fuentes, R. G.; Bautista-Hernández, A.; Pal, U. *J. Nanosci. Nanotechnol.* **2006**, *6*, 685-690.

(55) Sharma, P.; Baek, I. H.; Cho, T.; Park, S.; Lee, K. B. *Powder Technology* **2011**, *2008*, 7-19.

(56) Godson, L.; Raja, B.; Lal, D. M.; Wongwises, S. *Exp. Heat Transfer* **2010**, *23*, 317-332.

(57) Singh, A. K.; Raykar, V. S. *Colloid and Polymer Science* **2008**, *286*, 1667-1673.

(58) The National Research Council, In *Prudent Practices in the Laboratory: Handling and Management of Chemical Hazards*, The National Academic Press: Washington, D.C., 2001, Page 139.

(59) Gustafson, S. E. *Review of Scientific Instruments* **1991**, *62*, 797-804.

(60) Xun, F.; Wei, Y.; Yusheng, L.; Debao, W.; Huaqiang, S.; Fengyuan, Y. *Journal of Dispersion Science and Technology* **2005**, *26*, 575-580.

(61) Szejtli, J.; Zsuzsanna, B. *Acta Chim. Hung.* **1979**, *99*, 433-446.

(62) Hirsch, W.; Muller, T.; Pizer, R.; Ricatto, P. J. *Canadian Journal of Chemistry* **1995**, *73*, 12-15.

(63) Rao, C. R. K.; Trivedi, D. C. *Materials Chemistry and Physics* **2006**, *99*, 354-360.

(64) Creighton, J. A.; Eadon, D. G. *J. Chem. Soc. Faraday Trans.* **1991**, *87*, 3881-3891.

(65) Yang, J.; Lee, J. Y.; Chen, L. X.; Too, H. P. *Journal of Physical Chemistry B* **2005**, *109*, 5468-5472.

(66) Blazer, R. M.; Whaley, T. W. *J. Am. Chem. Soc.* **1980**, *102*, 5082-5085.

(67) Fraschini, C.; Vignon, M. R. *Carbohydrate Research* **2000**, *328*, 585-589.

(68) Michaelis, M.; Henglein, A. *J. Phys. Chem.* **1992**, *96*, 4719-4724.

(69) Ragaini, F.; Larici, H.; Rimoldi, M.; Caselli, A.; Ferretti, F.; Macchi, P.; Casati, N. *Organometallics* **2011**, *30*, 2385-2393.

(70) Dey, G. R.; El Omar, A. K.; Jacob, J. A.; Mostafavi, M.; Belloni, J. *J. Phys. Chem. A* **2011**, *115*, 383-391.

(71) Kamat, P. V. *J. Phys. Chem. C* **2007**, *111*, 2834-2860.

(72) *CRC Handbook of Chemistry and Physics*; 73rd ed.; Lide, D. R., Ed.; CRC Press, Inc.: Boca Raton, 1992.

Chapter 3

Preparation and Thermal Properties of CuO Particles

Introduction

Particles of interest in the nanofluid literature include SiO_2, Al_2O_3, Cu, Ag, Au, and CuO, the latter of which is focus of the current chapter.[1] Ammonium citrate-stabilized CuO particles were suspended in water and a 30% increase in thermal conductivity was reported according to the transient hotwire method.[2] CuO particles dispersed in ethylene glycol in the absence of any stabilizer produced thermal conductivity enhancements greater than 20%.[3,4] Conversely, sparse literature is available which considers CuO colloid or nanofluid research in nonpolar solvents such as alkanes due to the challenge of dispersing polar particles in nonpolar media. Oleic acid (OA) and sodium oleate (SOA) were used to disperse CuO in various alkanes but the result was large, micron-sized aggregates of particles in an acidic environment.[5] Measurements performed on CuO which was dispersed in paraffin by the aid of OA reveal an increase in thermal conductivity of 48%. One immediate complication, however, associated with colloidal CuO in acidic media is that the solute will readily dissolve according to the following equation:

$$CuO + 2H^+ \rightarrow Cu^{2+} + H_2O \qquad (1)$$

The current work reveals a reasonable and reproducible synthesis method for SOA-stabilized CuO particles of the nm size range that are readily soluble, and modestly stable, in hydrocarbons at high concentrations; preparation of concentrated oxide colloids has previously been limited to TiO_2 and ZnO in water or alcohols.[6,7] The potential of CuO/SOA hydrocarbon colloids for use

in nanofluid and PCM research will be considered herein by making use of an experimental design based on Newton's Law of Cooling as well as other thermodynamic measurements.[8]

Experimental

Caution: Piranha etch is a hazardous material that should only be handled by trained personnel using appropriate personal protective measures. Waste from this material should only be disposed of by approved procedures.[9] $Cu(NO_3)_2 \cdot 2.5H_2O$, NaOH, oleic acid, ethanol, hexane, octane, dodecane, eicosane, chloroform and DMF were purchased from Sigma-Aldrich and used as-received without further purification. Indium and sapphire certified standards were purchased from TA-Instruments. All glassware was treated with fresh piranha etch[9] prior to use and deionized water used in all experiments was supplied by a Barnstead model D7401 EASYpureII purification system.

For a product yield of ca. 3.5 grams, sodium oleate-stabilized copper(II) oxide particle preparation typically occurred as follows. Four grams of OA in 50 mL of methanol and 5.206 g of 97% pure NaOH were added to 900 mL of deionized water providing a 10% molar excess of hydroxide. The solution was heated under vigorous stirring to 100 ºC at which point the methanol had volatilized and the sodium salt of OA had formed. One hundred mL of 498.7 mM $Cu(NO_3)_2$ (aq) was heated separately prior to being titrated into the basic SOA solution over a period of two minutes instantly producing a dark brown color. The resulting solution was maintained at 100 ºC with continued stirring for 5 minutes followed by immersion in an ice bath. Once at room temperature, the mixture was removed and 700 mL of DMF was added followed by two minutes of stirring. The solution was returned to the ice bath for an additional 25 minutes with periodic swirling to promote aggregation. The particles were then filtered over a Whatman P8 qualitative filter paper, dispersed in 400 mL of a 50:50 mixture of DMF and

deionized water to remove surplus ions, and filtered again in the same manner after flocculation. It is important to note that in either flocculation step, filtration must occur when aggregates are in the ~1 to ~3 mm size range. The larger clumps that would otherwise ensue after prolonged cooling cause filtering to become immensely difficult. The resulting product was dried under vacuum at 100 ºC for 4 hours. Selective extraction of the well-coated particles was achieved by dissolving the product in 400 mL of chloroform followed by fractional filtration through P8, #42, and #50 Whatman filters. The filtrate was transferred to a 1L separatory funnel and extracted with 300 mL of DI water in order to remove any residual ions and poorly coated particles. As a last step, the organic layer was separated into a large crystallization dish from which the chloroform was removed under vacuum at 60 ºC. Once dryness was achieved, the temperature was raised to 90 °C for 4 additional hours to remove any remaining water. A material resembling black wax was obtained which adhered to the glass but could easily be removed with the aid of a razor blade. The product was stored until use in a vacuum dessicator; prolonged exposure to air resulted in insoluble particles. The hydrocarbon backbone of the SOA surfactant enabled easy particle solvation in low dielectric media. Therefore, colloid preparation involved merely dissolving the dried CuO/SOA particles in the hydrocarbon of interest and stirring at 80 ºC for 45 minutes.

Particle characterization occurred via several processes. Absorption spectra were obtained using an Ocean Optics CHEM2000-UV-Vis spectrophotometer. XRD patterns were obtained with a Bruker D8 X-ray diffractometer to verify CuO crystallinity. Copper and sodium content was determined by a Varian AA240 flame atomic absorption (FAA) spectrometer and the CuO and SOA contents were extrapolated. TEM images for particle size and morphology determination were obtained on a Zeiss EM10 transmission electron microscope at 60keV. Size distribution involved analysis of more than 300 particles imaged from multiple samples while the

diameter was taken as the widest portion of the particle regardless of the shape. Heat capacities, heats of fusion, and melting points, where applicable, were obtained using a Thermal Analysis DSC 2920 differential scanning calorimeter. DSC measurements were obtained in accordance with ASTM 1269-05 and warrant a brief discussion.[10] Two different methods were employed depending on the solvent used, each of which began by equilibrating at 22 ºC followed by a 4 minute isotherm. For the dodecane system, a ramp of 5 °C/min was utilized whereas for the eicosane system a ramp of 2 ºC/min was necessary to improve resolution about the phase change region. Both methods spanned a temperature range of 22 ºC to 100 ºC. Prior to each series of measurements the instrument was calibrated. The temperature calibration involved a single point calibration using indium, which also served to calibrate the cell constant, and a sapphire standard was used to determine the calorimetric sensitivity constant at various temperatures for heat capacity measurements. At the end of each run, the cell was quench-cooled with liquid nitrogen. All samples and standards were analyzed in hermetic, aluminum pans.

A simple device was assembled to measure relative heat transport properties of the prepared colloids. The apparatus includes a custom built Pyrex sample cell which houses a type K thermocouple (TC-Omega) in a centered location, as shown in Figure 3.1. Two heat sources were employed: (1) 300 mL of boiling water in a 400 mL beaker on a hot plate and (2) a Fisher Scientific model 9500 thermostatic bath held at 0.0 ºC. A fixed mass of sample was placed inside the sample cell and the apparatus was transferred to and from the hot and cold baths while temperature vs. time data were collected via a USB-TC 8-channel thermocouple input data shuttle by Measurement Computing. Data were recorded with a PC at a rate of 1 sec^{-1} and temperature vs. time cooling curves were plotted for data analysis. A reference thermocouple located approximately 4 cm away from the apparatus determined that no significant temperature fluctuations occurred in the thermostatic bath.

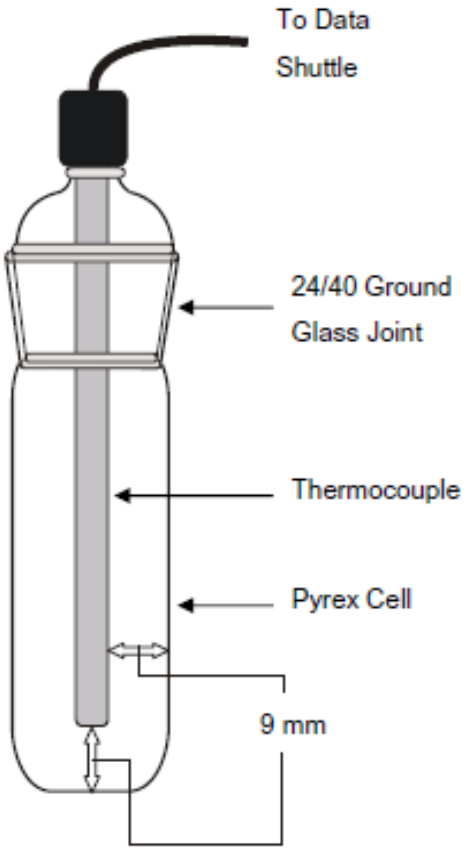

Figure 3.1. Apparatus employed to measure the relative heat transfer properties of prepared colloids.

The cooling curve data were obtained as follows (note that one thermodynamic cycle comprising a single "cooling curve" is marked by cooling the sample from 100 to 0 °C then heating again to 100 °C). To begin the process, 9.00±.005 g of sample were added to the clean, dry cell which was allowed to heat at 100 °C for 20 minutes after which data acquisition was initiated. After precisely 30 seconds, the cell was transferred to the thermostatic bath at 0.0 ºC where it remained for 40 minutes before being returned to the hot bath for an additional 20 minutes to complete one cycle. The reproducibility of the current technique was established by running a sample of eicosane through the cooling and heating cycle ten times; an overlay plot of runs 1, 5, and 10 is

presented in Figure 3.2. The cooling rate was averaged (by a method to be described) over ten runs yielding a mean square deviation of ±0.3%. Experiments to externally calibrate the device were not possible for the reason that analogous data is not available.

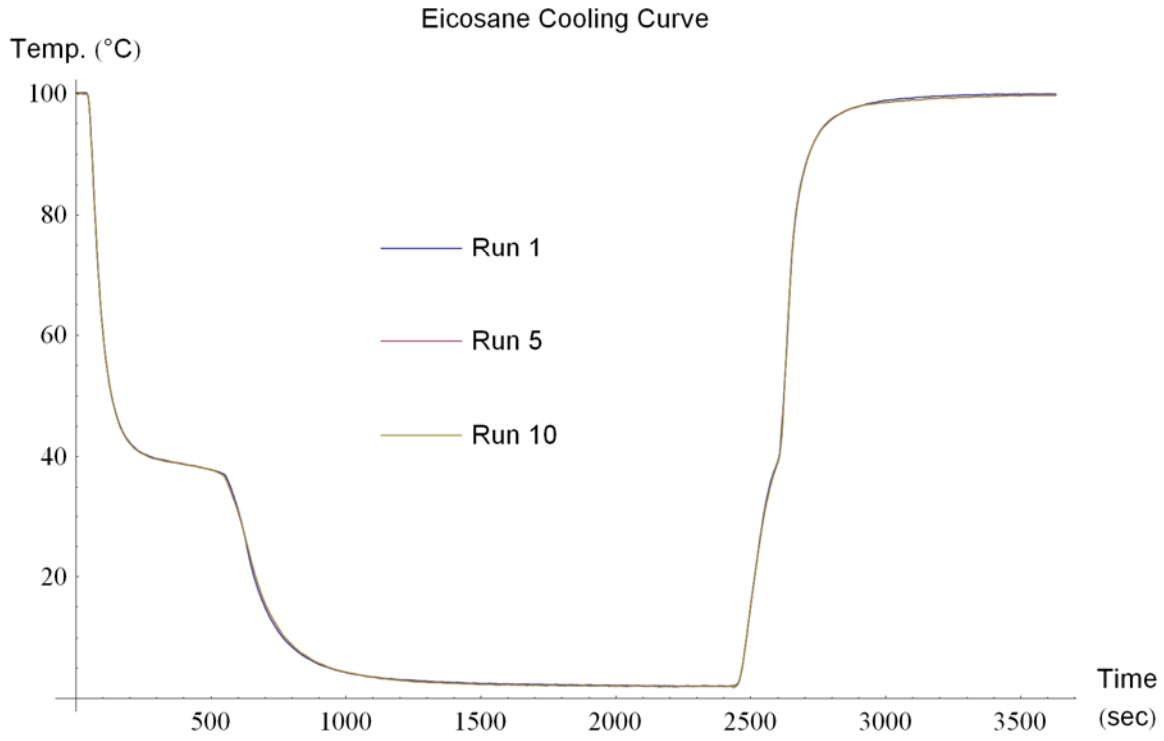

Figure 3.2. Cooling curves corresponding to the eicosane blank. Displayed are runs 1,5, and 10 out of 10 demonstrating the reproducibility of the technique used in the current investigation to measure the relative heat transport properties of the prepared colloids.

Results and Discussion

Figure 3.3 shows an XRD pattern of the SOA-coated particles which yielded signals consistent with crystalline CuO in accordance with the reflections listed in JCPDS Card No. 41-0254. Efforts to detect crystallinity in solid eicosane were unsuccessful. TEM images, one of which is shown in Figure 3.4(A), reveal a particle size distribution ranging from 3 to 29 nm. As shown in the histogram presented in Figure 3.4(B), 90% of the distribution exists within the range of 5 to 15 nm with the dominant size being 9 nm. In order to quantify the chemical composition of the CuO/SOA system, 50 mg of the particles was dissolved in piranha acid, diluted accordingly, and the copper and sodium were analyzed with FAA. The Cu:O

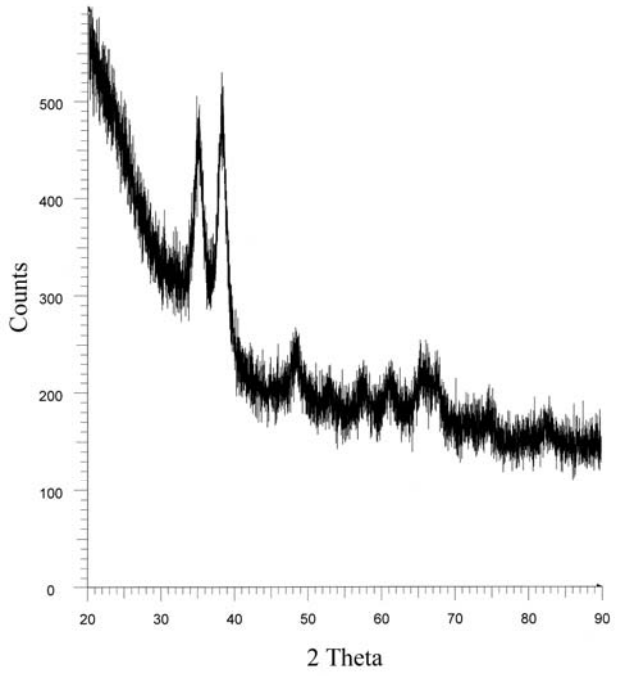

Figure 3.3. XRD pattern of CuO/SOA particles.

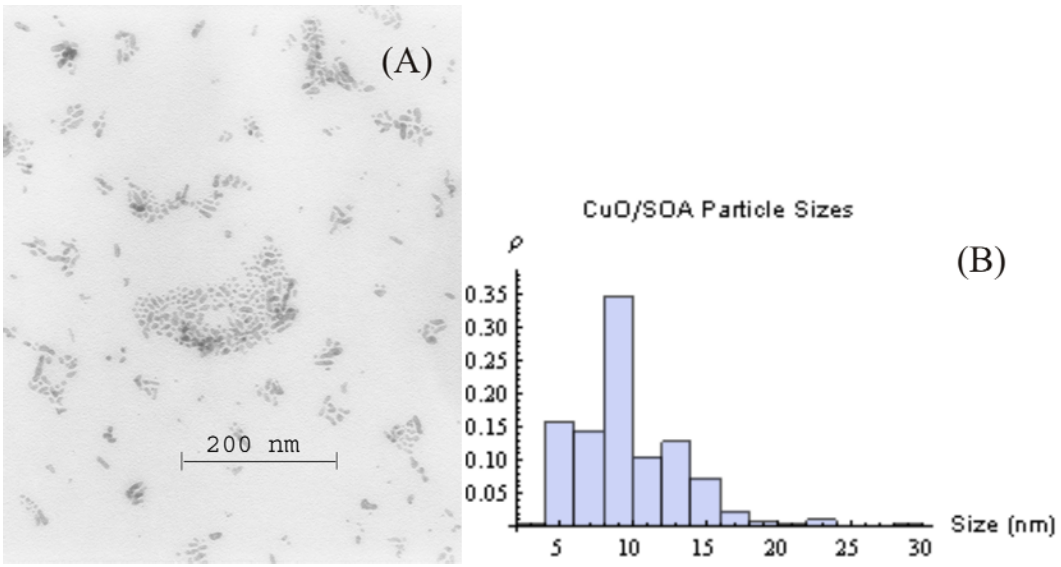

Figure 3.4. (A) TEM image of CuO/SOA Nanoparticles with (B) corresponding histogram of sizes assessed over 309 particles.

stoichiometry was taken as unity while the remaining mass was assumed to be SOA without significant impurities. The mass concentrations summed to the original mass digested ±1%. Following the synthesis method previously described, four particle samples were independently prepared and analyzed and the average mass composition was 69 ±1.4% copper oxide and 31 ±1.4% SOA, as shown in Figure 3.5. The precise nature of interaction between the surfactant and particle is not well known although it is reasonable to assume that the polar head group associates with the particle surface whereas the nonpolar tail interacts with the hydrocarbon solvent. Attempts to image the coating with TEM were unsuccessful for the reason that the surfactant tail lacks sufficient density to scatter electrons. A control experiment was performed, however, in which the particles were prepared according to the described procedure but in the absence of SOA. The resulting product was insoluble in hydrocarbon and produced a distinctly different morphology as demonstrated in the electron micrograph shown in Figure 3.6. An increase in size extending beyond 150 nm was observed as well as a shift in particle morphology from spherical or ellipsoidal to elongated box shapes which indicates that in addition to

stabilization and enabling dissolution in low dielectric media, the surfactant restricts particle growth.

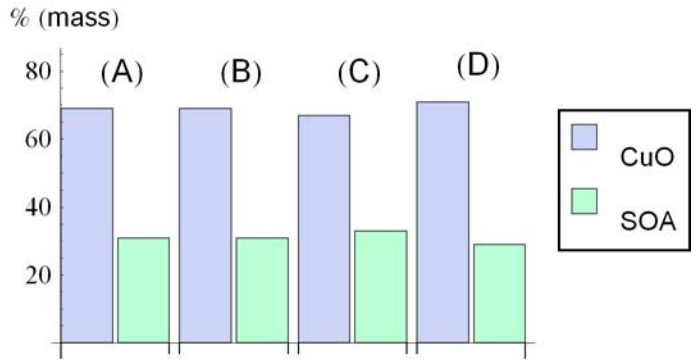

Figure 3.5. Component composition of four independently prepared CuO/SOA particle samples demonstrating the reproducibility of the synthetic method.

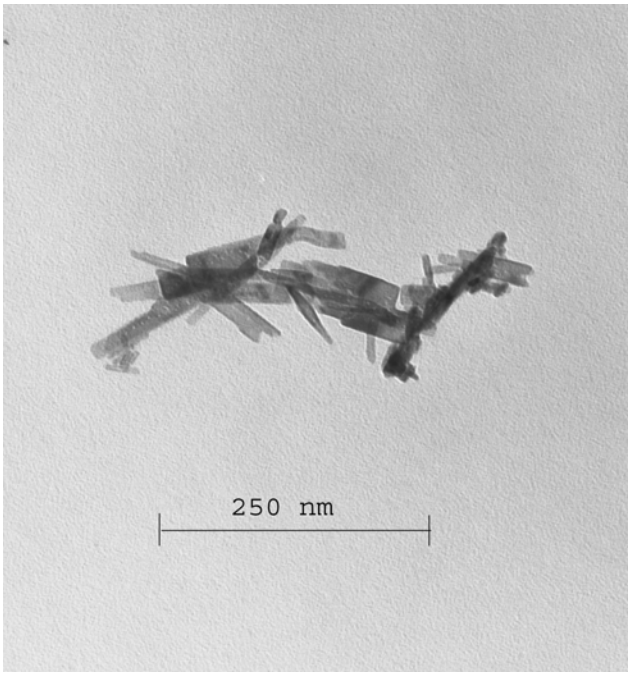

Figure 3.6. TEM image of CuO prepared according to the described synthesis method but in the absence of the SOA stabilizer indicating the role of the surfactant in restricting particle growth.

Absorbance Spectra

Of paramount concern in nanofluid research and colloid chemistry is particle instability which was considered here by monitoring CuO concentration spectroscopically. Signals from 280-600 nm follow Beer's law with an extinction coefficient, corresponding to the maximum centered at 282 nm, of 2010 $M^{-1}\cdot cm^{-1}$ based on moles of CuO formula units or .0177 $ppm^{-1}\cdot cm^{-1}$ based on CuO/SOA mass concentrations. The observed maximum is in good agreement with those values previously reported.[11-13] The absorption spectrum of single crystal CuO has been shown to be dominated by transitions involving states localized within the energy gap; such transitions are described by Urbach's rule in which ε scales in a logarithmic fashion with energy.[14] Conversely, in many semiconductors, indirect transitions dominate and the optical properties of these materials are described by equation 2:[15]

$$\alpha = B(h\nu - \kappa)^2/h\nu \qquad (2)$$

where α is the absorption coefficient converted from the molar extinction coefficient ($\alpha = 2.3 \times 10^3\ \varepsilon\delta/F_w$, where δ is the density of CuO and F_w is its formula weight), B is a constant characteristic of a given material (1 in the case of CuO[16]), and κ is the band gap energy. It is common practice to plot $(\alpha h\nu)^{1/2}$ vs. $h\nu$ and extrapolate the linear portion of this curve to the x-intercept, the numerical value of which is equal to the band gap energy. Analysis of the optical data, at wavelengths longer than 280 nm, for particles prepared in the current study is indicative of an indirect transition with $E_g = 1.6$ eV as shown in Figure 3.7.

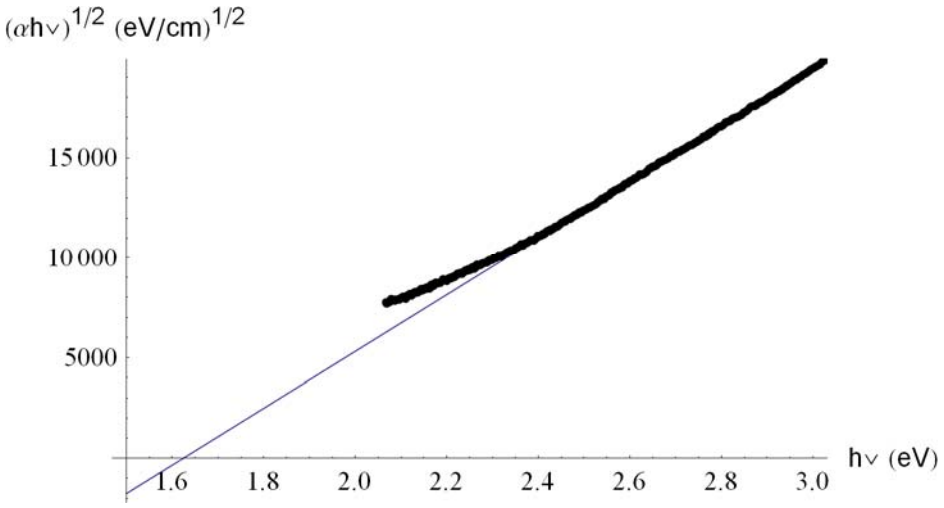

Figure 3.7. Analysis of the absorption spectrum of CuO/SOA colloids diluted in hexane according to an indirect optical transition.

Particle stability at room temperature was investigated by preparing colloids in octane at .072 (720 ppm), 1, 5, 10, and 20 % (mass), and in dodecane at 1, 5, 10, and 20% (mass). The lower concentration sample in octane was considered for long-term stability by diluting an aliquot to 60 ppm in hexane immediately after preparation and another more than eight months later and following the optical data. The corresponding spectra, shown in Figure 3.8, demonstrate that no change in absorbance between 280 and 600 nm occurred. The slight decrease in intensity below 280 nm suggests aggregation of the less stable particles with sizes ≤5 nm.[12] No precipitation was observed, either by visible or spectrophotometric inspection, over this extended period of time indicating remarkable stability at room temperature and at fairly low concentration. The higher concentration samples in both dodecane and octane were also periodically analyzed after dilution to 60 ppm in hexane. After a period of 10 days no precipitation occurred in any sample.

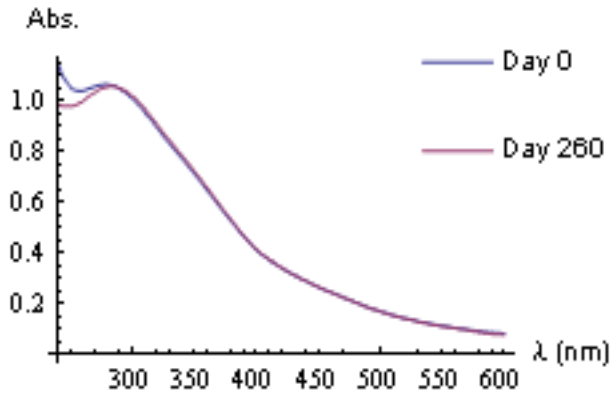

Figure 3.8. Absorbance spectra of CuO/SOA in octane demonstrating the stability of the particles at room temperature.

In order to determine the affect of colloid heating and cooling on particle stability, aliquots of the dodecane and eicosane systems were taken before and after one thermodynamic cycle, diluted to 60 ppm in hexane (based on starting concentration), and absorbance spectra recorded. The percent loss in particle concentration was taken as the change in absorbance at 282 nm. The experimental error was determined by repeating the dilution procedure for a 20% (mass) sample in dodecane 10 times. After one thermodynamic cycle no significant precipitation had occurred in either sample; any reported loss was well within experimental error, as shown in Table 3.1.

	Dodecane	Eicosane
1% CuO/SOA	−0.4 ± 3%	−5.6 ± 9%
5% CuO/SOA	−1.5 ± 3%	−2.0 ± 9%
10% CuO/SOA	1.3 ± 3%	3.9 ± 9%
20% CuO/SOA	−2.2 ± 3%	−3.8 ± 9%

Table 3.1. Percent precipitation for the CuO/SOA systems after one cycle of cooling and heating. Reported change is within experimental error indicating that no precipitation of CuO/SOA occurred during one thermodynamic cycle in either system.

Further investigation of the stability as well as thermodynamic properties of these particles was conducted in dodecane and eicosane, the latter of which experiences a phase change over the temperature range of interest. One control, consisting of only solvent, and four colloids were prepared in amounts of 1, 5, 10, and 20% by mass and labeled 1D-4D and 1E-4E for the dodecane and eicosane systems, respectively. Specific heat capacities (J/g/°C) were calculated according to equation 3

$$C_p = \left[\frac{60\,E}{Hr}\right] \times \left(\frac{\Delta h}{m}\right) \tag{3}$$

where *E* is the dimensionless cell calorimetric sensitivity constant at a given temperature, *Hr* is the heating rate, Δh is the difference in heat flow between the sample and reference which is found as the y-axis deflection in the DSC heat flow vs. temperature plot, and *m* is the mass of sample.[10] For both systems the measured values were fit to linear functions and extrapolated to zero in order to obtain heat capacity functions over the desired temperature range. Linear regression on these values was performed with an R^2-value of no less than 0.985 and a minimum of four data points per function. In the case of eicosane, data were fit to a piecewise function to accommodate the phase change. Enthalpies (J/g) were obtained by integrating the obtained functions according to equation 4:[17]

$$\Delta H = \int_{T1}^{T2} C_p dT + \Delta H_{fus} \tag{4}$$

where ΔH_{fus} is the enthalpy of fusion at 1 atmosphere. The quantity of interest, however, is the heat, ΔQ (J/g), which can be obtained by combining equations 4-6. When the temperature of

$$\Delta H = \Delta U + \Delta PV \tag{5}$$

$$\Delta U = \Delta Q + \Delta W \tag{6}$$

dodecane is raised from 0 to 100 °C at 1 atm, a volume change of 1.4×10^{-7} m^3/g occurs which corresponds to -14 mJ/g of work.[18] The same transition in eicosane results in -11.8 mJ/g.[19,20] Thus, with negligible change in volume or work, ΔPV and ΔW become zero to yield equation 7.

$$\Delta Q = \int_{T1}^{T2} C_p dT + \Delta H_{fus} \tag{7}$$

Thermodynamic measurements were performed not only on the colloids and solvents but on the particle components as well with unmodified CuO possessing the lowest heat capacity (component measurements were obtained using a particle sample that consisted of 71 % (mass) CuO). Figure 3.9 shows the corresponding heat capacity vs. temperature plots and demonstrates a trend of decreasing heat capacity with increasing particle concentration in both solvents, the values for which are tabulated in Table 3.2. With increasing particle concentration, the eicosane samples exhibited a decrease in ΔH_{fus} (Table 3.3) which is expected because as an extensive property, the of latent heat corresponding to the phase change observed at 35 °C depends only on the amount of eicosane present.[17]

The molal freezing point depression constant for eicosane was calculated according to the ideal solution equation 8:[17]

$$\Delta T_f = -\frac{R \cdot M_{solvent} \cdot \left(T_{fusion}\right)^2}{\Delta H_{fus}} \cdot m_{solute} = -K_f \cdot m_{solute} \tag{8}$$

where ΔT_f is freezing point depression, R is the ideal gas constant, $M_{solvent}$ is the molecular weight of the solvent in kg/mol, T_{fusion} is the melting point of the pure solvent in K, ΔH_{fusion} is the solvent fusion enthalpy in J/mol, m_{solute} is the molality of the solute, and K_f is the freezing point depression constant. Analysis of ΔT_f for eicosane in sample 4E resulting from the presence of SOA alone predicts a depression of 0.78 K. As can be seen from the values listed in Table 3.3, however, the melting temperature across five sample concentrations experienced a mean square deviation of only 0.1 °C and a maximum deviation of 0.3 °C indicating that SOA is not present as molecular species freely dissolved in eicosane. This in turn supports the interpretation that SOA interacts strongly with the CuO particles which limits the solute-solvent interactions which are responsible for freezing point depression.

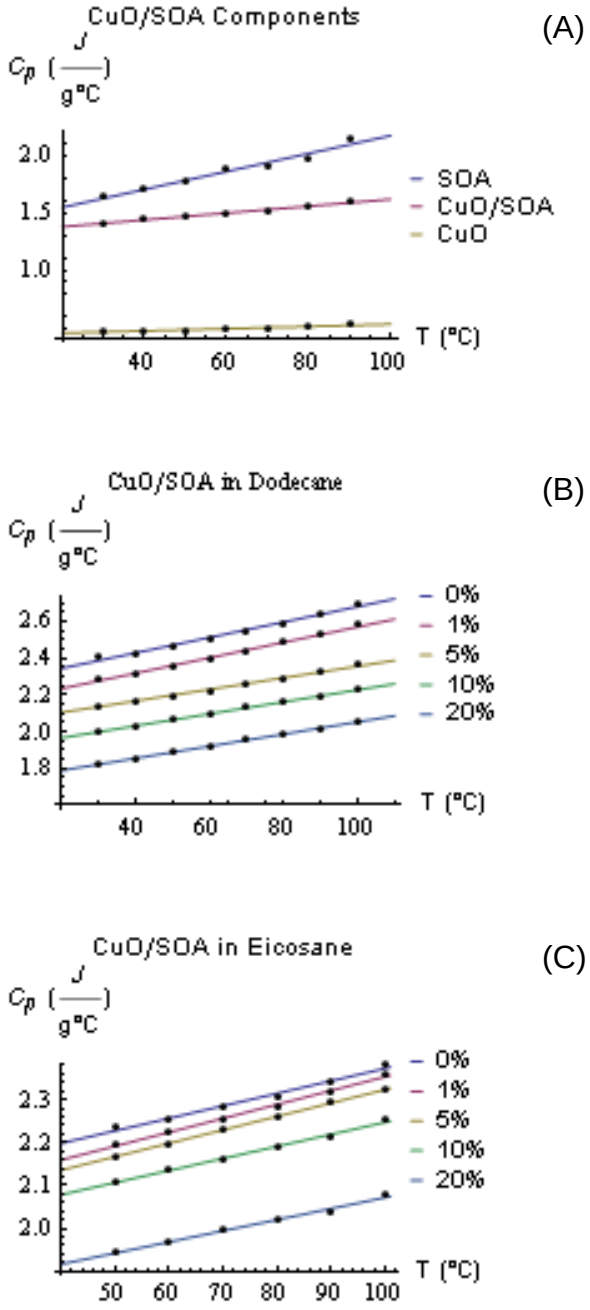

Figure 3.9. Specific heat capacity vs. temperature plots for the CuO/SOA components (A), CuO/SOA in dodecane (B), and CuO/SOA in eicosane (C).

	30°C	40°C	50°C	60°C	70°C	80°C	90°C	100°C
CuO (ref.)	0.578	0.587	0.594	0.601	0.608	0.614	0.619	0.624
CuO	0.473	0.473	0.475	0.480	0.495	0.511	0.531	0.529
SOA	1.642	1.705	1.775	1.880	1.915	1.966	2.153	2.175
CuO/SOA	1.409	1.444	1.470	1.498	1.525	1.559	1.593	1.619
Dodecane	2.403	2.428	2.464	2.507	2.547	2.591	2.639	2.696
1% CuO/SOA in Dodecane	2.286	2.321	2.355	2.398	2.437	2.484	2.529	2.580
5% CuO/SOA in Dodecane	2.143	2.171	2.196	2.225	2.256	2.292	2.327	2.363
10% CuO/SOA in Dodecane	2.001	2.034	2.063	2.096	2.133	2.161	2.193	2.231
20% CuO/SOA in Dodecane	1.824	1.856	1.887	1.920	1.954	1.991	2.020	2.054
Eicosane	1.947	2.198	2.236	2.256	2.280	2.305	2.339	2.385
1% CuO/SOA in Eicosane	1.990	2.159	2.196	2.222	2.254	2.285	2.320	2.358
5% CuO/SOA in Eicosane	1.926	2.136	2.167	2.196	2.231	2.261	2.294	2.321
10% CuO/SOA in Eicosane	1.862	2.079	2.109	2.135	2.162	2.190	2.215	2.252
20% CuO/SOA in Eicosane	1.796	1.917	1.945	1.967	1.996	2.020	2.041	2.077

Table 3.2. Table of specific heat capacities (J/g/°C) for CuO/SOA samples and components.[21]

	ΔH_{fus} ($\frac{J}{g}$)	M.P. (°C)
0% CuO/SOA	249.1	35.3 ±0.1
1% CuO/SOA	240.6	35.6 ±0.1
5% CuO/SOA	226.6	35.4 ±0.1
10% CuO/SOA	218.4	35.3 ±0.1
20% CuO/SOA	181.7	35.3 ±0.1

Table 3.3. Enthalpies of fusion (latent heat) and melting points associated with the eicosane blank and samples 1E-4E.

The efficacy of nanofluids is typically characterized by their thermal conductivity, *k* (W/m/K), for which several test methods exist. Each technique shares a common goal of measuring the migration of heat down a temperature gradient as a function of time and distance but in the absence of convection. The most common and most widely accepted technique appears to be the transient hotwire method in which a metal wire is vertically suspended in the center of a cylindrical sample cell.[22-24] The metal wire is typically composed of Pt because of the well characterized resistance/temperature relationship of this material and serves as both a heat source and a thermocouple with the distance term arising from the length of the wire. Another method involves using a plane heater and a heat-loss measuring layer separated by a volume of sample

with the length term arising from the separation distance which is kept minimal in order to reduce convection.[25] When considering the extent to which particles enhance the thermal properties of a nanofluid, relative thermal conductivity is the parameter of interest which is achieved by dividing $k_{nanofluid}$ by $k_{solvent}$.

The methods outlined above are designed to minimize or completely eliminate convective heat transport and measure exclusively thermal conductance. On the other hand, the current procedure, described in the experimental section, is an alternative to those previously discussed whereby conductive and convective modes of heat transfer are both incorporated. The rate of heat transfer as the bulk material is heated or cooled through a wide temperature range is determined according to equations 9 and 10

$$r = \left(\frac{\Delta Q}{\Delta T}\right) \cdot \left(\frac{\Delta T}{\Delta t}\right) = \frac{\Delta Q}{\Delta t} \tag{9}$$

$$r_{rel} = \frac{r_s}{r_{sol}} \tag{10}$$

where r is a general term describing the rate of heat transfer (J/g/sec) in unspecified media, T is the temperature in ºC, and t is the time in seconds. Values of r for specific media arise from equation 9 to produce equation 10 where r_{rel} is the relative heat transfer rate, r_s is the rate of heat transfer in the prepared sample, and r_{sol} is the rate of heat transfer in the solvent. $\Delta Q/\Delta T$ is determined by DSC whereas $\Delta T/\Delta t$ is obtained from the cooling curve plots. The cooling curve measurements were conducted between 0 and 100 ºC and the temperature limits for integration for ΔQ were 10 and 95 ºC. Equation 11 illustrates Newton's Law of Cooling which states that the cooling rate of a medium is proportional to the product of a constant, γ, and the difference in temperature between the surroundings and medium.[8]

$$\frac{\Delta Q}{\Delta t} = \gamma \cdot \left(T_{surroundings} - T_{medium} \right) \tag{11}$$

No cooling curves fit readily to any simple function such as equation 11. Thus, with cooling and heating treated as path-independent processes, two points, 95 & 10 ºC for the cooling process and 10 & 95 ºC for the heating process, were taken from each curve to obtain ΔT/Δt in order to lead to the desired ΔQ/Δt values.

Dodecane System

The results of the cooling and heating experiments indicate that the addition of CuO/SOA particles to a hydrocarbon solvent inhibits the rate of heat transfer through the resulting colloid. Figure 3.10 shows the cooling curve plots for samples 1D-4D and the solvent blank. Note that the two heat sources are significantly different thus producing different rates for cooling and heating. The influence of the particles in the cooling and heating portions, expanded in Figures 3.10B and 3.10C, becomes increasingly apparent because of the reduced temperature difference between the sample and surroundings. It is clear upon visual inspection of these plots that an increase in particle concentration produces a decrease in the dT/dt slope. ΔQ/Δt rates, $\pm r$, and relative heat transfer rates, $\pm r_{rel}$, were determined according to equations 9 and 10, respectively, and are tabulated in Table 3.4A with the maximum inhibition of 82% occurring in the dodecane sample containing 20% (mass) CuO/SOA.

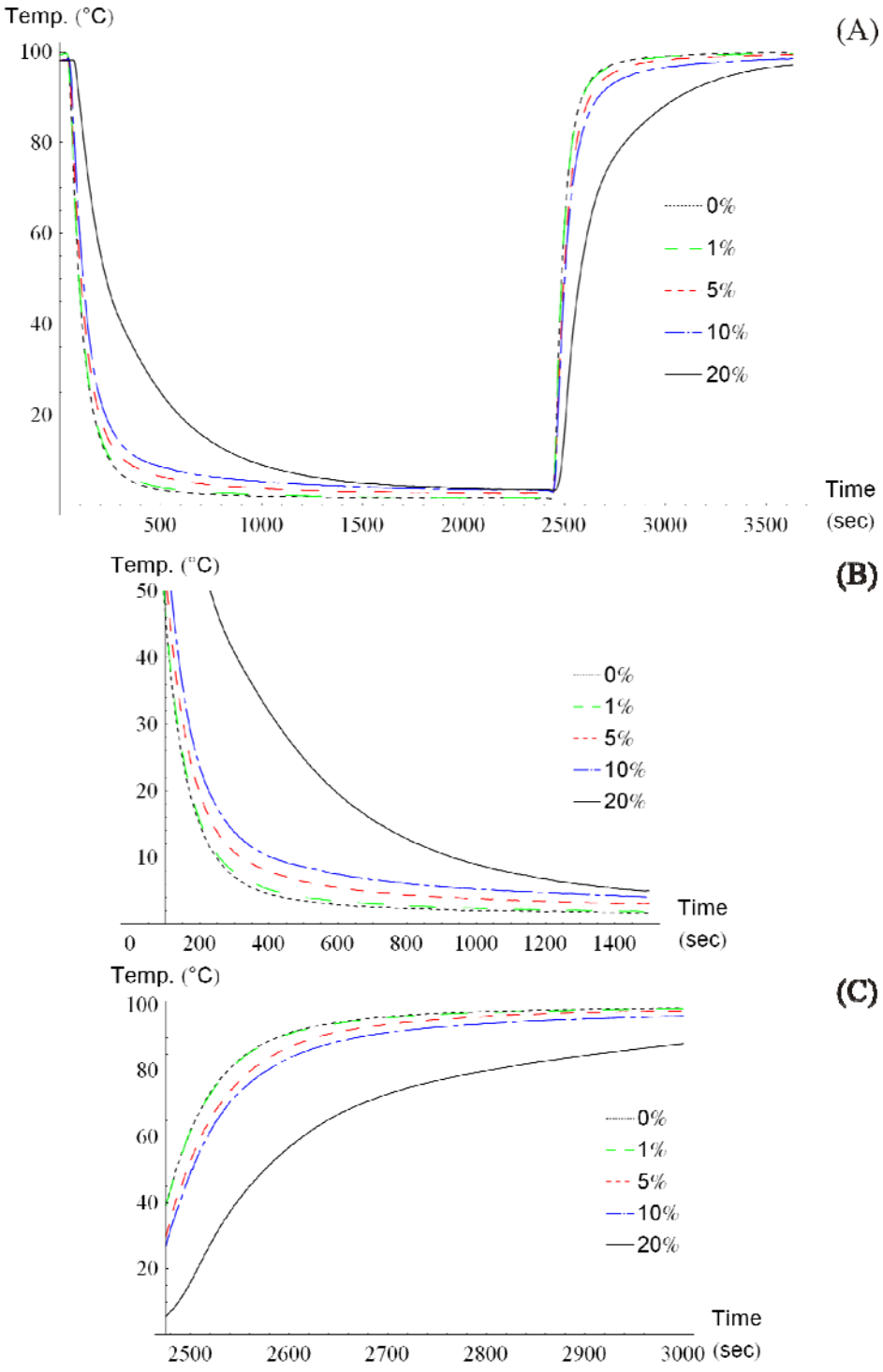

Figure 3.10. Temperature vs. time plots ("cooling curves") obtained during one thermodynamic cycle for the dodecane system corresponding to samples 1D-4D as well as the solvent blank. (A) Full cycle, (B) expansion of the cooling and (C) heating regions.

(A)

	$-r\ (\frac{J}{g \cdot s})$	$r\ (\frac{J}{g \cdot s})$	$-r_{rel}$	r_{rel}
0%	1.061	1.041	1.000	1.000
1%	1.017	1.014	0.959	0.974
5%	0.444	0.688	0.418	0.661
10%	0.501	0.464	0.472	0.446
20%	0.190	0.189	0.179	0.181

(B)

	$-r\ (\frac{J}{g \cdot s})$	$r\ (\frac{J}{g \cdot s})$	$-r_{rel}$	r_{rel}
0%	0.637	1.367	1.0	1.0
1%	0.615	1.060	.966	.780
5%	0.613	0.629	0.962	.460
10%	0.583	0.552	0.916	.403
20%	0.474	0.331	0.744	.242

Table 3.4. Rates and relative rates (dimensionless) of heat transfer for the dodecane (A) and eicosane (B) systems where $-r$ and $-r_{rel}$ correspond to the cooling and relative cooling rates, respectively, from 95-10 °C whereas r and r_{rel} correspond to the heating and relative heating rates from 10-95 °C.

There exists a seemingly unanimous consensus within the literature which states that the dispersion of nm-sized CuO particles in a given solvent will produce a nanofluid with enhanced thermal conductivity.[2-4,26-35] The current results, however, clearly demonstrate an inhibition of heating and cooling rates when both conductive and convective modes of heat transfer are involved. A significant increase in solvent viscosity becomes apparent upon the addition of CuO/SOA in the amounts used during this investigation. This increase is capable of drastically impeding convection that might overwhelm a smaller increase in thermal conductance.

Eicosane System

The contribution of CuO/SOA particles to the heat transport properties of eicosane-based nanofluids displays the same inhibiting trend as the dodecane colloid while the system exists in

the liquid phase. Figure 3.11 shows the cooling curves for samples 1E-4E and the solvent blank. $\Delta Q/\Delta t$ rates and relative heat transfer rates were determined in the same manner as the dodecane system and the results are tabulated in Table 3.4B. The largest inhibition observed was 76% which also occurred in the sample containing the largest mass of dispersed particles. In both the heating and cooling portions of the curves, the liquid and phase change regions display the most significant contribution from the suspended particles whereas the solid region remains relatively unaffected. The distinction between these two regions can be rationalized by considering the contribution of convection as in the case of the dodecane system. Again, a large decrease in convection overwhelms the relatively small increase in thermal conductivity while in the liquid phase. In the solid phase convective heat transfer is eliminated and conduction dominates. As seen in Figure 3.11, there is no significant change in the cooling or heating rates while in the solid phase which indicates that if there is an enhancement in thermal conductivity, the current technique is not capable of detecting it.

The area of the cooling curve corresponding to sample 4E where freezing occurs (Figure 3.11B) is a little later in time compared to the lower concentrations whereas the melting portion (Figure 3.11C) is delayed. This can be understood by considering the simple model which is depicted in Figure 3.12. Prior to introducing the hot sample and cell into the 0 ºC bath, the

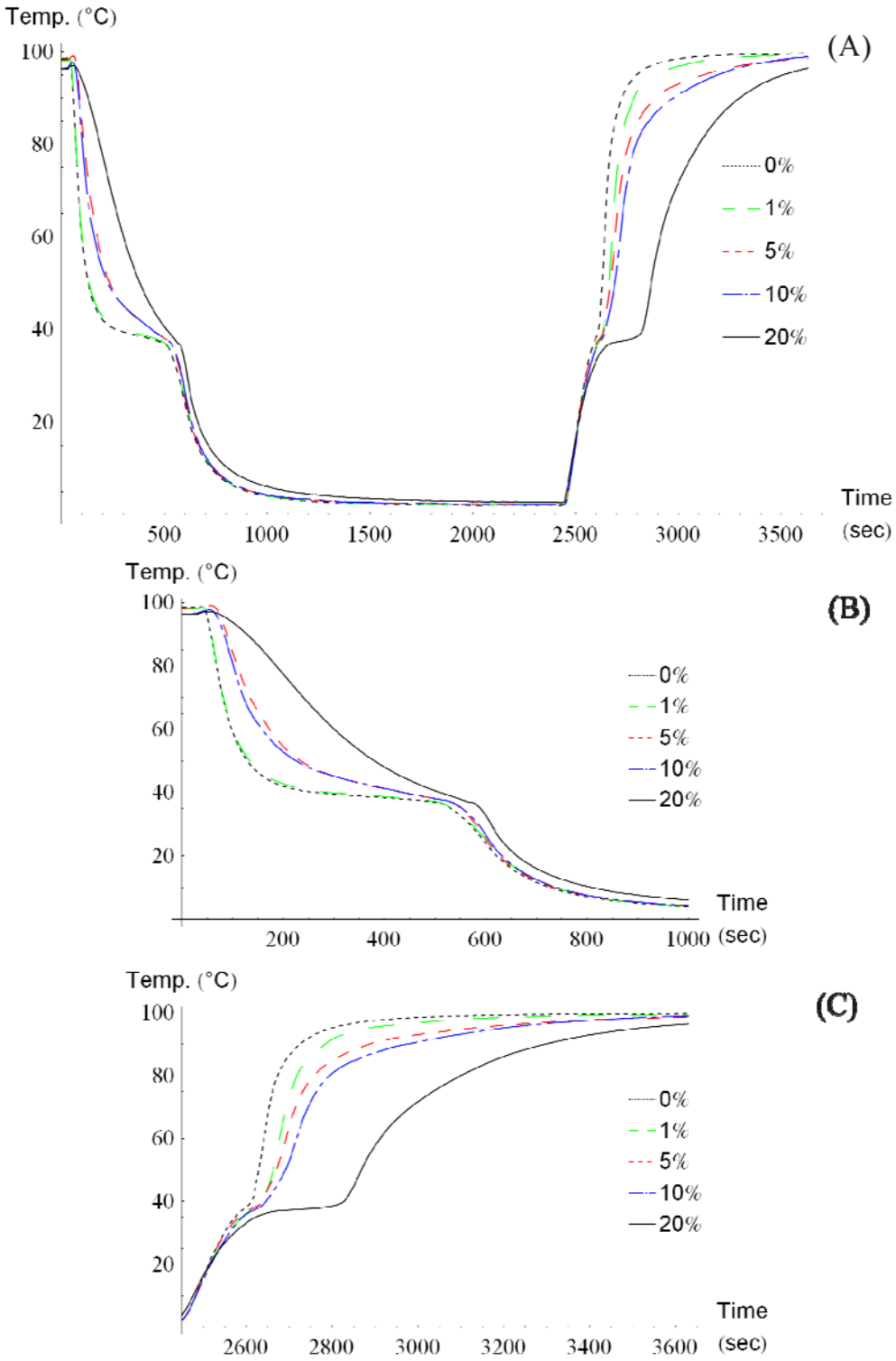

Figure 3.11. Cooling curves obtained during one thermodynamic cycle for the eicosane system corresponding to samples 1E-4E as well as the solvent blank. (A) Full cycle, (B) expansion of the cooling and (C) heating regions.

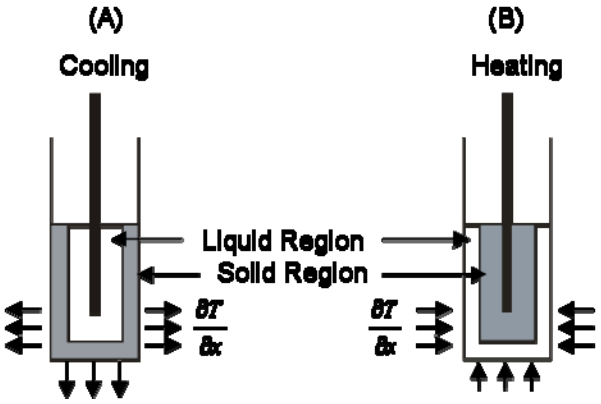

Figure 3.12. During cooling (A) and heating (B), regions of liquid and solid develop. The liquid region corresponds to slower heat migration due to a reduction in convective heat transport by the suspended CuO/SOA particles.

temperature distribution on a macroscopic level is uniform throughout, i.e. no significant gradient exists. Upon exposure to the lower temperature, the material nearest the sample cell wall rapidly looses thermal energy developing a temperature gradient between the wall and the thermocouple. But in the case of the unmodified eicosane, this gradient remains small provided that convection enables thermal energy to migrate rapidly through the liquid phase. A freezing front develops at the cell wall that moves significantly slower than the linear heat diffusion (Figure 3.12A). By the time this front begins to develop near the cell wall, sufficient energy has diffused through the sample to heat the layers adjacent to the thermocouple to near their melting temperature. In the corresponding region of the cooling curve for eicosane, the phase change is observed as a long, nearly horizontal transition. By the time freezing begins at the glass surface for sample 4E however, little temperature change has occurred near the thermocouple due to the inhibition of convective heat transfer by the particles. This results in a much larger temperature gradient. Heat now diffuses more slowly from the obstructed liquid into the developing solid

which causes the freezing front to migrate at a rate only slightly less than that of the heat diffusion. In this case, by the time the material adjacent to the thermocouple reaches its freezing point, only a small fraction of the sample remains in the liquid phase. This results in a very short transition in the corresponding region of the cooling curve for sample 4E. In the heating region of the eicosane cooling curves the trend is reversed. The absence of significant variation in the dT/dt slope below 35 °C with increasing particle concentration indicates that the particles exert little influence on the heat transfer rate through the solid. In the solid phase, the order of heat transfer rates becomes:

$$r_{solid}(1E) \approx r_{solid}(2E) \approx r_{solid}(3E) \approx r_{solid}(4E) \approx r_{solid}(\text{eicosane}) \quad (12)$$

where r_{solid} indicates the heat transfer rate of the corresponding sample in parentheses while in the solid phase. As a solid, the temperature gradient between the cell wall and the thermocouple surface remains fairly small for the blank as well as loaded eicosane samples. As a melting front evolves, however, the influence of particle loading becomes apparent. With increasing particle concentration, the phase transition becomes increasingly delayed. In the case of the blank, as the solid region is replaced by liquid, a negligible decrease in heat transfer rate is observed. In the cases of the loaded samples, however, the colloidal regions replacing the solid are loaded with particles which can reduce convection and slow the heat transfer rate. In the liquid phase, the order of heat transfer rates becomes

$$r_{liquid}(4E) < r_{liquid}(3E) < r_{liquid}(2E) < r_{liquid}(1E) < r_{liquid}(\text{Eicosane}) \quad (13)$$

where r_{liquid} is the heat transfer rate in the liquid phase of the corresponding sample in parentheses. As the liquid region grows, the rate at which heat is delivered to the remaining solid, and in turn, the layers adjacent the thermocouple, decreases due to the increasing volume of scattering medium, as illustrated in Figure 3.12B. Therefore, as r_{liquid} decreases, the time

required for the bulk phase change to occur increases. This result is independent of the inverse proportionality between latent heat and particle concentration (Table 3.3). The corresponding region of the cooling curve of sample 4E therefore becomes significantly broadened with respect to that of the control sample.

Conclusion

A synthesis method for the generation of hydrocarbon-soluble copper(II) oxide particles has been presented. Thermodynamic measurements clearly demonstrate that these particles inhibit the rate at which heat can travel through either dodecane or eicosane over a broad temperature range. In fact, the data show a very significant decrease in relative heat transport properties—as much as 82%—with increasing particle concentration. Adding particles to eicosane also significantly reduced the enthalpy of fusion of the solvent as well as the heating and cooling rates which suggests that these particles would poorly serve the purpose of enhancing the thermodynamic efficiency of phase change materials.

While thermal conductivity measurements have served as the benchmark criterion for characterizing nanofluids, the current investigation suggests that further measurements are necessary. The inhibition of convective heat transfer drastically overwhelms the much smaller enhancement of thermal conductivity when particle mass concentrations reach 1% or more. Current work is underway to produce a nanogel in which convection is significantly reduced.

References

(1) Trisaksri, V.; Wongwises, S. *Renewable Sustainable Energy Rev.* **2007**, *11*, 512-523.

(2) Zhu, H. T.; Zhang, C. Y.; Tang, Y. M.; Wang, J. X. *J. Phys. Chem. C* **2007**, *111*.

(3) Liu, M. S.; Lin, M. C. C.; Huang, I. T.; Wang, C. C. *Chem. Eng. Technol.* **2006**, *29*, 72-77.

(4) Lee, S.; Choi, S. U. S.; Li, S.; Eastman, J. A. *J. Heat Transfer* **1999**, *121*, 280-289.

(5) Li, C. C.; Chang, M. H. *Mater. Lett.* **2004**, *58*, 3903-3907.

(6) Kovtyukhova, N. I.; Martin, B. R.; Mbindyo, J. K. N.; Smith, P. A.; Razavi, B.; Mayer, T. S.; Mallouk, T. E. *J. Phys. Chem. B* **2001**, *105*, 8762-8769.

(7) Spanhel, L.; Anderson, M. A. *J. Am. Chem. Soc.* **1991**, *113*, 2826-2833.

(8) Newton, I. *Phil. Trans. Royal Soc. London* **1701**, *22*, 824-829.

(9) The National Research Council, In *Prudent Practices in the Laboratory: Handling and Management of Chemical Hazards*, The National Academic Press: Washington, D.C., 2001, Page 139.

(10) ASTM Standard E1269, 2005, "Standard Test Method for Determining Specific Heat Capacity by Differential Scanning Caloimetry," ASTM Internatiional, West Conshohocken, PA, 2005, DOI: 10.1520/E1269-05, www.astm.org.

(11) Borgohain, K.; Mahamuni, S. J. *J. Mater. Res.* **2002**, *17*, 1220-1223.

(12) Zhu, J.; Chen, H.; Liu, H.; Yang, X.; Lu, L.; Wang, X. *Mater. Sci. Eng., A* **2004**, *384*, 172-176.

(13) Chen, X. Y.; Cui, H.; Liu, P.; Yang, G. W. *Appl. Phys. Lett.* **2007**, *90*, 1-3.

(14) Marabelli, F.; Parravicini, G. B.; Salghetti-Drioli, F. *Phys. Rev. B: Condens. Matter* **1995**, *52*, 1433-1436.

(15) Mills, G.; Zongguan, L.; Meisel, D. *J. Phys. Chem.* **1988**, *92*, 822-828.

(16) Basov, N. G. In *Optical Properties of Semiconductors*, Consultant Bureau: New York, 1976.

(17) Noggle, J. *Physical Chemistry*, 2nd ed.; HarperCollins: New York, 1989.

(18) http://webbook.nist.gov/chemistry/fluid/, 9/14/2011.

(19) Dutour, S.; Daridon, J.-L.; Lagourette, B. *High Temperature-High Pressures* **2001**, *33*, 371-378.

(20) http://www.chemicalbook.com/ChemicalProductProperty_EN_CB1343496.htm, 23 Sep '11.

(21) Chase, M. W. J. *NIST-JANAF Thermochemical Tables, Fourth Edition*, **J. Phys. Chem. Data, Monograph 9**, 1998; pp 1-1951.

(22) Kestin, J.; Wakeham, W. A. *Physica* **1978**, *92A*, 102-116.

(23) Johns, A. I.; Scott, A. C.; Watson, J. T. R.; Ferguson, D. *Phil. Trans. R. Soc. London* **1988**, *A325*, 295-356.

(24) Roder, H. M. *J. Res. Nat. Inst. Stand. Technol.* **1981**, *86*, 457-493.

(25) Wang, B. X.; Zhou, L. P.; Peng, X. F. *Int. J. Heat and Mass Transfer* **2003**, *46*, 2665-2672.

(26) Choi, U. S. Enhancing Thermal Conductivity of Fluids with Nanoparticles. In *Developments and Applications of Non-Newtonian Flows*; Siginer, D. A., Wang, H. P., Eds.; ASME: New York, 1995; Vol. 66; pp 99-105.

(27) Ho, C. J.; Gao, J. Y. *Int. Commun. Heat Mass Transfer* **2009**, *36*, 467-470.

(28) Moghadassi, A. R.; Hosseini, S. M.; Henneke, D. E. *Ind. Eng. Chem. Res.* **2010**, *49*, 1900-1904.

(29) Lee, D.; Kim, J. W.; Kim, B. G. *J. Phys. Chem. B* **2006**, *110*, 4323-4328.

(30) Das, S. K.; Putra, N.; Theisen, P.; Roetzel, W. *J. Heat Transfer* **2003**, *125*, 567-574.

(31) Eastman, J. A.; Choi, S. U. S.; Li, S.; Yu, W.; Thompson, L. J. *Appl. Phys. Lett.* **2001**, *78*, 718-720.

(32) Jang, S. P.; Choi, S. U. S. *Appl. Phys. Lett* **2004**, *84*, 4316-4318.

(33) Kumar, D. H.; Patel, H. E.; Kumar, V. R. R.; Sundararajan, T.; Pradeep, T.; Das, S. K. *Phys. Rev. Lett.* **2004**, *93*, 1-4.

(34) Xue, Q.; Xu, W. M. *Mater. Chem. Phys.* **2005**, *90*, 298-301.

(35) Yu, W.; Choi, S. U. S. *J. Nanopart. Res.* **2003**, *5*, 167-171.

Chapter 4

Photochemical Generation of Nanometer-Sized Cu Particles in Octane

Introduction

The use of light to initiate the reduction of metal salts provides a well-known method for the generation of small metal particles in either liquid or solid media.[1] The direct irradiation of aqueous $AgClO_4$ and $HAuCl_4$ by UV photons in the presence of electron donors, such as an alcohol[2] or amine,[3] produces colloidal silver and gold. While some copper(II) complexes can undergo reduction via direct excitation, a photosensitizer is more commonly needed.[4] Acetone,[5,6] acetophenone,[7] benzophenone,[8-11] anthraquinone derivatives,[12] and sulfonated poly(ether ether ketone)[13] have been employed as photosensitizers in the presence of alcohols as H atom donors in the reduction of Cu^{2+} ions. Benzophenone has also been used in the photoreduction of aqueous silver[14,15] salts as well as $HAuCl_4$ dispersed in PVA films.[16] In addition to alcohols, primary, secondary, and tertiary amines containing α-hydrogen can serve as H atom donors for abstraction by triplet ketones.[17] The current work describes a method for the production of metallic copper nanoparticles whereby benzophenone is utilized as a photosensitizer to abstract hydrogen from a sacrificial donor to subsequently reduce cupric ions dissolved in the form of anhydrous copper(II) oleate. A comprehensive mechanism is also postulated in addition to the associated rate dependencies.

Experimental

Caution: Piranha etch is a hazardous material that should only be handled by trained personnel using appropriate personal protective measures. Waste from this material should only

be disposed of by approved procedures.[18] Oleic acid (OA), methanol, toluene, octane, NaOH, benzophenone (BP), $Cu(NO_3)_2 \cdot 2.5H_2O$, and additional organic solvents were obtained from Aldrich while oleoylsarcosine (OS) was purchased from TCIAmerica. Rigorous purification of OS proved to be crucial to obtaining reproducible results. In order to remove water and other volatiles, the sarcosine was twice diluted in excess dry toluene followed by solvent removal under vacuum and partial pressure distillation for 4 hours. BP was recrystallized from methanol and water while the remaining reagents were used as received. Prior to use, octane was scanned from 900 – 200 nm to ensure the absence of light absorbing impurities. All glassware was treated with fresh piranha etch, rinsed thoroughly, and oven dried. Water used during the synthesis of copper(II) oleate (to be described) was supplied by a Barnstead EasyPureII ultrafiltration system. A Shimadzu UV-2450 UV-Vis spectrophotometer was used to follow the cupric ion consumption and particle formation. Metal concentrations were determined using a Varian AA240 flame atomic absorption (FAA) spectrometer. TEM images for particle size and morphology determination were obtained on a Zeiss EM10 Transmission Electron Microscope at 60keV while electron diffraction data were obtained using a Hitachi HF-2000 TEM at 200keV. Ni/formvar grids were coated by evaporating a single drop of 0.5 mM Cu colloid in octane inside of a glove bag at 1 atm of N_2 and particle size distribution involved analysis of more than 400 particles.

In order to obtain an anhydrous copper(II) carboxylate capable of being dissolved in nonpolar solvents, a synthetic method was developed by modification of literature techniques and warrants a brief discussion.[19] An aqueous solution of sodium oleate (SOA) was prepared by stirring OA with equimolar NaOH in deionized water at 100 °C for 30 minutes. At room temperature, 7.225 mmol of SOA were added to 150 mL of deionized water and the pH adjusted

to 10.5 with 0.1 M NaOH. In order to achieve the desired SOA:Cu^{2+} mole ratio of 1.20:1, 6.019 mmol of $Cu(NO_3)_2$ were added to the surfactant solution under vigorous stirring. The reaction proved to be sensitive to both pH and mole ratio and under non-ideal conditions, an undesirable product was formed that appeared as a floating, light blue solid. A successful reaction resulted in a dark green precipitate which conveniently adhered to the walls of the pyrex beaker, as well as the stir bar, allowing easy isolation by decanting the liquid phase. The collected solid was rinsed thoroughly with deionized water and dried under vacuum at 50 ºC for 12 hours. Purification steps were conducted below 60 °C to prevent decomposition of the complex.[19] Removal of complexed water was achieved by refluxing in anhydrous toluene at 40 ºC under partial pressure for an additional 12 hours with periodic addition of dry solvent to maintain a relatively constant volume. Toluene was ultimately removed in a vacuum oven at 50 ºC under a partial pressure of N_2 for several hours beyond dryness to ensure complete evaporation. The resulting product, which appeared as a very dense, green, wax-like solid, was immediately transferred to a nitrogen-filled glove bag, weighed, and dispersed in anhydrous octane by the aid of mechanical stirring.

Photochemical reductions were conducted in a 1 cm pathlength quartz cuvette (Starna Cells) fitted with a quartz-to-Pyrex graded seal. Samples were prepared in the optical cell under nitrogen, sealed with a rubber septum, and agitated for 10 seconds. Irradiation was achieved by vertically and horizontally centering the cell inside a Rayonet 100 circular illuminator equipped with 16 RPR-3500A lamps generating photons of $\lambda = 350 \pm 15$ nm and chemical actinometry was conducted using Aberchrome 540.[20] In order to avoid undesirable sample illumination during the course of preparation and handling, room light was replaced by low intensity red light.

Results and Discussion

Due to sensitivity of copper particles to water and the need for ready dissolution in nonpolar media, the formation of an anhydrous cupric salt was imperative. The absence of a peak near 3500 cm^{-1} in an IR spectrum of the prepared copper(II) carboxylate deposited on KBr disks confirms the anhydrous nature of the complex. Further evaluation of the purity of the cupric salt was achieved by first dissolving a known mass of sample in a specified volume of solvent to obtain a solution of known mass concentration. The resulting solution was then analyzed for molar concentration of Cu via FAA spectroscopy and comparison of these two values revealed a calculated molar mass of 626.5 g/mol which matches precisely to the theoretical value for the $Cu(oleate)_2$ complex. The complex initially formed likely assumes the structure shown in Figure 4.1 where R = $(CH_2)_7CH{=}CH(CH_2)_7CH_3$, the hydrocarbon tail of oleic acid, and L = water, which is removed during the purification process.[19] Evidence for a binuclear structure is illustrated in the absorbance spectra of $Cu_2(oleate)_4$ dissolved in octane which is presented in Figure 4.2A. The peak centered at 670 nm (ε = 200 $M^{-1}\cdot cm^{-1}$) corresponds to Cu(II) transitions whereas the transition located at 370 nm (ε = 70 $M^{-1}\cdot cm^{-1}$) has been assigned to transitions centered on the metal-metal bond.[21] Upon addition of OS in concentrations at least twice that of the metal, the extinction maximum of the cupric salt shifts from 670 to 720 nm seemingly due to tetragonal distortion .[22] Furthermore, the peak at 370 nm disappears suggesting that the dimer decays into the monomeric species shown in the inset of Figure 4.2B. The great affinity of cupric ions for nitrogen-containing ligands enables coordination of OS, an amide, into the axial positions of the Cu^{2+} center. In a study of the Jahn-Teller effect, similar shifts in both λ_{max} and absorbance intensity were observed upon the addition of up to a 100 fold excess of

various ligands capable of occupying the axial positions of equatorial bound copper(II) complexes with the large excess being necessary to overcome the dissociation equilibrium.[23]

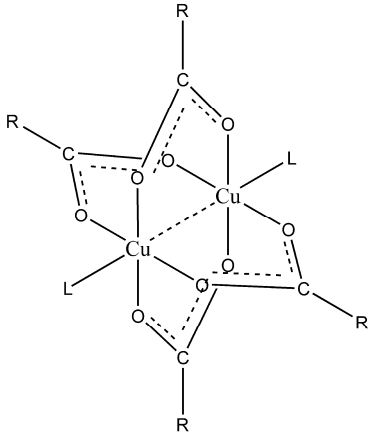

Figure 4.1. Structure of the cupric oleate prepared during the current investigation where R corresponds to the hydrocarbon tail of oleic acid and L corresponds to either water or OS.

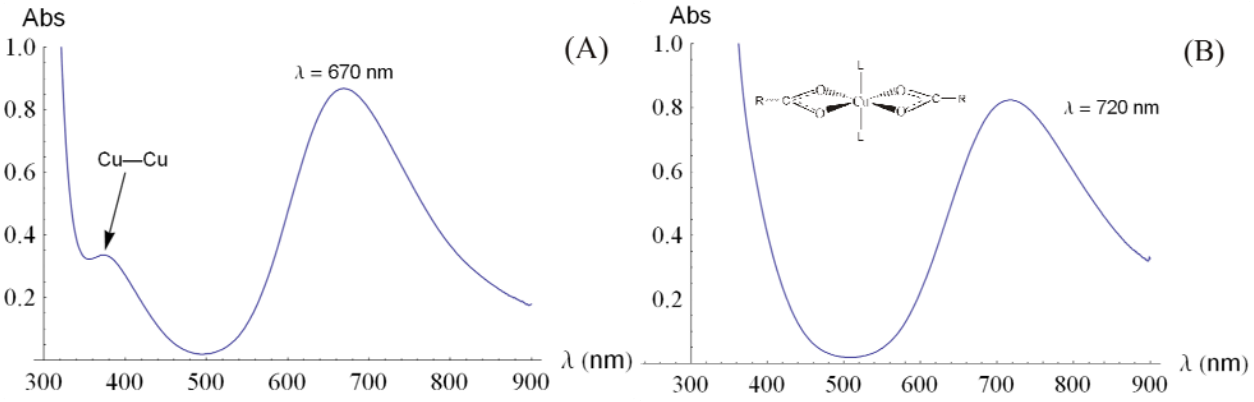

Figure 4.2. Absorbance spectra of (A) 5 mM copper(II) oleate in octane. Evidence for the binuclear structure of the cupric salt is provided by the peak centered at 370 nm which vanishes upon the addition of excess OS (B) which also involves a shift in λ_{max} from 670 to 720 nm. The spectral shifts are expected to result from the dissociation of the complex into the monomeric species shown in the inset of (B) where L thus corresponds to OS.

Irradiation of $Cu(oleate)_2$ with 350 nm photons in the presence of benzophenone and oleoylsarcosine in octane resulted in metal particles of the nm-size range which produce a deep,

burgundy red color. The same experiment conducted in the absence of BP produced very sparse reduction of Cu^{2+} to Cu^{+}, and no formation of Cu, but over the time scale of several hours rather than seconds. Visual inspection indicated that colloids stored under nitrogen showed no evidence of flocculation after four weeks and required a minimum of 12 h to decay upon exposure to air. The typical synthesis involves colloid preparation in octane but upon removal of the solvent, the particles can be redispersed in a variety of dry, low dielectric media such as chloroform, carbon tetrachloride, hexane, or toluene. Figure 4.3A presents an electron micrograph of the prepared Cu particles from which fairly spherical morphology can be observed. Size distribution ranged from 8 to 14 nm with a mean size of 11 nm, as shown in the histogram offered in Figure 4.3B.

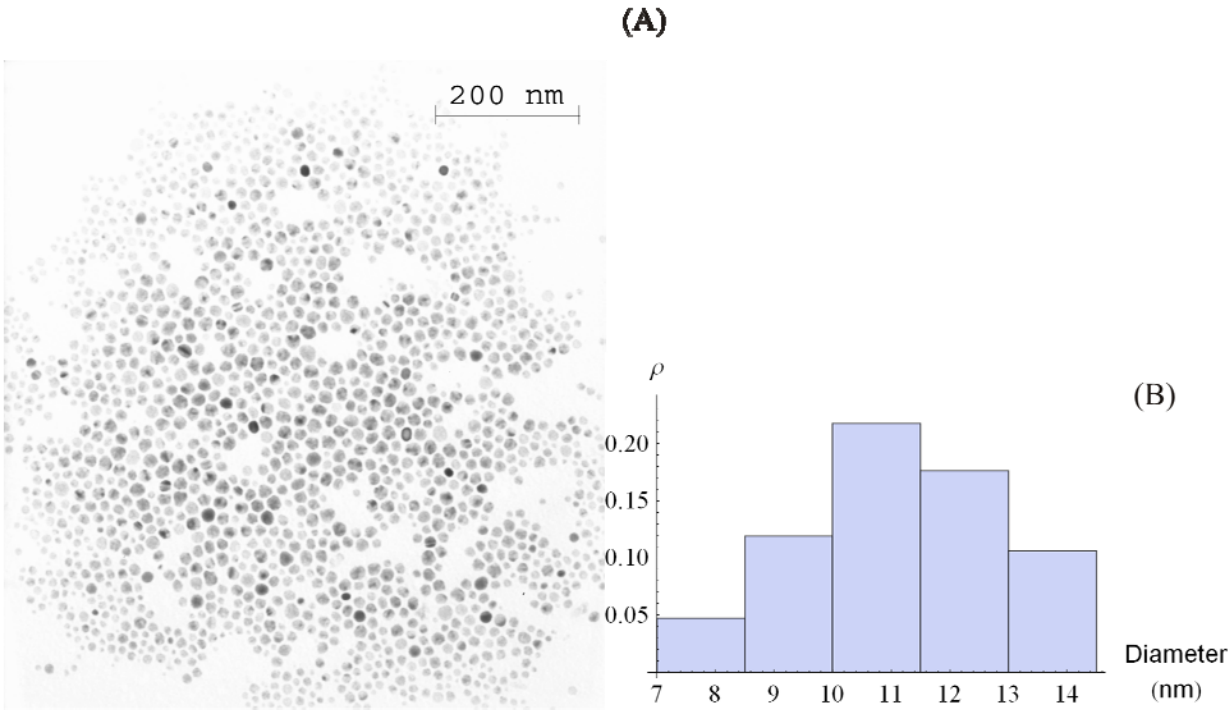

Figure 4.3. TEM image (A) of the photochemically generated Cu colloid and (B) the corresponding histogram of particle sizes.

The presence of crystalline, metallic copper was verified by electron diffraction; the Debye ring pattern shown in Figure 4.4 is in good agreement with the reflections listed in JCPDS card no. 4-0836. Further verification of the zero-valent state of copper included evaluation of the corresponding plasmon band centered at 565 which is typical of nm-sized, crystalline copper aggregates.[24] Figures 4.5A and 4.5B, respectively, depict the optical signals corresponding to

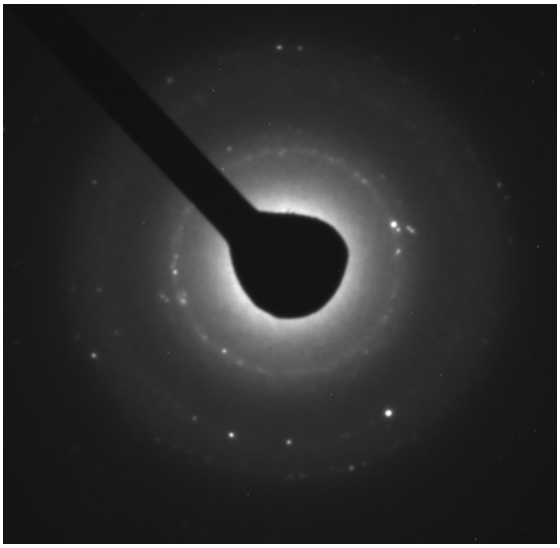

Figure 4.4 Electron diffraction pattern of the prepared Cu particles which is in good agreement with the reflections listed in JCPDS card no. 4-0836.

reactant consumption and product formation while the affiliated insets trace reaction progress with time. A one electron process is evident in that the Cu^{2+} peak decays completely (Figure 4.5A) prior to the emergence of the product peak (Figure 4.5B); however, the Cu^{+} species does not exhibit an electronic transition within the visible region. Figure 4.5C traces the oxidation process observed after pure O_2 is introduced into the solution while the associated inset emphasizes the Cu^{2+} peak before irradiation (i) and after introduction of oxygen (ii). The increase in optical density observed is likely due to the formation of light scattering products

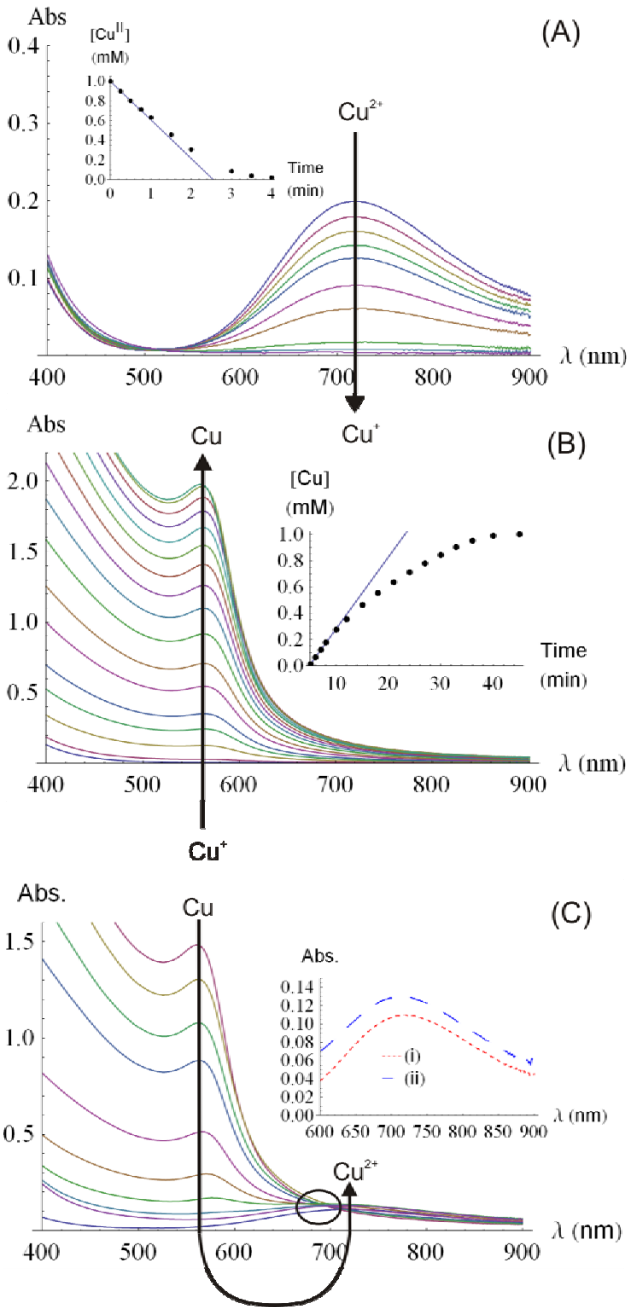

Figure 4.5. Copper(II) consumption (A) and Cu formation (B) in an octane solution containing 1 mM Cu^{2+}, 1 mM BP, 10 mM OS and with an average incident light intensity of 30 μM(hν)/s. The corresponding insets illustrate initial rate plots. Absorbance spectra (C) tracing the decay of a 0.75 mM Cu colloid (based on total Cu concentration) after the introduction of pure O_2 with the inset emphasizing the Cu^{2+} peak before irradiation (i) and after introduction of oxygen (ii).

generated during the redox processes which tend to create a baseline shift. The isosbestic point, circled in 4.5C, is indicative of a two electron process since the cupric peak begins to rise in concert with the decay of the Cu signal.

Reduction of aqueous Cu^{2+} ions typically involves a two stage process whose Cu^{+} intermediate experiences a visible electronic transition. When $CuSO_4$ was irradiated with gamma rays in the presence of H-atom donors, the initially blue solution, typical of Cu^{2+} ions, turned first to a pale yellow then finally to a pink resulting from the formation of Cu aggregates.[25] Analogous observations were made in the sulfonated poly(ether ether ketone)/poly(vinyl alcohol) (SPEEK/PVA) system in which the repeating polymeric chromophore unit consists of sulfonated benzophenone. The triplet state of SPEEK is similarly capable of H atom abstraction from PVA to produce the long lived, reducing SPEEK· radical. When an air-free SPEEK/PVA solution was irradiated with 350 nm photons in the presence of $CuSO_4$(aq), the solution also produced first a yellow color indicating the presence of a Cu^{+} species which was ascribed to CuOH.[13] Furthermore, in order to continue the reduction to atoms, protons generated during the oxidation of PVA were required to neutralize the cupric hydroxide and liberate Cu^{+}. Disproportionation thus produced Cu atoms and Cu^{2+} ions, the latter of which were again reduced by the photogenerated radicals with the highest quantum yield of Cu^{+} generation of 0.04. This two stage process observed in aqueous solution can be understood by considering the corresponding reduction potentials in which $E^{o}[Cu^{2+}/Cu^{+}] = 0.168$ V,[26] but $E^{o}[Cu^{+}/Cu_{(atom)}] = -2.7$ V.[27] Estimation of the potential for the SPEEK reduction to SPEEK· yielded $-1.2 \geq E^{o} \geq -1.4$ V,[13] meaning that α-hydroxy radicals derived from BP groups are unable to reduce Cu^{+} in H_2O. Unique to the current system, however, is not only the significantly larger quantum yields but the absence of Cu^{+} disproportionation which was confirmed by irradiating a

typical sample until the bulk of the metal was present in the cuprous form. After remaining in complete darkness for several hours, a subsequent absorbance spectrum revealed no change—neither Cu nor Cu^{2+} had formed in any measurable amount.

Cupric salt reduction is expected to occur via photogenerated radicals, a process which is initiated by the illumination of benzophenone to promote a nonbonding carbonyl electron to the π* LUMO (π*←n) generating a singlet excited state. Excited singlet BP, ^{1}BP*, rapidly undergoes intersystem crossing to yield $^3BP^*$ with near 100% efficiency.[28] The triplet state of benzophenone is capable of hydrogen abstraction from alcohols, amines, amides,[29] or hydrocarbons, the latter two of which are available in the current system.[30] The first step in $^3BP^*$ reduction by triethyl amine was suggested to be electron transfer from the non-bonding pair of nitrogen to form a short-lived contact ion pair, as shown below. [31,32]

$$^3BP^* + Et_3N \rightleftharpoons \left(BP^-, Et_3N^+\right) \quad (1)$$

In nonpolar media, ultrafast proton transfer follows to yield the ketyl and alkyl radicals.[33]

$$\left(BP^-, Et_3N^+\right) \rightarrow BPH\cdot + Et_2N\dot{C}HCH_3 \quad (2)$$

Hydrogen abstraction from amides is expected to occur by a process similar to the above model but with a slower rate due to the inductive effect of the adjacent carbonyl. The quenching of ^{3}BP* in acetonitrile by amides[29] occurred with a rate constant 2-3 orders of magnitude smaller than quenching in the same solvent by amines.[33] Triplet BP has also been shown to abstract hydrogen directly from alkanes to form α-hydroxy, or ketyl, and alkyl radicals.[34] Evaluation of

rate dependencies was conducted using the initial rate method, denoted r_i. Where appropriate, initial quantum yields, φ_i, are additionally reported where $\varphi_i = r_i/(\rho I_o)$, ρ = the fraction of photons absorbed by the chromophore at the given concentration, and I_o = light intensity recorded in μM(hν)/s. Unless noted otherwise, a standard reaction involves 1.0 mM Cu^{2+}, 1.0 mM BP, and 10 mM OS with an average incident light intensity of 30 μM(hν)/s. Presented in Figure 4.6 is a plot of initial rate vs. I_o whose slope is linear with light intensity for both Cu(II) consumption and Cu formation. Respective quantum yields are 1.76 and 0.208 which indicate that the first reduction occurs with a far greater efficiency.

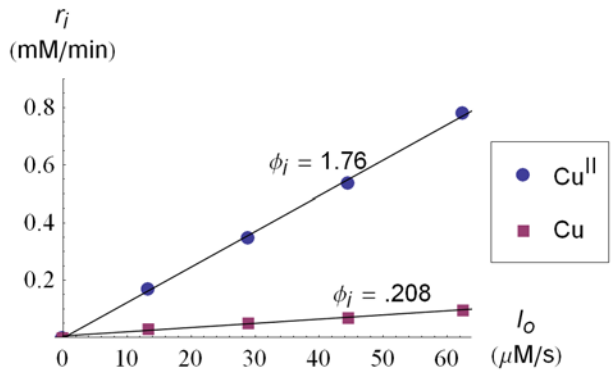

Figure 4.6. Plot of initial rate vs. incident light intensity obtained from solutions containing 1 mM BP, 1 mM Cu^{2+}, and 10 mM OS in octane. Initial quantum yields for Cu^{2+} consumption and Cu formation were 1.76 and 0.208, respectively.

Figure 4.7 demonstrates that the initial rate dependence on [BP] was first-order for both reduction products suggesting that radical formation is the rate limiting step. The dependence of initial rate on $[Cu^{2+}]_i$, shown in Figure 4.8, was also linear but with a negative slope suggesting that the cupric salt inhibits the first reduction while the second step appears unaffected. The corresponding quantum yield plot displayed the same decreasing trend signifying that the inhibition results from quenching of excited BP by Cu^{2+} ions which has previously been

observed.[13] The sarcosine stabilizer also showed a trend of linear inhibition as illustrated in Figure 4.9. A parallel trend was observed in the φ_i vs. $[OS]_i$ plot which implies that $^3BP^*$ does

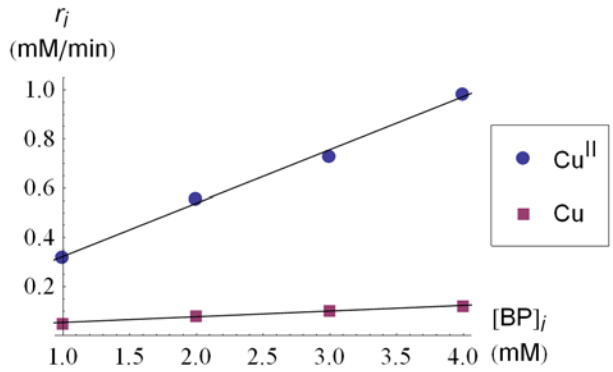

Figure 4.7. Initial rate as a function of initial BP concentration illustrating a first-order dependence for both reduction steps in the presence of 1 mM Cu^{2+}, and 10 mM OS in octane with an average incident light intensity of 30 μM(hν)/s.

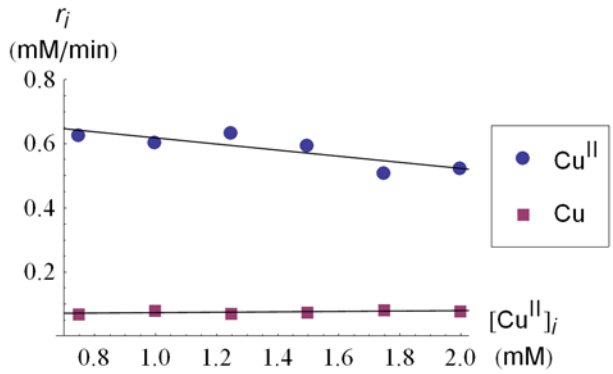

Figure 4.8. Dependence of initial rate on initial Cu^{2+} concentration in octane solutions containing 1 mM BP and 10 mM OS with an average incident light intensity of 30 μM(hν)/s.

react with sarcosine and perhaps forms a contact ion pair as expected, but the result does not lead to metal ion reduction. The ion pair can decay either by the back reaction of eq. 1 or the nascent ketyl and alkylamidyl radicals can rapidly combine.

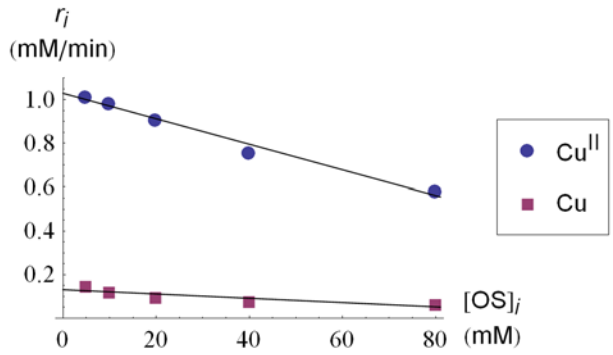

Figure 4.9. Variation of initial rate with initial OS concentration with 1 mM Cu^{2+}, 1 mM BP and with an average incident light intensity of 30 μM(hν)/s.

In order to consider the sacrificial H-atom source, a series of experiments were conducted in anhydrous toluene with varying amounts of added octane. Toluene is also capable of reducing excited BP but with a quantum yield of 0.4 which is much slower than aliphatic hydrocarbon.[35,36] Figure 4.10 presents a plot of initial quantum yield vs. octane concentration, in the presence of 1 mM Cu^{2+} and 10 mM OS, which reveals a sharp increase from 0.5 to 1.6 in going from 0 to 1 mM octane. A yield of 0.5 in the absence of octane implies that $^3BP^*$ oxidizes not only toluene but the hydrocarbon tail of either the cupric salt or the sarcosine. From 1 to 8 mM octane the quantum yield remains constant at $\varphi_i = 1.6$ implying that the hydrocarbon solvent serves as the dominant H-atom donor.

The simplest possible mechanism for the reduction of Cu^{2+} that explains the above data is that, under the assumption that radical formation is rate limiting, which is consistent with the first order dependence of r_i on I_o and [BP]. The initiating step is shown in eq. 3 whereas eqs. 4 and 5 entail the quenching of excited BP by the sarcosine and cupric complex, respectively,

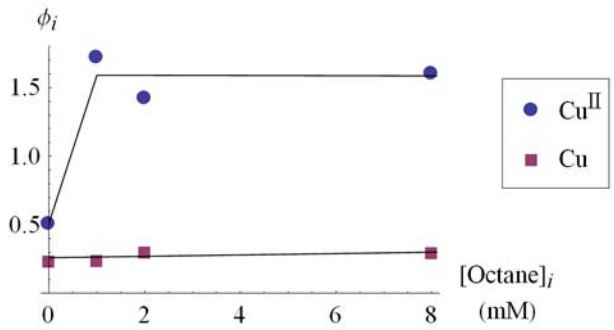

Figure 4.10. Initial quantum yield as a function of octane in toluene solutions containing 1 mM Cu^{2+}, 1 mM BP, 10 mM OS, and with an average incident light intensity of 30 μM(hν)/s.

and 6 illustrates the formation of ketyl and alkyl radicals (where RH_2 denotes octane and RH· the octyl radical). Reduction of the metal complex can occur by both steps 7 and 8.

$$BP + h\nu \rightarrow {}^1BP^* \rightarrow {}^3BP^* \quad (3)$$

$$^3BP^* + OS \xrightarrow{k_4} (BP^-, OS^+) \xrightarrow{k_4'} BP + OS \quad (4)$$

$$^3BP^* + Cu^{2+} \xrightarrow{k_5} BP + Cu^{2+*} \quad (5)$$

$$^3BP^* + RH_2 \xrightarrow{k_6} BPH\cdot + RH\cdot \quad (6)$$

$$BPH\cdot + Cu^{2+} \xrightarrow{k_7} BP + Cu^+ + H^+ \quad (7)$$

$$Cu^{2+} + RH\cdot \xrightarrow{k_8} Cu^+ + R + H^+ \quad (8)$$

According to this mechanism, Cu^{2+} is consumed via elementary steps 7 and 8 which results in the following rate law:

$$r = -\frac{d\left[Cu^{2+}\right]}{dt} = k_7[BPH\bullet][Cu^{2+}] + k_8[RH\bullet][Cu^{2+}] \quad (9)$$

Equation 10 represents the overall process of Cu^{2+} consumption. The oxidation of octane

$$^3BP^* + RH_2 + 2\,Cu^{2+} \xrightarrow{k_{obs}} BP + R + 2\,Cu^+ + 2\,H^+ \quad (10)$$

by $^3BP^*$ in CCl_4 at room temperature occurs with a rate constant of 4.7×10^5 M^{-1} s^{-1}. Assuming this reaction occurs with the same rate constant in octane, the same value is assigned to k_6.[34] Thus, $k_6' = k_6[C_8H_{18}] = 2.9 \times 10^6$ s^{-1} when the concentration of pure octane (6.15 M) is used which is a reasonable approximation provided that all reagents are present in low concentrations. Upon consideration of literature information for processes similar to steps 7 and 8, large values are anticipated for k_7 and k_8. Similar to step 7, reduction of Cu^{2+} by α-hydroxy radicals derived from 2-propanol occurs in water with a rate constant of $k = (0.5\text{-}1.6) \times 10^8$ M^{-1} s^{-1}.[37] Similarly, cupric ion reduction by alkyl radicals, such as 2-propyl· and *n*-butyl·, occurs in a 40% acetonitrile-acetic acid solution at 25.5 °C with respective rate constants of $k_{propyl} = 5 \times 10^6$ M^{-1} s^{-1} and $k_{butyl} = 3.1 \times 10^6$ M^{-1} s^{-1};[38] thus, step 8 is expected to occur with a rate constant of similar magnitude. These reductions involve Cu(II)-radical adducts, which probably form in the our system as well. The regeneration of BP in equation 7 was confirmed when irradiation of a solution containing a five-fold molar excess of $Cu(oleate)_2$ over BP resulted in complete metal ion reduction.

Using the steady state approximation, equations for the concentrations of BPH· and RH· under such conditions can be derived by considering equations 3-8

$$[BPH\bullet]_{ss} = \left(\frac{k_6'}{k_7[Cu^{2+}]}\right)\left(\frac{\varphi I_{abs}[BP]}{k_4[OS] + k_5[Cu^{2+}] + k_6'}\right) \tag{11}$$

$$[RH\bullet]_{ss} = \left(\frac{k_6'}{k_8[Cu^{2+}]}\right)\left(\frac{\varphi I_{abs}[BP]}{k_4[OS] + k_5[Cu^{2+}] + k_6'}\right) \tag{12}$$

where I_{abs} = the incident light intensity absorbed by benzophenone. By substituting (11) and (12) into (9), the following rate law can be obtained.

$$r = \frac{2\varphi I_{abs} k_6'[BP]}{k_4[OS] + k_5[Cu^{2+}] + k_6'} \quad (13)$$

Following the equation developed in eq. 13, Figures 4.11A and 4.11B exhibit the linear variation of inverse initial rate with [OS] and [Cu^{2+}], respectively. Evaluation of the corresponding slopes provide the values k_4 = 1.6 × 10^5 M^{-1} s^{-1} and k_5 = 6.1 × 10^5 M^{-1} s^{-1}. The H-atom abstraction reaction of step 6 to produce reducing radicals is able to favorably compete with the triplet deactivation processes because $k_6' > k_4$[OS] and also $k_6' > k_5$[Cu^{2+}]. The quenching by sarcosine is interesting because it can occur by either energetic or reactive quenching. Electron transfer is predominant in the case of amines but since OS is an amide, one would expect that the energy transfer (similar to step 5) to be competitive with reactive quenching.[29,33] Similar to step 5 is the deactivation of the $^3BP^*$ group of triplet excited SPEEK by Cu^{2+} ions which occurs in water with a rate constant of (2-3) × 10^9 M^{-1} s^{-1}.[13]

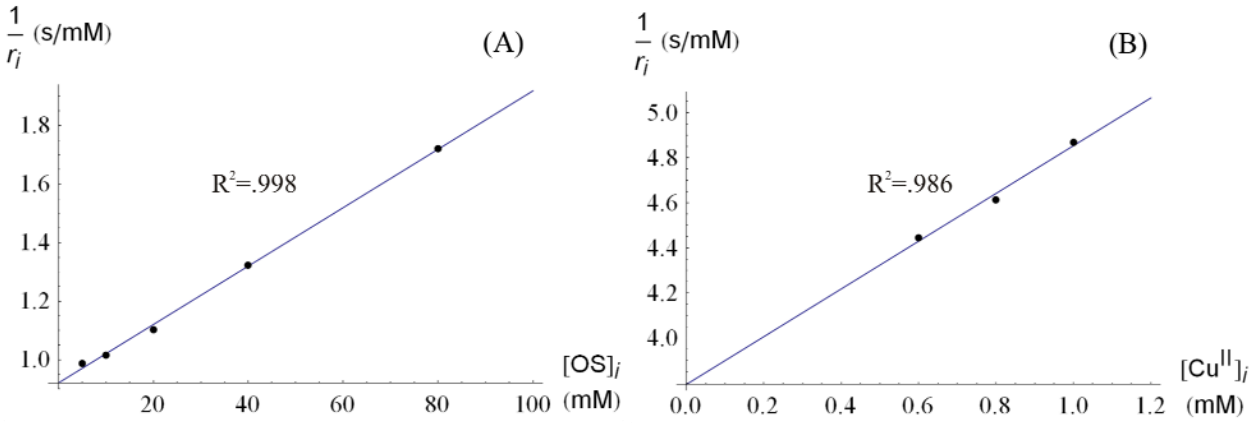

Figure 4.11. Linear variation of inverse initial rate with (A) OS and (B) Cu^{2+} concentrations in agreement with equation 13. The corresponding slopes provide the values $k_4 = 1.6\times10^5\ M^{-1}\cdot s^{-1}$ and $k_5 = 6.1\times10^5\ M^{-1}\cdot s^{-1}$.

When solutions containing $[Cu_2(oleate)_4]$ < 0.6 mM (total Cu) were irradiated in the absence of OS, initial quantum yields in excess of three were observed for Cu^{2+} reduction, as shown in Figure 4.12, while metal ion concentrations from 0.6 to 1 mM resulted in a fairly constant φ_i near 2. While the same trend was not observed in Cu^{+} reduction, an increase in the

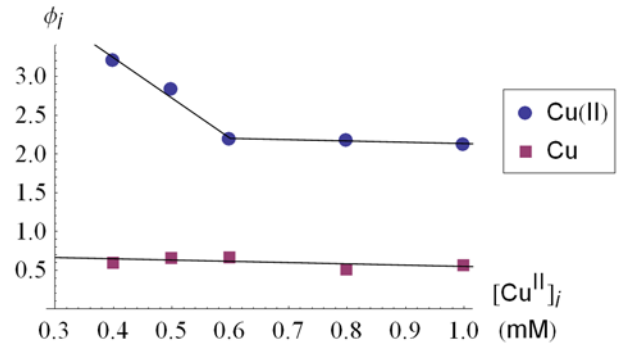

Figure 4.12. Variation of initial quantum yield with initial Cu^{2+} concentration in octane in the presence of 1 mM BP but no OS. Cu formation shows no dependence but at low cupric salt concentrations, the yield of Cu^{2+} reduction exceeds values of 2 indicating a chain process.

quantum yield for both steps occurred in the absence of OS which further demonstrates the inhibiting behavior of the sarcosine. Given the high quantum yields obtained in these experiments ($\varphi_i > 3$), the illuminations were repeated numerous times and similar yields were obtained. Equation 10 predicts a maximum quantum yield, with respect to Cu^{2+}/Cu^{+} reduction, of 2 so a chain mechanism is necessary to rationalize the larger yields observed when the reaction is conducted at lower metal concentrations and in the absence of OS. A chain process may arise from an oxidizing, mixed valence metal dimer resulting from the first reduction of the complex $Cu_2(oleate)_4$ provided that no dissociation of the dimer occurs in the absence of OS. Initiation plus ketyl and alky radical formation follows 3, 4, and 7 above, respectively. The Cu^{2+} dimer is then reduced by either radical species to generate a mixed valence intermediate

$$BPH\cdot/RH\cdot + Cu^{2+}—Cu^{2+} \rightarrow BP/R + Cu^{\alpha}—Cu^{\beta} + H^{+} \qquad (14)$$

where $\alpha + \beta = 3$ and $1 \leq \alpha, \beta \leq 2$. The intermediate dimer would then be free to oxidize another alkane molecule forming two Cu^{+} ions and another reductive alkyl radical.

$$Cu^{\alpha}—Cu^{\beta} + RH_2 \rightarrow 2\ Cu^{+} + RH\cdot + H^{+} \qquad (15)$$

A chain reduction ensues when reactions 15 and 14 (involving the RH· radical) operate in concert as chain propagation steps. Chain termination likely occurs via dimerization of the chain carriers. The occurrence of this alternate mechanism only at lower Cu^{2+} concentrations can be rationalized by deactivation of the intermediate by a Cu^{2+} dimer to produce one cuprous and three cupric ions.

$$Cu^{\alpha}—Cu^{\beta} + Cu^{2+}—Cu^{2+} \rightarrow Cu^{+} + 3Cu^{2+} \quad (16)$$

The constant $\varphi_i \approx 2$ obtained at higher copper ion concentrations indicates that the Cu^{2+} dimer is not an efficient quencher of $^3BP^*$.

Disproportionation of Cu^+ ions was an integral part of the metal formation process in water because SPEEK· and α-hydroxy radicals from isopropanol were not strong enough reductants to reduce the cuprous ions.[13,37] The present data, obtained in hydrocarbons such as octane and toluene, show that Cu^+ ions complexed with oleate ligands are reduced by photogenerated radicals. While the oxidation potential of octyl radicals is (to the best of our knowledge) not available in the literature, the value for toluene radicals has been estimated to be $E^o = 0.95$ V in acetonitrile.[39] As anticipated, BPH· is a stronger reductant with $E°(BP,H^+/BPH•) = -1.31$ V in 50% H_2O/ethanol.[40] If these values remain unchanged in the hydrocarbon solvents, then the lower quantum yields for reduction obtained in toluene (Figure 10) suggest that Cu(II) ions are efficiently reduced by octyl and BP radicals but not by the $C_6H_5CH_2$· radical. While participation of the octyl radical in the reduction of Cu(I) remains uncertain, the significant quantum yields of metal formation are strong evidence that BPH· is able to reduce the cuprous ions. Hence, the reduction of Cu^+ to yield Cu atoms is more favorable in nonpolar media than in water.

In the absence of complexing agents, Cu^+ ions hydrolyze in water to form the CuOH species which is difficult to reduce but no such species was detected in the dry hydrocarbon solvents employed during the present study. In the case of $Cu(oleate)_2$ reduction, the rate law for initial metal formation was first order with respect to I_o and [BP] indicating that the

photogeneration of reducing radicals can be considered as the rate-limiting step in Cu^{+} reduction. However, several observations indicate that reduction of the cuprous species takes place via a mechanism that is different from the one proposed for the Cu^{2+} consumption. For instance, φ_i for metal formation was at least 4 times smaller than the quantum yield of Cu^{2+} reduction. In addition, the data presented in Figures 3.8, 3.10 and 3.12 demonstrate that the slower metal formation process is not significantly affected by reaction conditions that altered the rate of the Cu^{2+} reduction. Although it is not entirely clear why the two reduction steps occur by different pathways, disproportionation does not provide a viable explanation since thermal formation of metal particles was not detected during the photoreduction of Cu^{2+} or after that process was completed.

A tentative explanation for the slow reduction of the cuprous complexes can be suggested based on observations made during the formation of metallic Cu in aqueous solutions containing formate ions.[41] In that system, Cu^{+} reacts with α-hydroxy and $\cdot CO_2^{-}$ radicals to form adducts and reaction of the adducts with Cu^{+} produces a metal atom. An analogous process can explain the observation that Cu particles form in hydrocarbons only when the cuprous ions are present together with the photogenerated reducing radicals. The slow metal generation process can be rationalized by assuming that complexation of Cu^{+} by the reducing radicals is slow or if the dissociation of the resulting adducts to form metal is fairly inefficient.

Conclusion

The present study describes an efficient method for the generation of crystalline Cu particles in hydrocarbon solvents. Reproducible quantum yields for the Cu^{2+}/Cu^{+} step of 3.21 were obtained and are rationalized in terms of a chain mechanism involving a reactive, mixed

valence Cu^{2+}/Cu^{+} intermediate. Initial rates of Cu^{2+} consumption depend linearly on incident light intensity and benzophenone concentration while decreasing rates result from increasing concentrations of Cu^{2+} and oleoylsarcosine. Metal formation occurs at least 4 times slower than the Cu^{2+}/Cu^{+} step which can be explained by considering the Gibbs free energy change associated with each step as measured in water. For the Cu^{2+}/Cu^{+} step, $\Delta G° = -16.2$ kJ/mol[26] whereas $\Delta G°(Cu^{+}/Cu_{atoms}) = 260.5$ kJ/mol[28] illustrating the large energy input required to form metallic Cu. Although the reaction can proceed in toluene, it occurs more slowly and with significantly lower quantum yields than in octane for the reason that the alkane solvent acts as a sacrificial H-atom donor presenting pseudo first-order conditions for the formation of ketyl radicals. The resulting colloids possess modest stability and resistance to air but they also have the capability of being dried and redispersed in a number of low dielectric media.

References

(1) Sakamoto, M.; Fujistuka, M.; Majima, T. *J. Photochem. Photobiol. C* **2009**, *10*, 33-56.

(2) Yonezawa, Y.; Sato, T.; Ohno, M.; Hada, H. *J. Chem. Soc., Faraday Trans.* **1987**, *83*, 1559-1567.

(3) Torigoe, K.; Esumi, K. *Langmuir* **1992**, *8*, 59-63.

(4) Kapoor, S.; Mukherjee, T. *Chem. Phys. Lett.* **2003**, *370*, 83-87.

(5) Yonezawa, Y.; Sato, T.; Kuraoda, S. *J. Chem. Soc. Faraday Trans.* **1991**, *87*, 1905-1910.

(6) Henglein, A. *Chem. Mater.* **1998**, *10*, 444-450.

(7) Sato, T.; Onaka, H.; Yonezawa, Y. *J. Photochem. Photobiol. A* **1999**, *127*, 83-87.

(8) Kapoor, S. *Langmuir* **1998**, *14*, 1021-1025.

(9) Kapoor, S.; Palit, D. K.; Mukherjee, T. *Chem. Phys. Lett.* **2002**, *355*, 383-387.

(10) Kometani, N.; Doi, H.; Asami, K.; Yonezawa, Y. *Phys. Chem. Chem. Phys.* **2002**, *4*, 5142-5147.

(11) Sato, T.; Maeda, N.; Ohkoshi, H.; Yonesawa, Y. *Bull Chem. Soc. Jpn.* **1994**, *67*, 3165-3171.

(12) Finter, J.; Lohse, F.; Zweifel, H. *J. Photochem.* **1985**, *28*, 175-185.

(13) Korchev, A. S.; Shulyak, T. S.; Slaten, B. L.; Gale, W. F.; Mills, G. *J. Phys. Chem. B* **2005**, *109*, 7733-7745.

(14) Scaiano, J. C.; Aliaga, C.; Maguire, S.; Wang, D. *J. Phys. Chem. B* **2006**, *110*, 12856-12859.

(15) Eustis, S.; Krylova, G.; Eremenko, A.; Smirnova, N.; Schill, A. W.; El-Sayed, M. *Photochem. Photobiolog. Sci.* **2006**, *4*, 154-159.

(16) Sakamoto, M.; Tachikawa, T.; Jujitsuka, M.; Majima, T. *Langmuir* **2006**, *22*, 6361-6366.

(17) Cohen, S. G.; Parola, A.; Parsons, G. H. *Chem. Rev.* **1973**, *73*, 141-161.

(18) The National Research Council, In *Prudent Practices in the Laboratory: Handling and Management of Chemical Hazards*, The National Academic Press: Washington, D.C., 2001, Page 139.

(19) Mehrotra, R. J.; Bohra, R. *Metal Carboxylates*; Academic Press: London, 1983;

Chapter 2.

(20) Heller, H. G.; Langan, J. R. *J. Chem. Soc., Perkin Trans. 2* **1981**, 341-343.

(21) Tonnet, M. L.; Yamada, S.; Ross, I. G. *Trans. Faraday Soc.* **1964**, *60*, 840-849.

(22) Atkins, P.; Overton, T.; Rourke, J.; Weller, M.; Armstrong, F. *Inorganic Chemistry*, 4th ed.; W. H. Freeman: New York, 2006.

(23) Protasiewyck, G. M.; Nunes, F. S. *Spectrochim. Acta, Part A* **2006**, *65*, 549-552.

(24) Salzemann, C.; Lisiecki, I.; Brioude, A.; Urban, J.; Pileni, M. P. *J. Phys. Chem. B* **2004**, *108*, 13242-13248.

(25) Khatouri, J.; Mostafavi, M.; Amblard, J.; Belloni, J. *Chem. Phys. Lett.* **1992**, *191*, 351-356.

(26) Ciavatta, L.; Ferry, D.; Palombari, R. *J. Inorg. Nucl. Chem.* **1980**, *42*, 593-598.

(27) Belloni, J.; Mostafavi, M. *Metal Clusters in Chemistry*; Wiley-VCH: Weinheim, 1999; Vol. 2.

(28) Gilbert, A.; Baggott, J. *Essentials of Molecular Photochemistry*; CRC Press: Boca Raton, 1991.

(29) Bensasson, R. V.; Gramain, J. C. *J. Chem. Soc., Faraday Trans. I* **1980**, *76*, 1801-1810.

(30) Cohen, S. G.; Baumgarten, J. *J. Am. Chem. Soc.* **1967**, *89*, 3471-3475.

(31) Cohen, S. G.; Cohen, J. I. *J. Am. Chem. Soc.* **1967**, *89*, 164-165.

(32) Davidson, R. F.; Lambeth, P. F. *Chem. Commun.* **1968**, 511-512.

(33) Devadoss, C.; Fessenden, R. W. *J. Phys. Chem.* **1991**, *95*, 7253-7260.

(34) Winnik, M. A.; Maharaj, U. *Macromolecules* **1979**, *12*, 902-905.

(35) Hammond, G. S.; Baker, W. P.; Moore, W. M. *J. Am. Chem. Soc.* **1961**, *83*, 2795-2799.

(36) Walling, C.; Gibian, M. J. *J. Am. Chem. Soc.* **1965**, *87*, 3361-3364.

(37) Buxton, G. V.; Green, J. C. *J. Chem. Soc. Faraday Trans. 1* **1978**, *74*, 697-714.

(38) Kochi, J. K.; Bemis, A.; Jenkins, C. L. *J. Am. Chem. Soc.* **1968**, *90*, 4616-4625.

(39) Griller, D.; Martinho-Simoes, J. A.; Mulder, P.; Sim, B. A.; Wayner, D. D. M. *J. Am. Chem. Soc.* **1989**, *111*, 7872-7876.

(40) Canonica, S.; Hellrung, B.; Wirz, J. *J. Phys. Chem. A* **2000**, *104*, 1226-1232.

(41) Grodkowski, J.; Neta, P. *J. Phys. Chem. B* **2001**, *105*, 4967-4972.

Chapter 5

Photochemical Generation of Ag, Pd, and Pt Particles in Octane

Introduction

The use of light as the driving force in metal salt reduction provides an interesting tool for the generation of colloidal particles which was discussed in detail in Chapter 4 and has additionally been reviewed.[1] Significant investigations include the photochemical preparation of silver colloids from aqueous solutions of $AgClO_4$ by either direct irradiation[2,3] or via the action of α-hydroxy radicals generated by irradiation of solutions containing acetone and 2-propanol.[4] Semiconductors, such as CdSe and CdS,[5] have been employed as photosensitizers in the generation of aqueous colloids of Pd and Pt while anatase TiO_2 has similarly been used in aqueous alcohol solution to produce Ag[6] and Pt[7] particles. $Pt(acac)_2$ was made water soluble by inclusion inside the cavity of β-cyclodextrin and irradiation of the resulting complex with both UV and visible light resulted in metal particles.[8] Likewise, direct irradiation of H_2PtCl_6[9] and $PdCl_2$[10] with UV photons resulted in ion reduction. Little work, however, has been published regarding the photochemical generation of Ag, Pd, or Pt in hydrocarbon media. At the time of publication, one reference was available in which Ag and Pt particles were photochemically generated in aqueous ethanol solutions, isolated, and redispersed in benzene and THF.[11] Filtration was required, however, to remove the fraction of particles which initially precipitated.

Previous attempts to generate noble metal colloids in non-polar solvents have been dominated by two-phase systems in which aqueous metal salts are extracted into an organic layer with the aid of phase transfer agents such as phosphines or quaternary amines.[12] Salt reduction ensues by the addition of a strong reducing agent such as $NaBH_4$ or hydrazine.[13-23] Provided that

salt dissolution can be achieved, in-situ reduction can, at times, be made possible in the organic phase by the input of thermal energy. Silver lactate, for example, was thermally decomposed in mineral oil in the presence of Korantin SH as a reductant as well as particle stabilizer to produce particles in large concentrations that were stable for several weeks.[24] Further methods for the thermal decomposition of various organic-soluble salts of silver and gold have lead to isolable particles which could be dispersed in an assortment of low dielectric solvents, including hexane, heptane, chloroform, toluene, cyclohexane, MIBK, THF, and benzene.[25-27] Additional achievements in non-polar media include the electrochemical generation of Ag in DMSO[28] and the formation of silver-encapsulated reverse micelles that could be isolated then dispersed in hexane.[29]

The study of nanofluids, colloids which function as liquids with enhanced thermal properties, has traditionally been limited to highly polar media such as ethylene glycol and water with little published work utilizing nonpolar solvents.[30] Silver nanoparticles were prepared by thermal reduction of aqueous $AgNO_3$ with ascorbic acid, isolated by centrifugation, and redispersed in kerosene. The resulting nanofluid was evaluated for thermal conductivity enhancement using a computer controlled transient calorimeter which showed an increase of nearly 20% for a colloid at 50 °C containing 0.5 mass% Ag.[31] The current study will report a method for the photochemical generation of colloidal Ag, Pd, and Pt in octane and the resulting enhancement of thermal conductivity as measured by the thermal HotDisk method.

Experimental

Caution: Piranha etch is a hazardous material that should only be handled by trained personnel using appropriate personal protective measures. Waste from this material should only

be disposed of by approved procedures.[32] $Pd(acac)_2$ and $Pt(acac)_2$, where acac denotes the acetylacetonate anion, were purchased from VWR, silver 2-ethyl-2,5-dimethylhexanoate (AgOOR) and oleoyl sarcosine (OS) from TCIAmerica, and all other chemicals were from Sigma-Aldrich. Rigorous purification of OS proved to be crucial to obtaining reproducible results. In order to remove water and other volatiles, the sarcosine was twice diluted in excess dry toluene followed by solvent removal under partial pressure and continued distillation for 4 hours. Benzophenone (BP) was recrystallized from methanol and water while the remaining reagents were used as received. Prior to use, octane was scanned from 900-200 nm to ensure the absence of light absorbing impurities. All glassware was treated with fresh piranha etch, rinsed thoroughly, and oven dried. Stock solutions of $Pd(acac)_2$ and $Pt(acac)_2$ were prepared daily in dry toluene in the concentration range of 25-50 mM whereas working stocks of AgOOR were prepared daily in anhydrous octane. Absorbance spectra were obtained on a Shimadzu UV-2450 spectrophotometer. Electron micrographs were obtained on a Zeis EM10 Transmission Electron Microscope at 60keV while selected area electron diffraction data were obtained on a Hitachi HF-2000 TEM at 200 keV and thermal conductivity measurements were conducted with a Hot Disk Transient Plane Source TC detector.[33] Ten mL aliquots of each colloid were deposited in Pyrex sample holders, fitted with a cover containing a slit to accommodate the Thermal Hot Disk sensor, and the containers were then inserted into matching cavities within an aluminum block submerged in a thermostatic bath. Samples were equilibrated until they remained at the desired temperature, ±0.1 °C, for at least 5 minutes and the reported TC value is the average of five independent measurements, the standard deviation of which was used to approximate the experimental error. Specimens were prepared for TEM observation by dip coating a 300 mesh Cu/formvar grid into a 0.5 mM colloid and oven drying at 60 °C under vacuum for 10 minutes.

Photochemical reactions were conducted in a 1 cm pathlength cuvette fitted with a quartz-to-pyrex graded seal. Samples were prepared in the optical cell within a nitrogen-filled glove bag, sealed with a rubber septum, and agitated for 10 seconds. Sample irradiation was achieved by vertically and horizontally centering a the cell inside of a Rayonet 100 circular illuminator equipped with 16 RPR-3500A lamps generating photons of λ = 350 ±15 nm and chemical actinometry was conducted using Aberchrome 540.[34]

Results and Discussion

Irradiation of octane solutions containing AgOOR, $Pd(acac)_2$, or $Pt(acac)_2$ with 350 nm photons in the presence of BP resulted in metal particles with nanometer dimensions. Absorbance spectra of the resulting yellow, dilute-black, and light-brown solutions, respectively, are presented in Figure 5.1. The sharp peak at 400 nm for silver is due to the collective oscillation of electrons about the particle surface whereas the broad absorption bands which extend throughout the visible region in the Pd and Pt spectra is a result of the superposition of

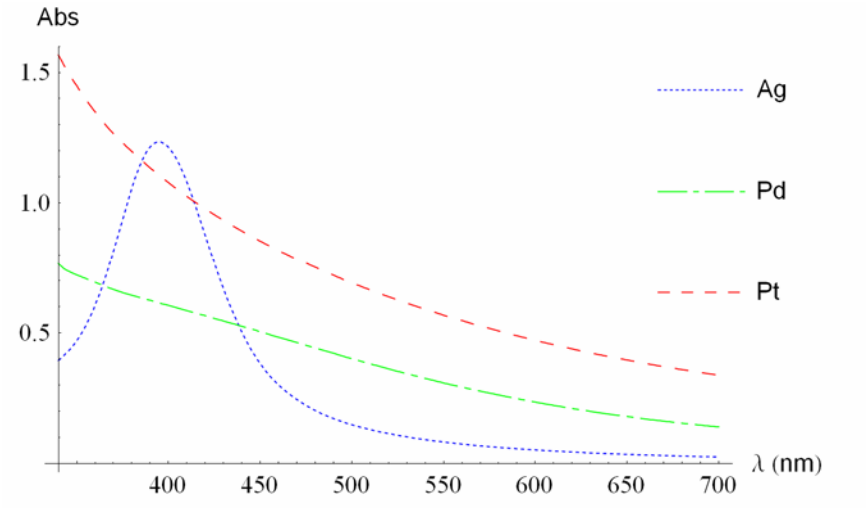

Figure 5. 1 Absorbance spectra of 0.1 mM Ag, 0.5 mM Pd, and 0.5 mM Pt in octane.

interband demonstrate that the particles appear to be spherical while the histograms in Figures 5.2D-5.2F reveal mean particle diameters of 11, 3, and 12.5 nm for Ag, Pd, and Pt, and provide corresponding size distributions. Colloidal stability was evaluated by visible inspection and Ag and Pt at 0.1 and 0.5 mM, have remained stable for more than four months. The Pd colloids unfortunately precipitate within a week of preparation, which is in contrast to the results for

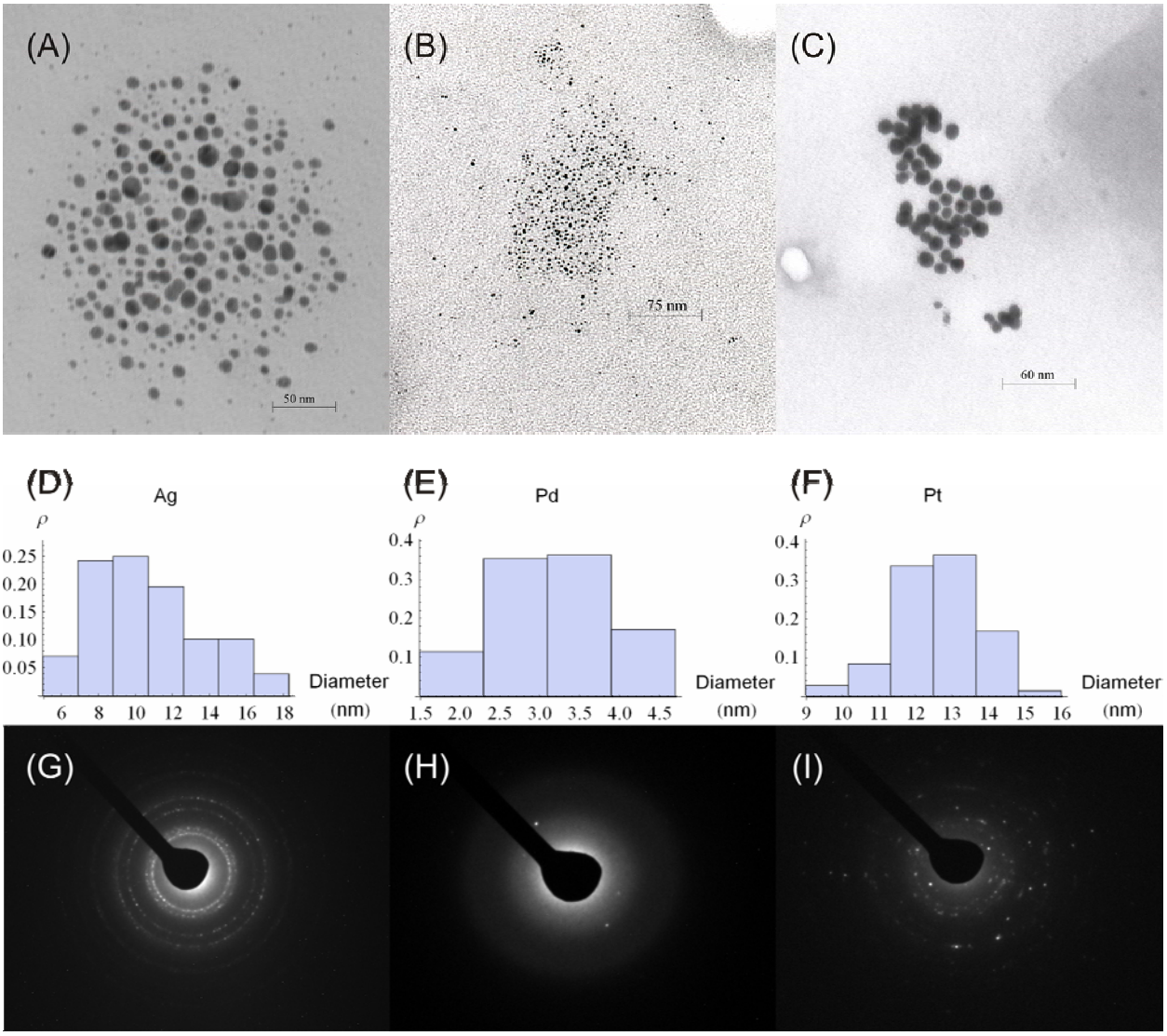

Figure 5. 2 TEM images of (A) Ag, (B) Pd, and (C) Pt particles revealing spherical morphology; histograms of particle sizes with mean diameters of 11, 3, and 12.5 nm, respectively (D-F); and corresponding electron diffraction patterns verifying particle crystallinity (G-I).

aqueous phase Pd particles presented in Chapter 2. The instability of the organic phase Pd particles is likely a result of the unusually small material dimensions which results in energetic surfaces leading to rapid aggregation and subsequent precipitation. Selected area electron diffraction (SAED) was employed to verify the crystallinity of each colloid. The Debeye rings shown in Figures 5.2G-5.2I are in good agreement with the reflections published by the JCPDS.[35]

The direct irradiation of $Pd(acac)_2$ and $Pt(acac)_2$ in the absence of BP resulted in metal particles whereas Ag required the aid of a photosensitizer. BP-sensitized metal ion reduction in octane is expected to occur via photogenerated ketyl radicals as previously illustrated in the photoreduction of Cu(oleate)2 in hydrocarbon solvent.[36] Absorption of a 350 nm photon by BP results in an excited singlet state which rapidly undergoes intersystem crossing, with near 100% efficiency, to yield the triplet excited state of BP, as shown in equation 1. The excited triplet

$$BP + h\nu(350\ nm) \rightarrow {}^1BP^* \rightarrow {}^3BP^* \qquad (1)$$

state is capable of hydrogen abstraction from alcohols, amines, amides, or hydrocarbons, the latter two of which are present in the current system. The first step in $^3BP^*$ reduction by tertiary amines was suggested to be electron transfer from the non-bonding pair of nitrogen to form a short-lived contact ion pair, as shown below where.[37,38] In nonpolar media, ultrafast proton

$$^3BP^* + Et_3N \rightarrow \left(BP^-, Et_3N^+\right) \rightarrow BP + Et_3N \qquad (2)$$

transfer follows to yield the ketyl and alkyl radicals.[39] Triplet BP has also been shown to

$$\left(BP^{-}, Et_3N^{+}\right) \rightarrow BPH\cdot + Et_2N\dot{C}HCH_3 \qquad (3)$$

abstract hydrogen directly from alkanes to form α-hydroxy, or ketyl, and alkyl radicals.[40] As previously established, ^{3}BP* does react with sarcosine and perhaps forms a contact ion pair as expected, but the result does not lead to metal ion reduction.[36] The ion pair can decay either by the back reaction shown in eq. 2 or the nascent ketyl and alkylamidyl radicals formed in eq. 2 can rapidly combine.[36] The dominant pathway for the reduction of BP was shown to occur by the oxidation of octane by ^{3}BP*, as shown in equation 4:

$$^3BP^* + RH_2 \xrightarrow{k_1} BPH\cdot + RH\cdot \qquad (4)$$

Since the oxidation of octane by $^3BP^*$ in CCl_4 at room temperature occurs with a rate constant of 4.7×10^5 M^{-1} s^{-1}, the same value is assigned to k_1.[40] Thus, $k_1' = k_1[C_8H_{18}] = 2.9 \times 10^6$ s^{-1} when the concentration of pure octane (6.15 M) is used which is a reasonable approximation provided that all reagents are present in low concentrations.

Evaluation of metal formation rate was conducted using the initial rate method, denoted r_i. Where appropriate, initial quantum yields, φ_i, are additionally reported where $\varphi_i = r_i/(\rho I_o)$, ρ = the fraction of photons absorbed by the chromophore at the given concentration, and I_o = light intensity recorded in μM(hν)/s. Figure 5.3 displays a plot illustrating the evolution of optical density of an octane solution containing 0.1 mM AgOOR, 0.1 mM BP, 10 mM OS and I_o = 29 μM/s with $\epsilon_{400}=1.2\times10^4$ $M^{-1}\cdot cm^{-1}$. The extinction coefficient is assumed to be

independent of wavelength and particle size.[41,42] A corresponding rate plot shown in the inset of Figure 5.3.

Each time step in Figure 5.3 corresponds to the irradiation of a fresh sample since temporarily interrupting the irradiation process of a single sample to perform measurements lead to undesirable products, the nature of which are currently under investigation. As has been extensively described in the literature, evolution of the plasmon band in Figure 5.3 is characterized by an initially broad peak centered at 415 nm, corresponding to clusters and small

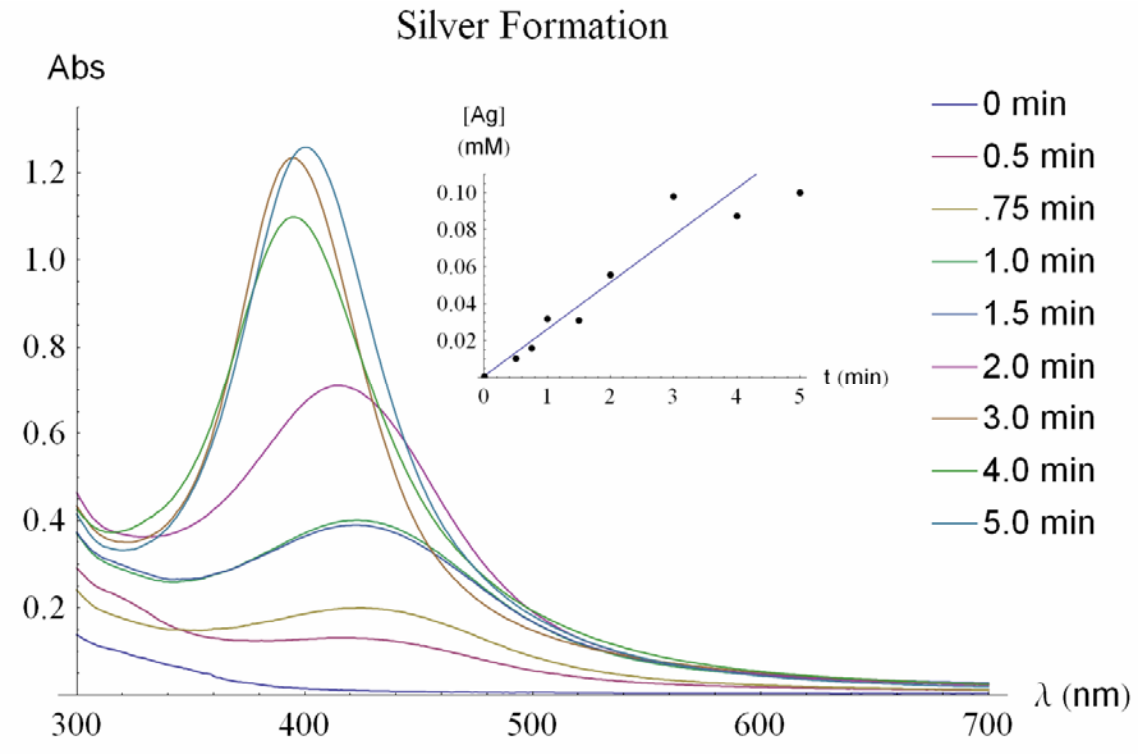

Figure 5. 3. Evolution of optical spectra during the photolysis of octane solutions containing 0.1 mM AgOOR, 0.1 mM BP, 10 mM OS, and I_o = 29 μM/s with an initial rate plot shown in the inset. Each time step corresponds to the irradiation of a fresh sample as opposed to the continuous irradiation of a single sample with intermittent pauses for measurement.

particles, followed by a sharpening of, and increase in, optical signal which blue shifts to 400 nm with the maturation of particles.[40] Metal formation occurred with an initial rate of 4.2×10^{-7} M/s and an initial quantum yield of 0.44. The latter value is nearly an order of magnitude larger than that which was reported for the reduction of silver ions in the aqueous SPEEK/PVA system ($\varphi_i = .06$)[43] and 5 times smaller than the reduction of Cu^{2+} ions in octane by BPH· radicals.[36]

Direct UV irradiation of $M(acac)_2$ (M = Pd or Pt) induces homolytic cleavage of the ligand—metal bond according to equations 5 and 6 resulting in a metal atom and two acac· radicals.[8] The two radicals then abstract hydrogen from a donor, such as the octane solvent, to yield 2 Hacac molecules as shown in equations 7 and 8 where R denotes the alkene product.[8]

$$M(acac)_2 + h\nu \rightarrow M(acac) + acac\cdot \quad (5)$$

$$M(acac) + h\nu \rightarrow M + acac\cdot \quad (6)$$

$$acac\cdot + RH_2 \rightarrow Hacac + RH\cdot \quad (7)$$

$$acac\cdot + RH\cdot \rightarrow Hacac + R \quad (8)$$

Due to the lack of a sharp peak, initial rates and yields for Pd and Pt formation were estimated by following the optical signal at 450 nm. When dry, air-free octane solutions containing 0.5 mM $M(acac)_2$ and 10 mM OS, as a particle stabilizer, were irradiated, metal formation was achieved. Figure 5.4 presents absorbance spectra which trace the formation of metallic Pd (A), $\varepsilon_{450} = 318$ $M^{-1}\cdot cm^{-1}$, and Pt (B), $\varepsilon_{450} = 1.2\times10^4$ $M^{-1}\cdot cm^{-1}$, by direct irradiation (no BP) with corresponding rate plots shown in the insets. Ion reduction occurred with an initial rate of $r_i = (3 \pm 0.5)\times10^{-8}$ M/s for Pd and $r_i = (4 \pm 0.7)\times10^{-8}$ M/s for Pt. In both cases, initial quantum yields were on the order of 10^{-3} which is at least one order of magnitude larger than values obtained under the same

conditions in dichloromethane with $\lambda \geq 300$ nm.[44] When the above experiments were repeated in the presence of 2 mM BP, the rates of metal formation increased by a factor of 3.8 for Pd and 2 which is significantly larger than the typical experimental error of 15%. The resulting initial rates were $r_i = (1.3 \pm 0.2)\times10^{-7}$ M/s and $(9 \pm 1.4)\times10^{-8}$ M/s, respectively, while the yields increased in accordance with the larger rates. Figure 5.5 illustrates the formation of Pd (A), $\varepsilon_{450} = 1\times10^4$ $M^{-1}\cdot cm^{-1}$, and Pt (B), $\varepsilon_{450} = 1.4\times10^4$ $M^{-1}\cdot cm^{-1}$, under photosensitized conditions with initial rate plots presented in the corresponding insets.

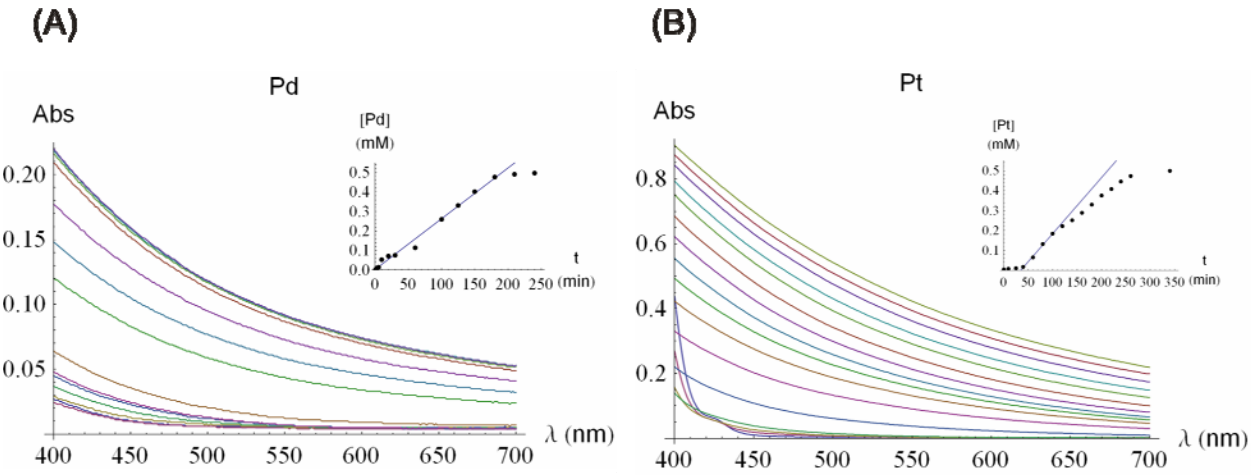

Figure 5. 4. Evolution of optical spectra during the photolysis of octane solutions containing 0.5 mM $M(acac)_2$, 10 mM OS, and $I_o = 53$ μM/s where (A) M = Pd^{2+} or (B) Pt^{2+} with corresponding initial rate plots shown in the insets.

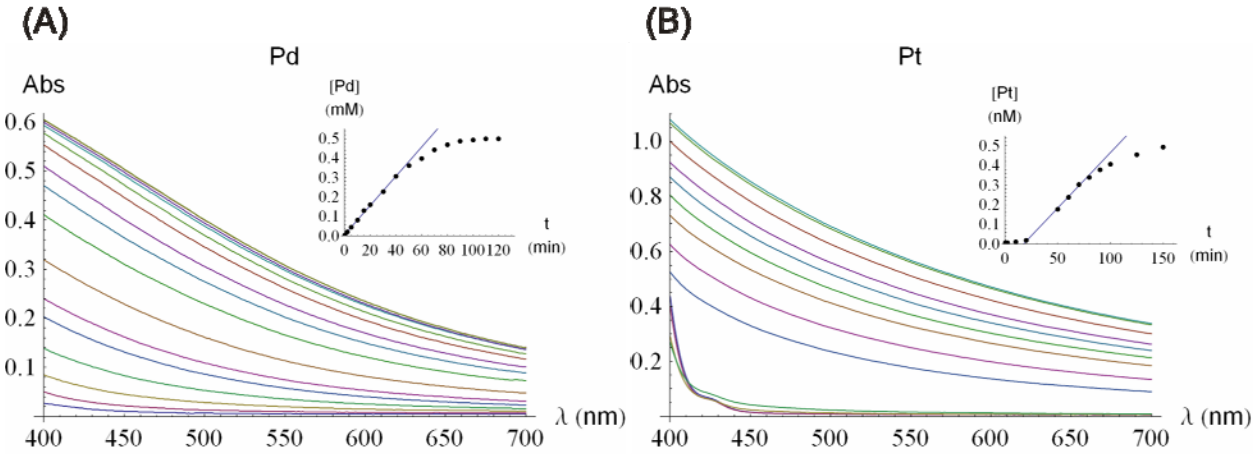

Figure 5. 5. Evolution of optical spectra during the photolysis of octane solutions containing 0.5 mM $M(acac)_2$, 2 mM BP, 10 mM OS, and I_o = 53 μM/s where (A) M = Pd^{2+} or (B) Pt^{2+} with corresponding initial rate plots shown in the insets. Presence of the sensitizer increases the rate of metal formation by a factor of 3.8 for Pd and 2 for Pt.

Thermal conductivity measurements were performed on colloids containing 5 mM M (M = Ag, Pd, or Pt), 20 mM BP, and 40 mM OS. Each sample was evaluated at 10, 30, and 50 °C with absolute TC values plotted in Figure 5.6A. The efficacy of nanofluids, however, is typically evaluated by their relative TC values, k_{rel} according to equation 9, where k_{nf} = colloid

$$k_{rel} = k_{nf}/k_{sol} \qquad (9)$$

TC and k_{sol} = TC of octane. Figure 5.6B demonstrates a plot of k_{rel} for each colloid with the maximum enhancement of ~10% occurring at 50 °C in both the Ag and Pt systems and Pd displaying an increase of 7% with an experimental error of ±1%. These values are significantly higher than the corresponding values in water, listed in chapter 1, of 2, 1, and 2%, respectively. The difference in the aqueous nanofluids vs. the hydrocarbon colloids is, however, intuitive for

the reason that the TC of octane is 6 times lower than that of water enabling the metal particles to make a greater contribution in hydrocarbon.

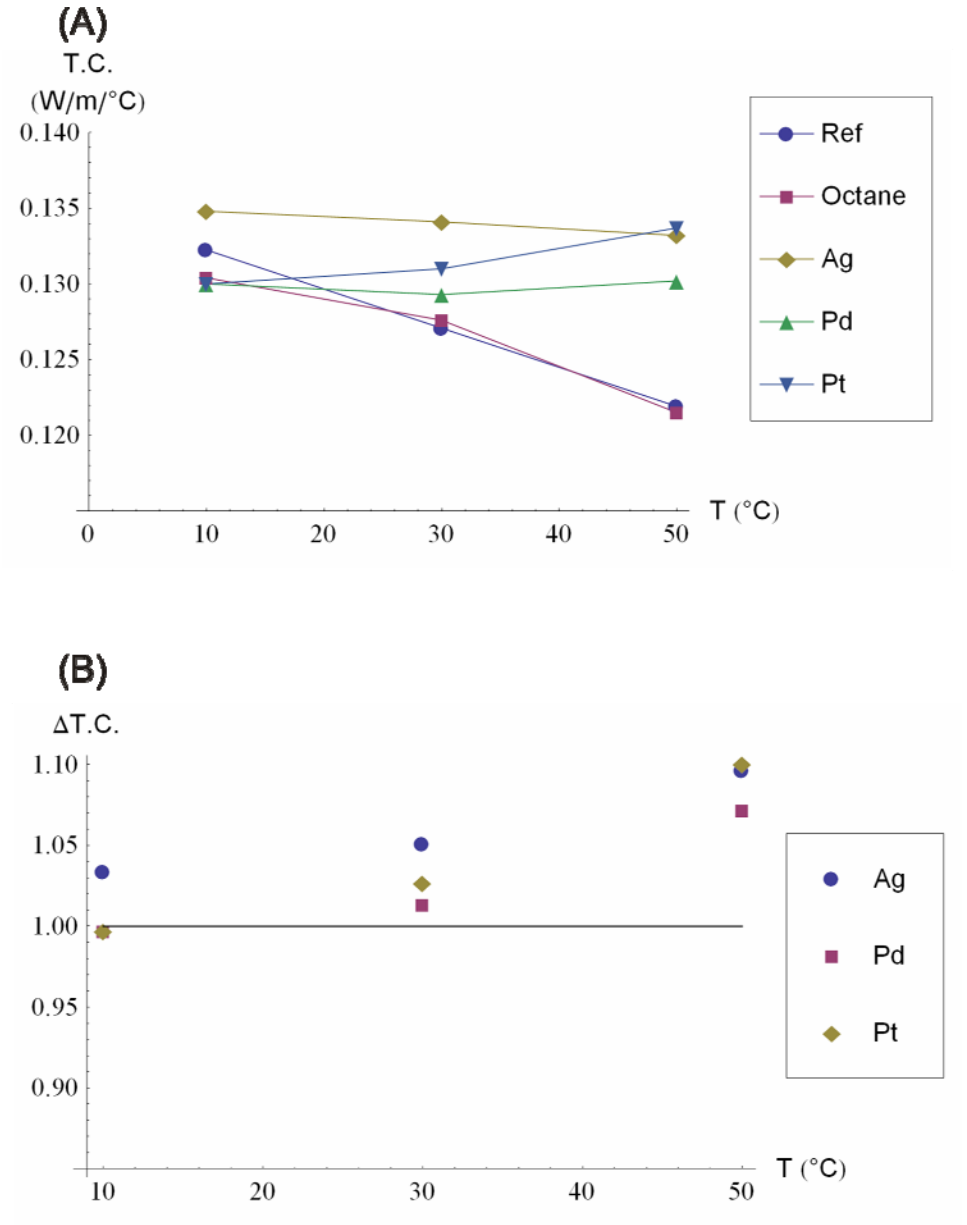

Figure 5. 6. Plots of (A) absolute and (B) relative TC. The experimentally determined values for octane are in good agreement with reference data.[45]

In the photochemical generation of Pd and Pt colloids, metal particles can result from the direct irradiation of the metal precursor. Silver, on the other hand, required the aid of a photosensitizer. Obtaining rate data for Ag was not trivial for the reason that periodic irradiation of a single sample, interrupted to obtain absorbance measurements, diverted the reaction pathway leading to an undesirable product, the precise nature of which is currently under investigation. Current reasoning suggests that when sample irradiation is interrupted during the early stages of particle growth, the surfaces of nascent clusters become coated with Ag^+ which shifts the Fermi level of the silver aggregates to a more negative potential causing the decay of ketyl radicals by alternate pathways to be favored over metal ion reduction. When 0.1 mM aqueous silver colloids were contaminated with iodine, the particle surfaces became oxidized, in turn coating the particle surface with a layer of AgI, resulting in the formation of a short wavelength peak and broadening of the plasmon band similar to that shown in Figure 5.7 from the current study.[46]

The BP-sensitized photoreduction of $Pd(acac)_2$ resulted in colloidal solutions with an extinction coefficient 3 times larger than that which was observed in Pd colloids prepared by direct irradiation. In order to verify that the smaller extinction was not due to incomplete ion reduction, a control experiment was conducted. A solution containing 0.5 mM Pd^{2+} and 10 mM OS in octane was irradiated until the evolution of optical density at 450 nm was complete. Four mM BP was then added and irradiation continued for one hour yet no increase in absorbance was observed indicating that all dissolved metal ions had been reduced. The decrease in extinction cross section is expected to be a result of smaller particle sizes with increased adsorption of chemical species onto the highly energetic particle surface. TEM analysis of the corresponding samples revealed particle sizes $\leq$2 nm; smaller sizes are below the resolution of the employed instrument.

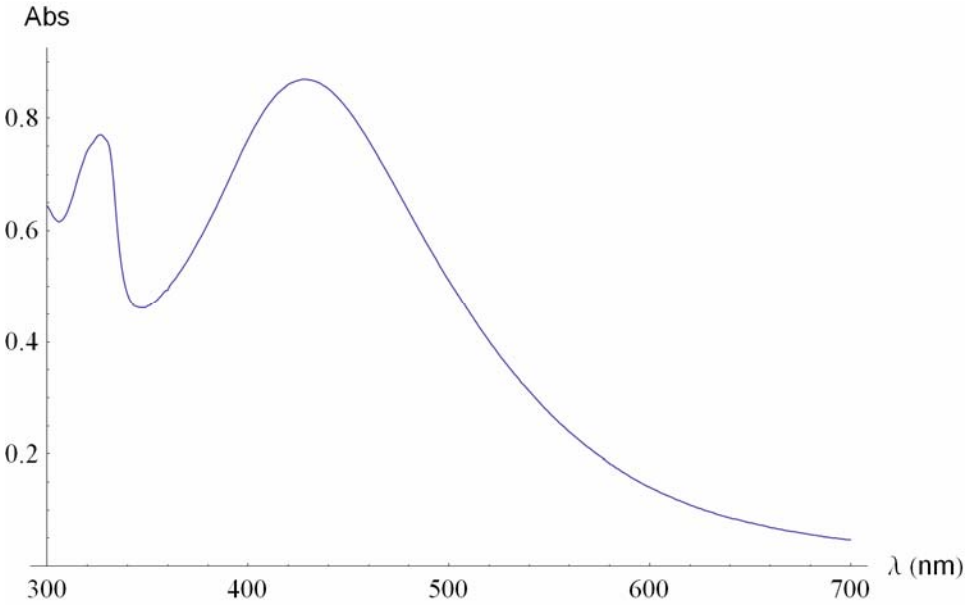

Figure 5.7. Final absorbance spectrum of Ag colloid after periodic interruption of irradiation in order to obtain measurements. Appearance of the short wavelength transition and broadening of the plasmon band are expected to be the result of adsorbed Ag^+ onto the surface of the growing particles which BPH· radicals are not capable of reducing.

Conclusion

Colloidal solutions of Ag, Pd, and Pt have been photochemically generated in octane using oleoyl sarcosine as a particle stabilizer. Solutions containing 0.1 mM Ag and 0.5 mM Pd have thus far remained stable for more than four months. On the other hand, Pd particles, prepared by either direct or photosensitized irradiation, precipitate within one week. Measurement of TC for the 5 mM colloids results in as much as 10% (±1%) enhancement in k_{rel} which is as much as five times larger than an analogous system evaluated in water (chapter 2). Maxwell's theory states that TC enhancement is a function of the volume fraction of dispersed metal; as such, further investigations are underway to determine the stable upper limit of metal concentration within the current colloidal system.

References

(1) Sakamoto, M.; Majima, T. *J. Photochem. Photobiol., C* **2009**, *10*, 33-56.

(2) Yonezawa, Y.; Sato, T.; Ohno, M.; Hada, H. *J. Chem. Soc., Faraday Trans.* **1987**, *83*, 1559-1567.

(3) Torigoe, K.; Esumi, K. *Langmuir* **1992**, *8*, 59-63.

(4) Henglein, A. *Chem. Mater.* **1998**, *10*, 444-450.

(5) Alemseghed, M. G.; Ruberu, P. A. *Chem. Mater.* **2011**, *23*, 3571-3579.

(6) Li, H.; Duan, X.; Liu, G.; Liu, X. *J. Mater. Sci.* **2008**, *43*, 1669-1676.

(7) Ismail, A. A.; Bahnemann, D. W. *J. Phys. Chem. C* **2011**, *115*, 5784-5791.

(8) Giuffrida, S.; Ventimiglia, G.; Petralia, S.; Conoci, S.; Sortino, S. *Inorg. Chem.* **2006**, *45*, 508-510.

(9) Harada, M.; Einaga, H. *Langmuir* **2006**, *22*, 2371-2377.

(10) Harada, M.; Inada, Y. *Langmuir* **2009**, *25*, 6049-6061.

(11) Murakata, T.; Higashi, Y.; Yasui, N.; Higuchi, T.; Sato, S. *J. Chem. Eng. Jpn.* **2002**, *35*, 1270-1276.

(12) Nath, S.; Jana, S.; Pradhan, M.; Pal, T. *J. Colloid Interface Sci.* **2010**, *341*, 333-352.

(13) Brust, M.; Walker, J. M.; Bethell, D.; Schiffrin, D. J.; Whyman, R. *J. Chem. Soc., Chem. Commun.* **1994**, 801-802.

(14) Esumi, K.; Shiratori, M.; Ishizuka, H.; Tano, T.; Torigoe, K.; Meguro, K. *Langmuir* **1991**, *7*, 457-459.

(15) Manna, A.; Imae, T.; Iida, M.; Hisamatsu, N. *Langmuir* **2001**, *17*, 6000-6004.

(16) Nath, S.; Praharaj, S.; Panigrahi, S.; Ghosh, S. K.; Kundu, S.; Basu, S.; Pal, T. *Langmuir* **2005**, *21*, 10405-10408.

(17) Song, X.; Sun, S.; Zhang, W.; Yin, Z. *J. Colloid Interface Sci.* **2004**, *273*, 463-469.

(18) Xun, F.; Wei, Y.; Yusheng, L.; Debao, W.; Huaqiang, S.; Fengyuan, Y. *J. Dispersion Sci. Technol.* **2005**, *26*, 575-580.

(19) Lala, N.; Lalbegi, S. P.; Adyanthaya, S. D.; Sastry, M. *Langmuir* **2001**, *17*, 3766-3768.

(20) Zeiri, L.; Efrima, S. *J. Phys. Chem.* **1992**, *96*, 5908-5917.

(21) Vorobyova, S. A.; Lesnikovich, A. I.; Sobal, N. S. *Colloids Surf., A* **1999**, *152*, 375-379.

(22) Kang, S. Y.; Kim, K. *Langmuir* **1998**, *14*, 226-230.

(23) Yang, J.; Lee, J. Y.; Chen, L. X.; Too, H. P. *J. Phys. Chem. B* **2005**, *105*, 5468-5472.

(24) Bönnemann, H.; Bladergroen, B.; Linkov, V. M. *Appl. Organomet. Chem.* **2005**, *19*, 768-773.

(25) Yamamoto, M.; Kashiwagi, Y.; Nakamoto, M. *Langmuir* **2006**, *22*, 8581-8586.

(26) Rao, C. R. K.; Trivedi, D. C. *Mater. Chem. Phys.* **2006**, *99*, 354-360.

(27) Hiramatsu, H.; Osterloh, F. E. *Chem. Mater.* **2004**, *16*, 2509-2511.

(28) Wadkar, M. M.; Chaudhari, V. R.; Haram, S. K. *J. Phys. Chem. B* **2006**, *110*, 20889-20894.

(29) Taleb, A.; Petit, C.; Pileni, M. P. *Chem. Mater.* **1997**, *9*, 950-959.

(30) Fan, L.; Khodadadi, J. M. *Renewable Sustainable Energy Rev.* **2011**, *15*, 24-46.

(31) Li, D.; Hong, B.; Fang, W.; Guo, Y.; Lin, R. *Ind. Eng. Chem. Res.* **2010**, *49*, 1697-1702.

(32) The National Research Council, In *Prudent Practices in the Laboratory: Handling and Management of Chemical Hazards*, The National Academic Press: Washington, D.C., 2001, Page 139.

(33) Gustafson, S. E. *Review of Scientific Instruments* **1991**, *62*, 797-804.

(34) Heller, H. G.; Langan, J. R. *J. Chem. Soc., Perkin Trans 2* **1981**, 341-343.

(35) JCPDS card numbers Ag: 4-0783; Pd: 46-1043; Pt: 4-0802.

(36) Clary, D. R.; Mills, G. *J. Phys. Chem. C* **2011**, *115*, 14656-14663.

(37) Cohen, S. G.; Cohen, J. I. *J. Am. Chem. Soc.* **1967**, *89*, 164-165.

(38) Davidson, R. F.; Lambeth, P. F. *Chem. Commun.* **1968**, 511-512.

(39) Devadoss, C.; Fessenden, R. W. *J. Phys. Chem.* **1991**, *95*, 7253-7260.

(40) Winnik, M. A.; Maharaj, U. *Macromolecules* **1979**, *12*, 902-905.

(41) Kreibig, U.; Vollmer, M. *Optical Properties of Metal Clusters;* Springer-Verlag: Berlin, 995.

(42) Belloni, J., Mostafavi, M. In *Metal Clusters in Chemistry*; Braunstein, P.; Oro, L. A.; Raithby, P. R., Eds.; Wiley-VCH: Weinheim, 1999; Vol 2, P 1213.

(43) Korchev, A. S.; Shulyak, T. S.; Slaten, B. L.; Gale, W. F.; Mills, G. *J. Phys. Chem. B* **2005**, *109*, 7733-7745.

(44) Lewis, F. D.; Miller, A. M.; Slavi, G. D. *Inorg. Chem.* **1995**, *34*, 3173-3181.

(45) *Handbook of Thermal Conductivity of Liquids and Gases*; Vargaftik, N. B.; Filippov, L. P.; Tarzimanov, A. A.; Totskii, E. E., Eds.; CRC Press: Boca Raton, 1994.

(46) Linnert, T.; Mulvaney, P.; Henglein, A. *J. Phys. Chem.* **1993**, *97*, 679-682.

Chapter 6

Conclusion

From the early days of stained glass windows to the modern day of colloid chemistry, small metal particles have established a commanding presence within the global research community. The collective oscillation of surface electrons enables solutions of nanometer-sized metal particles to produce brilliant colors distinct from the bulk. It was these colors that originally enchanted researchers and lead to the evolution of nanotechnology. Today it is well known that in addition to the unusual colors of colloidal solutions, the tiny crystallites also possess unusual electronic, optical, and surface properties that can be harnessed for a variety of applications. Of interest in the current work, however, has been the ability to stably disperse particles into a solvent of interest resulting in a colloid with enhanced thermal properties.

Due to interest in novel applications, the need has arisen to custom build stable colloids of precise composition fitted for each specific application. As such, a cyclodextrin-glucose host-guest complex was synthesized which enabled the reduction and stabilization of aqueous Ag, Au, Pd, and Pt colloids. The replacement of strong reductants, such as hydrazine or $NaBH_4$, with physiologically benign, environmentally "green" sugars may pave the way for these highly stable colloids to be employed in the course of various biological investigations. Thermal conductivity measurements of the prepared colloids showed an increase of only 2 ±1% at 50 °C but this value is still significant because it's far larger than what Maxwell's theory predicts for a colloid of such low volume fraction (~5×10^{-5} vol%).

The increase in thermal conductivity of a nanofluid is clearly a function of volume fraction of the suspended particles as well as the thermal properties of the starting materials.

With the vast majority of nanofluid and colloid chemistry literature describing particles dispersed in strongly polar media,[1] the current work was motivated to prepare and evaluate colloids with large particle concentrations in solvents of very low polarity, such as hydrocarbons ($\epsilon \approx 2.0$), that surpass expectations regarding particle stability. Dodecane and eicosane solutions of copper(II) oxide particles, stabilized by the sodium salt of oleic acid, were achieved with particle concentrations up to 1.65 M, or 20% by mass, which remained stable for weeks. Reducing the concentration by a factor of ten enabled particle stability to endure for more than 8 months. At such high concentrations, however, the thermal properties were found to diminish. Measurement of the relative heat transport properties, encompassing both conduction and convection, revealed a significant decrease at high concentration. Any enhancement in thermal conductivity was overwhelmed by a large decrease in convective heat transport.

A good model for TC enhancement in nanofluids is metallic copper due to this metal's large TC value (k = 401 w/m/K[2]). A photochemical system was established and characterized which was capable of producing highly stable Cu particles in octane. The resulting colloids, however, are air sensitive. A unique mechanism was discovered during the investigation of this system whereby a reactive intermediate oxidizes the hydrocarbon solvent. Future graduate students adopting this project will focus efforts into elucidating this mechanism. Future efforts also include eliminating the obstacle of air-sensitivity of the Cu particles by employing a transmetallation reaction whereby a layer of Cu atoms is replaced by a layer of Ag atoms, the latter of which has demonstrated robust stability toward oxidation.

With interest in air stable particles, octane colloids of Ag, Pd, and Pt have been photochemically prepared and evaluated. Both the Ag and Pt colloids display significant enhancement of thermal properties as well as excellent stability, persisting thus far for more than

four months ([M] = 0.1 and 0.5 mM, respectively), but Pd decays within a week of preparation. Thermal conductivity values, relative to the unmodified solvent, of up to 10% were achieved for [M] = 5 mM which is five-fold higher than analogous systems in water.

The increases in thermal conductivity, demonstrated for [M] = 5 mM, during the current work range from 1-10 ±1%. These values, which may appear of limited significance at face value, are of particular interest because they drastically exceed predictions made by Maxwell's theory for nanofluids composed of non-interacting, spherical particles, which is shown in equation 1.[3] The strong influence of the dispersed material imparts significance on the TC of the metal particles, bulk values for which were shown in Table 1.2, with TC values reported in W/m/°C.

Although the TC of Ag is 6 times larger than that of Pt, colloids prepared from these two metals in octane both resulted in a 10% enhancement at 50 °C. Of greater significance, however, is the significant deviation from theory. Maxwell's theory predicts very small enhancements for colloids prepared with [M] = 5 mM. In all cases, the predicted enhancement is on the order of 1.5×10^{-2} %,[3] approximately 600 times lower than what was reported in Chapter 4.

The unusual performance of the nanofluids evaluated during the current investigation is not uncommon. In fact, there is a great deal of controversy over not only the theories involved in predicting TC, but the measurement techniques as well.[4,5] The challenge, however, in developing useful models which accurately describe the mechanism of heat conduction in nanofluids is left to the theoreticians.

A greater obstacle which hinders the practical aspect of such heat transfer liquids is particle instability. The fact that such small volume fractions produce significant TC enhancements will enable the use of significantly smaller metal concentrations than predicted

and reduce that challenge to potentially achievable levels. Products of the current work conducted in aqueous media include highly stable aqueous colloids of Ag, Au, Pd, and Pt. Those seeking to enhance nonpolar cooling media, on the other hand, are presented herein with viable options of CuO, Ag, or Pt particles. One initiative during the continuation of the current work will involve maximizing the concentration of dispersed Ag in octane while maintaining particle stability. It is the hope of the current author that the materials developed during the current investigation will aid in the advancement of nanofluid technology from the experimental laboratory to practical use in a commercial environment; that the detailed characterization of each prepared colloid will assist colleagues in developing the much-needed models used to characterize heat transfer in such complicated, heterogeneous media; and that these findings will ultimately help dissolve the challenge that asks, ". . . is the controversy over?"[4] Not yet but soon . . . .

References

(1) Fan, L.; Khodadadi, J. M. *Renewable Sustainable Energy Rev.* **2011**, *15*, 24-46.

(2) *CRC Handbook of Chemistry and Physics*; 73rd ed.; Lide, D. R., Ed.; CRC Press, Inc.: Boca Raton, 1992.

(3) Eapen, J.; Rusconi, R.; Piazza, R.; Yip, S. *J. Heat Transfer* **2010**, 132, 102402/1-102402/14.

(4) Keblinski, P.; Prasher, R.; Eapen, J. *J. Nanopart. Res.* **2008**, *10*, 1089-1097.

(5) Buongiorno, J.; Venerus, D. C.; Prabhat, N.; McKrell, T.; Townsend, J.; Christianson, R.; Tolmachev, Y. V.; Keblinski, P.; Hu, L.-w.; Alvarado, J. L.; Bang, I. C.; Bishnoi, S. W.; Bonetti, M.; Botz, F.; Cecere, A.; Chang, Y.; Chen, G.; Chen, H.; Chung, S. J.; Chyu, M. K.; Das, S. K.; Paola, R. D.; Ding, Y.; Dubois, F.; Dzido, G.; Eapen, J.; Escher, W.; Funfschilling, D.; Galand, Q.; Gao, J.; Gharagozloo, P. E.; Goodson, K. E.; Gutierrez, J. G.; Hong, H.; Horton, M.; Hwang, K. S.; Iorio, C. S.; Jang, S. P.; Jarzebski, A. B.; Jiang, Y.; Jin, L.; Kabelac, S.; Kamath, A.; Kedzierski, M. A.; Kieng, L. G.; Kim, C.; Kim, J.-H.; Kim, S.; Lee, S. H.; Leong, K. C.; Manna, I.; Michel, B.; Ni, R.; Patel, H. E.; Philip, J.; Poulikakos, D.; Reynaud, C.; Savino, R.; Singh, P. K.; Song, P.; Sundararajan, T.; Timofeeva, E.; Tritcak, T.; Turanov, A. N.; Vaerenbergh, S. V.; Wen, D.; Witharana, S.; Yang, C.; Yeh, W.-H.; Zhao, X.-Z.; Zhou, S.-Q. *J. Appl. Phys.* **2009**, 106, 094312/1-094312/14.